THE EFFECT OF SUBSTRATE TOPOGRAPHY AND MECHANICAL STRAIN ON THE REGULATION OF NEURITE DEVELOPMENT IN NEURON CELLS

by

FURQAN HAQ

Under the Direction of Guigen Zhang

ABSTRACT

Many studies have shown that substrate topography and mechanical strains affect various cellular activities in most cell types. However, very few studies have shown the comparative analysis of the substrate topography features with different shape and size or the combined effect of substrate topography and mechanical strain on cellular activities in neuron cells. This study investigates the effect of micro/nanopillar and pore substrate topography features and the combined effect of substrate topography and mechanical strain on neurite development in PC12 (neuron) cells. Cells were cultured on substrates with nanopillars, nanopores and micro-island features to determine the effect of substrate topography on neurite development. Similarly, cells were cultured on deformable micro-textured substrates under no strain (static) and strain levels of 4%, 8% and 16% at strain rates of 0.1Hz, 0.5Hz and 1.0Hz, to determine the effect of substrate topography and mechanical strain on neurite development.

It was found that micro-islands enhanced neurite development while nanopillars enhanced proliferation compared with smooth substrates. Cells on nanopores had intermediate neurite development and proliferation. These findings suggest that the dimension of the substrate topography did affect neurite development. Under a mechanical environment, micro-textured

substrates enhanced neurite development only in the static and 4% at 0.1Hz conditions. Also, on smooth and micro-textured substrates, at a lower strain level increasing the strain rate promoted enhanced neurite development while at a higher strain level high strain rate inhibited neurite development compared to their static counterparts. These findings suggest that strain level and strain rate have a combined effect on neurite development, and the effect of micro-texture on neurite development is more prominent in static and lower strain conditions than in higher strain conditions.

The results of this study suggest that substrate topography and mechanical strain can be used to control neurite development in PC12 cells. These findings suggest using substrate topography and mechanical strain to control differentiation and proliferation in other neuron cell lines and neural progenitor cells. This will be therapeutically significant for treating degenerative diseases like Parkinson's disease, multiple sclerosis, spinal injury and other neuron related diseases.

INDEX WORDS: Topography, mechanical strain, proliferation, differentiation, cytoskeleton, neurite development, cell density, filopodia and neurite orientation.

THE EFFECT OF SUBSTRATE TOPOGRAPHY AND MECHANICAL STRAIN ON THE REGULATION OF NEURITE DEVELOPMENT IN NEURON CELLS

by

FURQAN HAQ

Bachelors of Arts, West Virginia University, 1997

Master of Science, West Virginia University, 1999

A Dissertation Submitted to the Graduate Faculty of The University of Georgia in Partial Fulfillment of the Requirements for the Degree

DOCTOR OF PHILOSOPHY

ATHENS, GEORGIA

2005

THE EFFECT OF SUBSTRATE TOPOGRAPHY AND MECHANICAL STRAIN ON THE REGULATION OF NEURITE DEVELOPMENT IN NEURON CELLS

by

FURQAN HAQ

Major Professor:	Guigen Zhang, PhD.
Committee:	Charles Keith, PhD. William Kisaalita, PhD. Steve Stice, PhD.

Electronic Version Approved:

Maureen Grasso
Dean of the Graduate School
The University of Georgia
December, 2005

DEDICATION

At this juncture in my professional life it is only appropriate to dedicate this research work to the people who have supported my academic and research pursuits. First and foremost the moral support provided by my family is paramount. It has been the stepping stone towards achieving a well rounded education, research and career goals. Some things in life are far too precious to be mentioned in words. I hope that you will consider this work as a token of my appreciation of your unconditional support. The advice supplied by teachers and academic counselors has been a great source of guidance in traversing the long and winding road called higher education. Friends in academic and social settings have also been a source of inspiration in their own special ways. To you all, I would like to say “kindly lead the light that illuminates the mind and brighten the soul.”

ACKNOWLEDGEMENTS

This research work has been a collaborative effort between different departments at the University of Georgia. First and foremost, I would like to thank the Department of Biological and Agricultural Engineering for the financial support. The grants from National Science Foundation (NSF) and UGA Engineering Grant under the auspices of Dr Zhang have been paramount in financing my research. I would like to thank the Center for Ultrastructural Research**,** in particular Dr. Shields for providing the training and knowledge to work on Scanning Electron Microscope (SEM). I would also like to thank Dr. Yiping Zhao's laboratory in the Physics department for providing nano-substrates for this study. Dr. Steve Stice has been extremely understanding in allowing me to use his laboratory to work on embryonic stem (ES) cells and human umbilical vein endothelial cells (HUVECs) under the guidance of Dr. Raj Rao.

I am eternally obliged to Dr. Charles Keith for teaching me everything I know about cell culture and providing laboratory space for carrying out this research work. Above all, Dr. Zhang has been instrumental in molding this project and was a refreshing source of inspiration through the course of my study. Dr. Zhang's research group has been an integral part of this research work. I would like to extend special thanks to all of them for their collaborative effort. Dr Kisaalita's guidance as a graduate co-ordinator was pivotal in orchestrating a timely completion of my degree requirements. I am obliged by the friendly service provided by the staff and secretaries at the Driftmier Engineering Center. You all have made my education and research at University of Georgia a pleasant experience.

TABLE OF CONTENTS

Page

LIST OF TABLES

Page

LIST OF FIGURES

Page

CHAPTER 1

INTRODUCTION

Purpose of Study

The study of how cells respond to physical cues in its surroundings represents a new and important area of tissue engineering research. Physical cues such as substrate topography and mechanical strain have been shown to influence various cellular activities such as cell adhesion, differentiation, proliferation, and gene expression [1, 2]. The fact that most biological cells and tissues have been shown to be affected by topographical features of its basal membrane and by mechanical strain of its surroundings raises an important question if these physical cues can be used to control cellular activities.

Most of the biological moieties in a cell such as cell body, filopodia (sense receptors) and integrins (cell adhesion proteins) are at the micro and nanoscale and hence they can be influenced by topographical features of similar sizes [1, 2]. Similarly, mechanical stresses in the cell's environment affect the regulation of cell and tissue morphology and function through integrins, the main receptor that connects the cell's cytoskeleton to the extracellular matrix (ECM). Hence, tractional forces developed in the cytoskeleton are transferred to the ECM through integrins [3]. Hence, the physical cues that the cells experience affects downstream processes such as cell adhesion, cell shape and spreading, differentiation, proliferation and gene regulation [1-3].

To develop physiologically relevant in vitro models that support normal cell functions and activities, the in vitro environment has to possess the major components of the basal

membranes to which cells are attached in vivo. Basal membranes are dense sheets of ECM formed by various cell types that along with chemotrophic factors are known to play a fundamental role in modulating cellular activities such as adhesion, migration, proliferation, and differentiation through biochemical interactions. The surface topography of various basement membranes is composed of ECM mesh of pores, ridges and fibers in the 30-190 nm range under dynamic strain due to the cell's biological function in the body [4]. To fully understand these cell-ECM interactions in vivo it is important to develop modified matrices that can incorporate topographical features and mechanical strains to closely mimic cell environment found in vivo.

A majority of cell-substrate interaction studies has shown the role of patterned grooves with various widths and depths on cell alignment but few studies looked at the effect of pillars and posts [5-9]. However, basal membranes found in vivo are more like arrays of nanaoscale pillars and pits, rather than grooves and ridges.

Even though various studies have investigated the effect of topography and mechanical strain on various cellular activities and cell lines, very few studies have shown how the applied strain might alter the effect of topographic texture on cell activities. No study has demonstrated the combined effect of these physical cues on neurite development in neurons. Most of the cellular-strain interaction investigations in neuron cells are focused on recreating experimental models of traumatic neuronal injury induced at relatively high mechanical strain conditions (>30% strain amplitude and >10.0Hz strain frequency) [10-12]. The physiological strain conditions of cells are governed by their biological functions. Neuronal cells do not have dynamic function as with osteoblasts (high strain rates of 10-20Hz) [13] and skeletal muscle cells (high strain levels of 25% to 35%) [14].

In this study, substrates with nanopillars, nanopores and micro-island structures were used to investigate the effect of substrate topography on neurite development in neuron-like cells. The substrate topography features used in this study have similar critical dimensions as the neuron cells. Typical neurites are 1-10 μm thick and the neuron cell body is about 10-20 μm in diameter. Similarly, filopodia have cross-sectional diameter of 120-160 nm [15]. Filopodia's are thin protrusions with actin-bundles as their core and comprises about 15-20 actin filaments oriented with their barbed ends towards the tip [15]. The formation and extension of filopodia in response to physical cues determines the path of growth cone advancement. Actin-filament bundling and actin polymerization at the tips supply the driving force behind the formation and elongation of neurites by assembly of microtubules. Neurite development in response to physical cues can thus be quantified by analyzing the cytoskeleton, which is directly connected to the ECM by integrins. This allows an in vitro analysis of the structure-function relationship of the cell's cytoskeleton in regulating cellular activities such as cell adhesion, cell differentiation and proliferation in response to physical cues in the cell's surrounding. Hence, the formation of actin and microtubules was investigated in this study to analyze the role of topography in eliciting neurite development at the intracellular level.

This work has importance for the design and development of implantable cell-based devices that interfaces and moves in relation to the movement of the host tissue. Furthermore the texture at the nano- and microscale might improve the device biocompatibility. Hence, a novel cell-based device that combines physiologically relevant movement (strain environment) and controlled topographical features can be used to enhance biocompatibility and regulate specific cellular activities such as cell adhesion, differentiation and proliferation.

The findings of this research suggest using substrate topography and mechanical strain as a factor in switching neurons between differentiation and proliferation by controlling the physical cues that the cell experiences. Hence, topography and mechanical strain can be used synergistically to understand the precursory role of physical cues in inducing intracellular functions like actin polymerization and microtubule assembly to maintain and regulate neurite development.

Cells integrate not only the chemical but also the physical aspects of their environment (substratum topography and mechanical forces) to regulate cellular activities including cell proliferation, differentiation, and gene expression [1-3]. The transmembrane adhesion proteins (integrins) provide a mechanical linkage between the cells environment and its cytoskeleton. Therefore, the chemical and physical attributes of the cell's environment as well as integrins and the cytoskeleton act as functional units to modulate intracellular activities that determine cell fate [3]. A quantitative analysis of cell morphology and biochemical activity can thus be used to measure the effect of different substrate topographies and mechanical strain conditions on cellular activities such as differentiation and proliferation. In this dissertation, nano-pillared, nano-porous and micro-island substrates, and different strain levels and strain rates are the structural and mechanical aspects of the cell's environment. Neurite development and cell multiplication are the cellular responses to these structural and mechanical aspects in the cell's environment. An analysis of the combined effect of the substrate topography and mechanical strain will help elucidate the interaction between these two physical cues in regulating cellular activities.

Hypothesis

The dimension of the substrate topography features and the magnitude of the mechanical strain level and strain rate can be used as factors to control neurite development in PC12 cells.

Objective

The primary goal of this study is to quantify the effects of substrate topography and mechanical strain on neurite development in PC12 cells. The specific aims of this study are:

Specific Aim-1: To investigate the effect of substrate topography on neurite development.

A quantitative analysis of neurite length, neurite density and cell density was performed to determine the effect of substrate topographical features with different size (nano and microscale) and shape (nanopillars and nanopores) on neurite development.

Specific Aim-2: To investigate the combined effect of substrate topography and mechanical strain on neurite development.

A quantitative analysis of neurite length, neurite density, cell density and neurite orientation were performed to determine the effect of deformable micro-textured substrates on neurite development in cultures subjected to a range of uniaxial strain levels and strain rates.

Significance

A great understanding of cellular and intracellular activities can be achieved by subjecting cells to topographical features and mechanical strains. A complete analysis at the cellular and intracellular level can be monitored via existing laboratory techniques. This approach helps in understanding the role of cell's environment in regulating cell shape and spreading, which affects cell differentiation and proliferation.

Modified substrates can mimic the basal membrane found in vivo. Using micro-and-nanofabrication permits the development of modified substrates to accommodate cell's spreading for desired cell growth. Similarly a tight control of the applied strain that the cell experiences will aid in understanding the role of different strain conditions on neuron cells. Furthermore, using a range of different strain conditions will help determine a physiological relevant strain condition for eliciting desired differentiation and proliferation activities in neuron cells. This will have significant impact to the development of artificial tissues and organs for treating various diseases.

CHAPTER 2

BACKGROUND LITERATURE

Most cells in the human body are attached to extracellular matrix (ECM) or to other cells to perform their physiological functions and to organize themselves into tissues and organs. Cell's ECM is connected to its microfilamentous cytoskeleton through transmembrane receptors called integrins. Integrins transmit physical cues such as mechanical strain and substrate topography across the cell-membrane to the actin-cytoskeleton. Cytoskeletal elements such as actin and microtubules mediate the transduction of these physical cues into biological responses. Cell functions can be influenced by changes in the ECM environment (both chemical and physical), culturing conditions and the cell-ECM interactions. Elucidation of both biochemical and mechanical mechanisms by which external forces affect cell morphology may reveal entirely new approaches to treat disease [16].

Currently there is a great deal of interest in developing modified substrates that can mimic cell-ECM interactions found in cells attached to basal membrane. Basal membranes are found in most mammalian tissue. The topography of the basal membrane is a complex network of pores (30-190 nm), fibers (20-90 nm), ridges and other features of nanometric sized dimensions [4]. The basal membrane also experiences a dynamic mechanical environment as a result of tissue function and activity in the body [17].

In neuronal cells, the attachment of the peripheral actin network of the growth cone via focal adhesion contacts to the substrate plays a leading role in the elongation of the neurites by advancing microtubules and cytoplasm [18]. Stimulatory signal transduction promotes the

polymerization of G-actin into F-actin and the bundling of the microtubules [18, 19]. The actin polymerization and microtubule bundling lead to the advancement of the growth cone. Inhibitory signal transduction causes rapid depolymerization of the F-actin and leading to the depletion of the P-region followed by the retraction of the microtubule rich neurite [18, 20]. Neurite development and orientation in response to physical cues can be explained by cytoskeleton changes that control and regulate the cell morphology. Cells undergoing deformation reorganize their actin cytoskeletons and consequently align the long axes in the direction of the minimal substrate deformation [21, 22].

To date, studies on cell mechanics have only dealt with one aspect of the physical cues in cell's environment. Usually these studies have been aimed toward investigating the influence of substrate topography features or mechanical strain on cell adhesion, cell morphology, cell differentiation and proliferation. However, very few studies have investigated the combined effect of topography and mechanical strain on cellular activities. In order to mimic cell environment found *in vivo* it is necessary to understand the combined effect of substrate topography and mechanical strain on fundamental cellular activities such as cell adhesion, cell differentiation and proliferation.

Effect of Topography on Cellular Activities

The fields of tissue engineering and bio-nanotechnology aim to restore the functionality of complex human tissues and other biological systems by integrating living and synthetic components together. To be successful, fundamental knowledge of interactions between the living and synthetic components, or more specifically cell-substrate interactions, is needed. To most closely mimic living systems, substrates should possess topographical features that are

similar to those encountered by cells in vivo [6]. Basement membranes are found throughout the vertebrate body serving as substrates for overlaying cellular structures, and they are made of a complex mixture of pores, ridges, and fibers with sizes in the nanometer range [23-25]. Basal membranes found in most mammalian tissue serve as substratum for attaching cells. Studies show that cells (15-50 μm range) are attached to basal membrane with a felt-like feature of grooves and ridges in the 400 nm to 4000 nm range [23-25]. The basal membrane topography of the Rhesus Macque, human and matrigel (a commercially available basal membrane-like complex) have pores and fibers in the nanometer size range [25]. The topographical features of the basement membranes play a very important role in regulating cellular activities, including spreading, adhesion, proliferation, gene expression, differentiation, and apoptosis [4, 5, 7].

It is known that cells react to micro-topography by changes in cell adhesion, contact guidance, cytoskeletal organization, apoptosis, macrophage activation and gene expression [26]. Recent findings have shown that nano-topography can affect both protein and cell behaviors essential for tissue development; these responses include adhesion, morphology cytoskeleton and pattern of gene expression [26, 27]. Teixeira et. al. found that ridges 70 nm wide induced human corneal epithelial cells to elongate and align along the topographic features [4]. Micro- and nano-featured substrates provide an extracellular topographic feature with size close to that of cell (10-20 μm) and filopodia (100-120 nm).

Micro-featured substrates with grooves of various depths, width and spacing have demonstrated that initial axon growth of neurons from different species is directed by topographic cues [28, 29]. Hippocampal neurons have shown increased initial axon growth on micro-pillared (0.5-2.0 μm diameter) surfaces compared to smooth regions [5]. Similar size micro-pillars have also been shown to promote cells of oligodendrocyte lineage to align and

migrate along surface contours as they do along axons in the developing optic nerve [30]. Neuroblasts from the central nervous system orient their neurites in both perpendicular and parallel directions on artificial micro-features that mimic a neurite bundle (diameter, approx. 0.5 μm) [31]. Micro-features may mimic biological structures by providing topographical cues with appropriate dimensions. Cells grown on micro-grooved as opposed to smooth substrates are generally more elongated and tend to conform to the shape of the micro-groove [32].

Recently, cellular behavior on substrates with nanometer scale topographical features has been investigated [33-37]. Nano-featured substrates were found to induce alignment of oligodendrocytes but not of rat hippocampal or cerebellar neurons [30]. Fibroblasts and endothelial cells have been shown to adhere and spread on 13 nm high nano-islands of 50-500 nm in diameter and 150-600 nm in separation produced by phase separation of poly(styrene) and poly(bromostyrene) [34]. A similar study showed that fibroblasts response to nanometric islands (13, 35, and 95 nm in height) of similar diameter and separation produced by polymer demixing [35]. The results of this study showed that 13 nm islands produced the most spread cells and 95 nm islands produced the least spread cells. Table 3 in Appendix-A shows the various fabrication techniques used to develop substrate topographies to study cellular activities in different cell types and cell lines [38-45].

Studies show that cells responded strongly to nanometer scale features by extending a large number of filopodia, or sensory organelles [27]. Since cells probe their surrounding by forming and extending filopodia to gather information, the development of such a large number of filopodia in cells seeded on nano-featured substrates suggests that the cells are ‘spatially aware’ of the nano topography of the substrates [27]. In neuronal cells, extension of filopodia is an up-stream event for productive neurite outgrowth [46, 47]. But it is not known if such a strong

up-stream filopodia extension event would lead to the down-stream neurite outgrowth activities in these neuronal cells.

Most of these studies have investigated the effects of nanometer or micrometer scale substrate features on cell morphology in comparison with smooth substrates. Comparison on the effects of the topographical features between nanometer scale and micrometer scale has not been made directly. Similarly, the effect of different shape topographies has not been addressed through a parallel analysis of vertically aligned and porous structures. A comparative analysis of different shape and size substrate topography features in cell-substrate interaction studies can offer insights into controlling cellular structures with a similar scale and morphology.

Effect of Mechanical Strain on Cellular Activities

Most cells *in vivo* are exposed to topographical features of the basement membranes and mechanical deformation due to the biological function of the host tissue and organ [48, 49]. Cells sense and respond to mechanical environment by initiating a variety of cellular activities, including morphological changes, protein synthesis, and gene expression [50-56]. Because of the complexity of the *in vivo* environment, systematic study of phenomena of cellular response to mechanical stimulation has relied heavily on the use of *in vitro* setups. To investigate the effect of mechanical strain on cellular activities such as cell adhesion, cell morphology, cell differentiation and proliferation, protein expression and gene regulation, many *in vitro* studies have been performed by culturing cells on flexible substrates with [50, 51] or without [52-56] micro-groove features and subjecting them to mechanical stimulation. In these studies, a wide range of strain levels and strain rates has been applied to the substrates to stimulate various cell types.

The magnitude level of amplitude, frequency and the direction of applied strain determine a specific cellular response [57]. Living cells respond to increasing levels of applied stress by a linear increase in cytoskeleton (CSK) stiffness [58]. Stretching forces pull on integrins (transmembrane focal adhesion contacts) causing the internal CSK and nuclear scaffolds to immediately align along the main axis of the applied tension field [58]. However, the magnitude and the type of applied strain eventually determine cell alignment and orientation. Cell alignment and orientation depends on the stretching magnitude – the larger the stretch, the farther the cells oriented away from the stretching direction [59, 60]. Almost every type of cells has been found to align nearly perpendicular to the primary cyclic stretching direction [59]. It has been observed that cells subjected to cyclic stretching (12% amplitude) oriented predominantly 60–70° about the stretching direction, which is the direction of minimal substrate deformation [59]. Biochemical assay and modeling studies have validated that stress fiber formation and cell alignment are in the direction of minimal substrate deformation [61].

Cells have shown various cellular responses to different strain level and strain rate. A high cyclic sinusoidal stretch of 25% at a frequency of 1 Hz in porcine vascular smooth muscle cells (PVSMCs) has been shown to cause an increase in PVSMC apoptosis [62]. Mechanical stretching magnitudes greater than 4% have been shown to cause an increase in the production of inflammatory mediator prostaglandin E_2 [63]. An increasing strain level and strain rate has been shown to cause an increased activation of G-protein subunits (role in mechanotransduction) in cardiac fibroblasts [64]. Autoradiography of labeled G-proteins showed a 4.7 fold increase at 0.1Hz and 6% maximum strain; 5.5 fold at 0.3Hz and 3% maximum strain; no increase at 0.1Hz and 3% maximum strain and with no stretch (control) [64]. Increasing the rate of applied strain elicited an increased activation of G-proteins and lower strain rates at lower strain magnitudes

failed to elicit any cell response. These studies suggest that the magnitude of both the strain level and strain rate have an influence on cellular activities. Furthermore, strain level and strain rate have a combined effect on cellular activities. While most groups have investigated the effect of different strain level and strain rate on various cell lines, few groups have looked at the relationship between strain level and strain rate on cellular activities in neuron cell lines.

To date, most mechanical stimulation studies on neurons have been limited to studies of axonal injury and neuronal cell death induced by subjecting the cells to relatively high non-physiological strains (≥ 30% strain level and 10Hz frequencies) [10-12]. The physiological strain conditions of cells are governed by their biological functions. Neuronal cells do not have dynamic function as with osteoblasts (high strain rates of 10-20Hz) [13] and skeletal muscle cells (high strain levels of 25% to 35%) [14]. Thus, the physiological strain conditions of neuronal cells are not as high as osteoblasts or skeletal muscle cells. Work done by Morrison et. al. has shown that strain level of 20% at strain rates above 10Hz represent a transition between non-injurious and injurious mechanical conditions in rat hippocampal cultures [65]. Very little damage was caused by strains of 10% at a strain rate less than 10Hz. Acute stretching of the peripheral nerve at 11% strain showed ischemic changes but not mechanical damage to the motor neurons while at 6% strain level there were no ischemic changes or mechanical damage to the motor neurons [66]. Based on these mechanical studies and information available a strain range of 4%-15% within 1-2Hz is considered as physiological mechanical conditions in neuron cell types.

Mechanical stimulation apparatus have included matrix coated flex plates (flexcell) [48], pulsatile fluid shear [56], deformable collagen sponges [67], laser trap optical stretchers [68], and deformable substrates (usually silicone) clamped between one immobile and a mobile end or

both mobile ends [49-51, 69]. A wide variety of laboratory apparatuses devised for mechanical stimulation of cell and tissue cultures is discussed in Table 4 in Appendix-B [70-76]. It provides a list of various types of cell-stretching apparatuses used to study influence of mechanical stimulation on different cell lines and cellular activities. These devices are categorized in terms of their primary loading modalities; compression, longitudinal stretch, bending, asymmetric substrate bulge, in plane substrate distortion, fluid shear. A wide range of substrate strain and amplitudes and frequencies on various types of cells have been used in these experiments. However, very little information is available on the effect of topography on the mechanical stimulation of fundamental cellular activities such as differentiation and proliferation. Furthermore, the relationship between different strain levels and strain rates on fundamental cellular activities such as differentiation and proliferation is not fully understood.

CHAPTER 3

RESEARCH QUESTIONS

Research Question 1: **What is the effect of size and shape of the substrate topography feature on neurite development in PC12 cells?**

Research Approach: This research question will be addressed by the following specific aims:

Aim 1: Characterizing Cell Morphology Response to Substrate Topography. PC12 cells will be cultured and maintained on substrates with nanopillars, nanopores and micro-islands under identical experimental conditions. The effect of different dimension and shape substrate topography features on neurite development and cell density will be observed using various microscopy techniques. The performed tasks to achieve this aim are:

Task 1: Substrate Fabrication. Nano- and micro-featured substrates will be fabricated using micro and nanotechnology. The morphology of the fabricated substrate features will be characterized to determine its dimensions.

Task 2: Preparing Substrates for Cell Culture. All the substrates will be first sterilized to prepare them for cell-culture. The sterilized substrates will then be chemically treated to promote cell-adhesion of PC12 cells.

Task 3: Cell Culture. PC12 cells will be seeded in an equal number on all the types of substrates in triplicates and maintained for 4 days. The effect of substrate feature size on cellular activities will be determined by seeding cells on substrates with nanopillars and micro-islands features in parallel. Similarly, the effect of substrate feature shape will be determined by seeding cells on substrates with nanopillars and nanopores in parallel. Smooth substrates (non-modified)

serve as the control in these studies. Two sets of experimental setups will be prepared: one for scanning electron microscopy (SEM) and the other for fluorescent microscopy (FM) analysis.

Task 4: Cell Density Analysis. After 4 days of culture, the cells density will be enumerated on all types of substrates.

Task 5: Neurite Development Analysis. After the cell density count, the cultures will be fixed and prepared for SEM and FM analysis.

Aim 2: Determining Plating Efficiency on Different Types of Substrates. A separate setup with all types of substrates will be used to determine the plating efficiency of different types of substrates. This plating efficiency analysis is to determine if there are any differences in cell adhesion on the different types of substrates that might have contributed to cell density and neurite development analysis. The percentage of the adhered viable cells out of the total plated cells will be calculated as the plating efficiency.

Aim 3: Quantification of Neurite Development and Cell Density. Neurite length and neurite density will be measured to quantify neurite development and cell multiplication will be measured to quantify cell density on different types of substrates. The performed tasks to achieve this aim are:

Task 1: Measuring Neurite Development and Cell Density. Neurite development will be quantified by measuring the length and number of neurites per cell (neurite density) and cell density will be quantified by cell enumeration. Correlation between the number of filopodia and the number of neurites per cell will be performed to determine how cells sense and respond to specific physical cues.

Task 2: Statistical Analysis. Statistical comparisons will be made between neurite length, neurite density and cell density on different types of substrates to determine the effect of

substrates with different topography features on cellular activities. The relationship between the number of filopodia and the number of neurites per cell on different types of substrates will be determined by calculating the correlation coefficient.

Aim 4: Biochemical Verification of Differentiation and Proliferation. A separate setup with nano, micro-featured and smooth substrates will be used to determine the differentiated state of neurons by a biochemical assay. This biochemical assay serves as a means of verification for the morphological observation of neurite development on nano and micro-featured substrates.

Research Question 2: **What is the combined effect of substrate topography and mechanical strain on neurite development in PC12 cells?**

Research Approach: This research question will be addressed by the following specific aims:

Aim 1: Characterizing Cell Morphology Response to the Combined Effect of Substrate Topography and Mechanical Strain. PC12 cells will be seeded on smooth and micro-textured substrates and subjected to various strain levels and strain rates. The influence of different strain on the effect of micro-textured substrates on neurite development and cell density will be observed using various microcopy techniques. The performed tasks to achieve this aim are:

Task 1: Substrate Fabrication. Deformable smooth and micro-textured substrates will be developed by casting polymer gel into membranes on smooth and micro-textured templates, respectively. The morphology of the developed micro-textured substrates will then be characterized to determine its dimensions.

Task 2: Preparing Substrates for Cell Culture. All the different types of substrates and the cell stretching apparatus will be sterilized for cell culture. The different types of substrates will then be chemically treated to promote cell adhesion.

Task 3: Cell Culture. Cells will be seeded at an equal seeding density in triplicates in all experimental setups. Two sets of setups will be prepared: one for SEM and the other for FM analysis. The cells on both the smooth and micro-textured setups will be subjected to different strain levels (4%-16%) and different strain rates (0.1Hz-1Hz). Cells on the smooth and micro-textured substrates in the non-stretched setups (static) serve as the controls for their counterparts in the stretched setups (dynamic). All the dynamic setups will be subjected to their respective strain conditions for 24 hours. All the setups will be cultured for a total of 4 days.

Task 4: Cell Density Analysis. After 4 days of culture, the cells density will be enumerated in all setups.

Task 5: Neurite Development Analysis. After cell enumeration, the cells in all setups will be fixed and prepared for SEM and FM analysis.

Aim 2: Determining Plating efficiency on Different Types of Substrates. A separate setup with smooth and micro-textured substrates will be used to determine the plating efficiency on different types of substrates. The percentage of the adhered viable cells out of the total plated cells will be calculated as the plating efficiency.

Aim 3: Quantification of Neurite Development and Cell Density. Neurite length and neurite density will be measured to quantify neurite development and cell multiplication will be measured to quantify cell density in different setups. The proposed tasks to achieve this aim are:

Task 1: Measuring Neurite Development and Cell Density. The length and the number of neurites per cell will be measured and counted respectively to quantify neurite development and the cells will be enumerated to quantify cell density. Furthermore, the angle of neurite orientation in respect to the direction of applied strain in the dynamic setups and randomly marked axis in the static setups will also be measured using the SEM. This serves as a measure

of neurite alignment in response to different strain conditions. The relationship between the development of the length and number of neurites and mechanical energy (strain level x strain rate) that the cells experience will be analyzed to determine the effect of mechanical energy on neurite development.

Task 2: Statistical Analysis. Statistical comparisons will be made between neurite length, neurite density, cell density and neurite orientation in the different setups to determine the combined effect of micro-textured substrates and mechanical strain on neurite development. The relationship between development of length and number of neurites and energy will be determined by calculating the correlation coefficient.

CHAPTER 4

MATERIALS & METHODS

Aim 1 & Task 1: Substrate Fabrication

Five different types of substrates topographies were used to determine the effect of substrate features on cellular activities. These substrates include: substrates with an array of vertically aligned nanopillars and nanopores having diameters close to the size of the filopodia found on neuron cells (150 nm), substrates with an array of micro-islands of 1.5 μm in height with diameters close to the size of the neuron cell-body (10-20 μm), substrates with an array of micro-islands of 4.0 μm in height with size close to the thickness of the neurites (1-5 μm, and smooth substrates as control. In addition, two different types of deformable polydimethylsiloxane (PDMS) substrates were used: substrates with micro-islands having diameters close to the size of the neuron cell-body and smooth PDMS substrates.

Silicon Nanopillars: Nano-featured substrates (or nano-substrates) with arrays of vertically standing silicon nanopillars of 890 nm in height, 103 nm in diameter and 131 nm in separation were deposited onto smooth silicon wafers using glancing angle deposition (GLAD) technique. GLAD is a physical vapor deposition technique that can fabricate aligned nano-pillar arrays using azimuthal rotation of the substrate at an oblique incident angle. An RCA1 (a wafer cleaning solution made of a mixture of ammonia hydroxide, hydrogen peroxide and water in a ratio of 0.25:1:5) cleaned 10×10 mm^2 silicon (100) substrate was placed on a substrate holder in an electron beam evaporator chamber under vacuum. The source material (silicon) was heated by an electron beam and the vapor of the source material was deposited onto the silicon substrate.

During deposition, the substrate was kept rotating azimuthally at a large fixed angle (>75°) with respect to the vapor flux. In this experiment, the incident angle of the silicon vapor flux was set at 86° with respect to the substrate surface normal, the growth rate at 0.2 nm/s, and the substrate rotation speed at 0.05 rev/s. Due to the shadowing effect [77] this technique produced vertically aligned arrays of nanopillars.

Silicon Micro-Islands: For micro-featured substrates (or micro-substrates), a square array of circular shaped islands of equal height was fabricated on silicon wafers using photolithography and wet etching processes [78]. A photomask having a square array pattern of micro-islands with diameter of 15 μm and the center-to-center distance of 30 μm was used. Figure 1 shows the procedure used to fabricate micro-featured substrates on silicon wafers with spin-coated photoresist by UV exposure in a mask aligner. The fabrication procedure is as follows. An RCA1 cleaned p-type silicon (100) wafer was first prebaked at 85°C for 5 minutes to remove any moisture. Positive photoresist (Microposit S1818, Shipley Corp, Marlborough, MA) was spin-coated onto the wafer using a spin coater (P6700, Specialty Coating System Inc., Indianapolis, IN) at 4000 rpm for 30 seconds. The wafers were soft baked at 90°C for 2 minutes to drive off solvents. The desired pattern was transferred to the photoresist layer through UV exposure in a mask aligner (Karl Suss MJB 3, Karl Suss America Inc., Waterbury Center, VT). The exposed sample was then developed in MF-319 developer (MF-319, Shipley Corp, Marlborough, MA) to reveal the photoresist pattern on the silicon substrate. The specimen was then hard-baked at 100°C for 10 minutes followed by wet etching in a mixture of acetic acid, nitric acid and hydrofluoric acid with a volume ratio of 13:8:4 at room temperature. The exposed wafers were etched in the etching mixture for 30 seconds to develop shallow micro-islands (1.5 μm, shallow micro-substrate) and 90 seconds to develop higher micro-islands (4.0 μm, high micro-substrate).

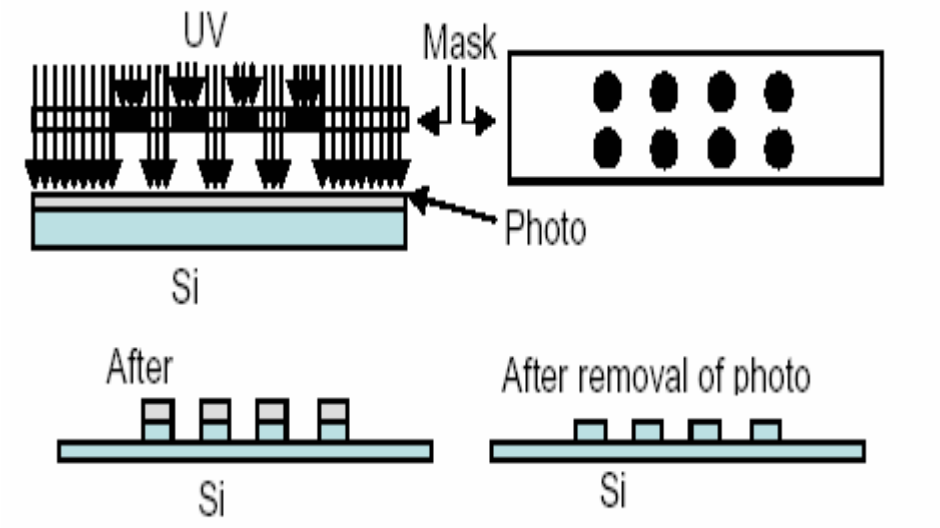

Figure 1. Procedure used to fabricate micro-featured substrates on silicon wafers. Silicon wafers with spin-coated photoresist are exposed to UV exposure in a mask aligner.

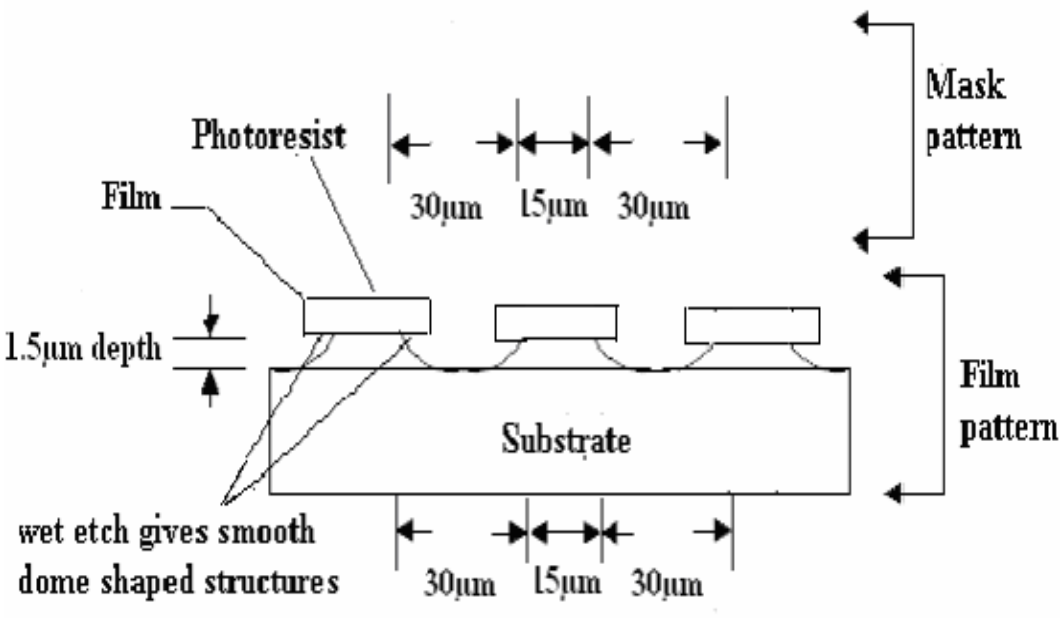

Figure 2. Smooth dome shaped micro-island features developed using isotropic wet etching.

Since the photoresist acted as an etching mask, this step resulted in micro-island arrays on a silicon substrate. After chemically stripping the remaining photoresist, the specimen was washed in deionized water and blow-dried with nitrogen. Figure 2 shows the micro-island like features obtained after isotropic wet-etching. The height of the developed micro-islands was characterized using a profilometer (XP-1, Ambios technology). The diameter and spacing of the micro-islands were characterized using an optical microscope (Nikon Eclipse ME600, Nikon Inc., Melville, NY).

Smooth Silicon Substrates: Clean bare silicon wafers (RCA-1 cleaned) served as a control for the nano and micro-featured substrates to study the effect of substrate topography feature size on cellular activities in PC12 cells.

Gold Nanopillars: Nano-featured substrates with arrays of standing gold nanopillars of 229 nm in diameter, 69 nm in separation and 2123 nm in height were developed using electrochemistry [79]. To fabricate vertically aligned nanopillar array features, porous anodic alumina (PAA) discs (Whatman Inc., England) were used as templates for electrodepositing metallic materials through the pores of the PAA templates. Prior to electrodeposition, a thin layer of gold of about 150 nm thick was sputter-coated on one side of PAA discs to provide a conductive coating. Electrodeposition was conducted in a three-electrode system (Solartron 1480 multistat): a gold-coated PAA disc was used as the working electrode; platinum (Pt) wire gauze was used as the counter electrode, and Ag/AgCl as the reference electrode. For gold nanopillar feature development, an OROTEMP24 gold plating solution (Tehnic Inc) was used. Prior to the electrodeposition of gold into the pores of the template, a thick gold film of approximately 3 μm was electrodeposited on top of the sputtered coating in order to provide a strong supporting base to the nanopillar array features. Then the supporting base was masked with Miccrostop solution

(Tolber division, pyramid plastics, Inc) and gold was deposited into the pores of the PAA disc from the uncoated side under a constant current density of 5-mA/cm^2 for 5 minutes at 65^{o}C. The height of the nanopillars can be controlled by varying the duration of electrodeposition. The PAA template was then removed by dissolving it in a 2.0M NaOH solution. After the removal of the PAA template, vertically aligned gold nanopillar array features on thick gold base were obtained. The morphology of the nanopillars was examined under scanning electron microscopy (SEM).

Gold Nanopores: For nanoporous substrates we used pre-fabricated porous anodized alumina 25 mm diameter discs (Whatman Inc, England) with pores (through holes) of 200 nm diameter were used for porous featured substrates. The PAA was coated with gold to give it the same surface material for cell adhesion as that of the gold nanopillars. A thin layer of 50 nm gold was deposited on the PAA using a high vacuum evaporator (BOC Edwards, Wilmington MA) with a built-in thickness detector. The morphology of the nanopores was characterized using an SEM.

Gold Coated Coverslips and Bare Coverslips: 25 mm diameter coverslips coated with 50 nm layer of gold (using the same procedure used for gold coating PAA) and 25 mm diameter non-coated (bare) coverslips were used as the two controls. These control setups allowed a comparative analysis on the effect of substrate topography feature shape on cellular activities in PC12 cells.

Micro-Textured PDMS: For micro-textured PDMS substrates, a hard silicon mold with a square array of circular shaped islands of 15 μm in diameter, 30 μm in separation and 1.5 μm in height was fabricated on silicon wafer using photolithography and wet etching processes. The detailed fabrication procedure of this silicon mold is described previously (Aim 1 & Task 1, Silicon Micro-Islands). In brief, a photoresist (Microposit S1818, Shipley Corp, Marlborough,

MA) was spin-coated onto a cleaned p-type silicon (100) wafer followed by prebake at 85°C for 5 minutes. The pattern from a photomask with arrays of micro-islands was transferred to the photoresist layer through UV exposure using a mask aligner (Karl Suss MJB 3, Karl Suss America Inc., Waterbury Center, VT). The exposed specimen was developed in MF-319 developer (MF-319, Shipley Corp, Marlborough, MA) to reveal the photoresist pattern on the silicon wafer. The specimen was then hard-baked at 100°C for 10 minutes followed by wet etching in an etching mixture (CH_3COOH, HNO_3 and HF, volume ratio of 13:8:4) at room temperature for 30 seconds. The etched silicon wafer was then washed in deionized water and blow-dried with nitrogen. After that, a parylene negative copy of the silicon mold was developed by coating a thin layer of parylene using chemical vapor deposition (PDS 2010 labcoater, Cookson Electronics, Rhode Island). To make PDMS micro-textured substrates, silicone gel mixed with its curing agent in a 10:1 ratio was cured into membranes by evenly pouring into the parylene mold at 100ºC for 45 minutes. Substrates with dimensions of 2.5×1.0×0.01 (inch) were made.

Figure 3 shows the a schematic diagram of the procedure used to fabricate micro-island on PDMS substrates using silicon mold and the subsequent development of parylene mold for curing silicone gel into micro-textured PDMS substrates. The height of the developed micro-islands was determined using a step-profilometer (XP-1, Ambios technology, Santa Cruz, CA). The diameter and the spacing of the developed micro-islands were measured using an optical microscope (Nikon Eclipse ME600, Nikon Inc., Melville, NY).

Smooth PDMS: Smooth PDMS substrates were developed by mixing silicone gel (Sylgard 184, Dow Chemical) with its curing agent in a 10:1 ratio for two minutes and poured between two parallel plates and cured at 100ºC for 45 minutes.

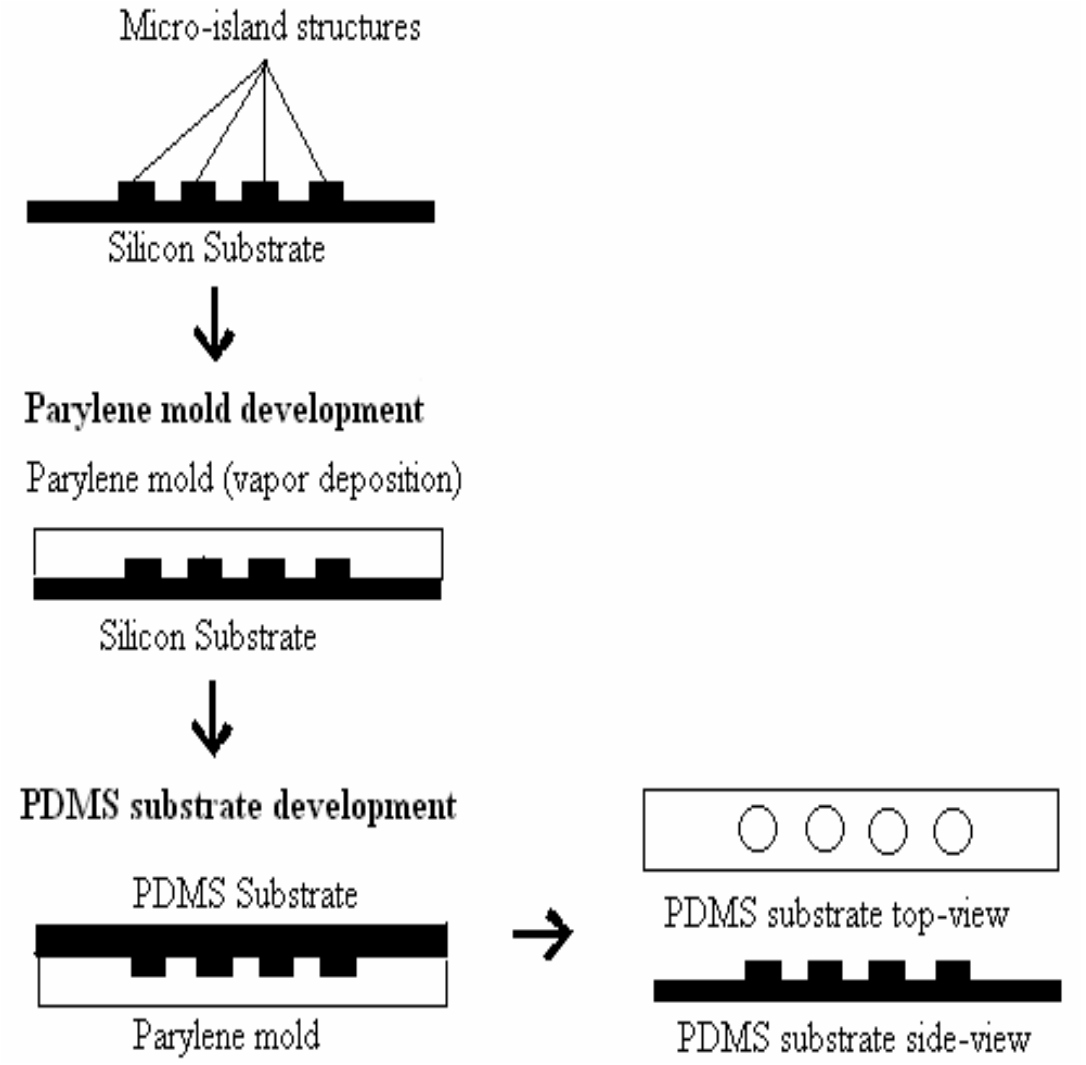

Figure 3. Procedure used to fabricate micro-textured PDMS substrates. Micro-patterned silicon wafers served as the template for the development of parylene mold for curing silicone gel into micro-textured PDMS substrates.

Aim 1 & Task 2: Preparing Substrates for Cell Culture

Substrate Sterilization: All the substrates were sterilized for cell culture using two basic sterilization techniques, heat and ethanol treatment. Silicon nano-, micro- and smooth substrates, and PDMS substrates (smooth and micro-textured) were sterilized by autoclaving at 135°C for 30 minutes using the gravity cycle. Gold nanopillars, nanopores, gold coated coverslips and bare coverslips were sterilized in 95% ethanol for 30 minutes, followed by two water washes and air dried in a laminar hood. These substrates were sterilized in ethanol because heat sterilization introduced cracks and pitting on the gold-coated substrates leading to the peeling off the gold layer.

Chemical Treatment of Substrates to Promote Cell Adhesion: Cell adhesion is dependent on proper anchorage of cells to the growth surfaces. For most cell lines, and especially for post-mitotic neurons, coated tissue culture plates are prerequisite for seeding. The most commonly used coating reagents are positively charged polymers such as poly-L-lysine or biologically purified adhesive molecules such as collagen.

Gold substrates used in this study are inert and did not allow creation of surface charges with commonly used synthetic and protein treatments. The gold surfaces of the substrates were modified with a self-assembled monolayer (SAM) of cysteamine, to provide a thiol group (-SH) for molecular binding. The cysteamine SAMs were prepared by treating all the types of gold substrates with 2.0 mM solution of cysteamine dihydrochloride in ethanol for 24 hours at room temperature in the dark and then rinsing with ethanol, 1.0 mM NaOH and sterile water. The SAM on gold surfaces was then readily functionalized to allow the binding of polymeric molecules such as poly-L-lysine and collagen that promote cell adhesion.

All the substrates were treated with 0.05% poly-L-lysine (70-150 kD.) for four hours at room temperature followed by two 10-minute washes in sterile deionized water. The reason for choosing Poly-L-lysine is that this treatment does not induce focal adhesions [80-82] but instead it generates ionic bonds to cells. Its working principle is that the polycationic poly-L-lysine molecules adsorb strongly to various solid surfaces, leaving cationic sites which interact by means of electrostatic interactions with the anionic sites on the cell surfaces [83, 84]. Since poly-L-lysine is a synthetic molecule it does not bind to chemically specific receptors to stimulate biological activity other than those elicited by physical interactions with the substrate. In addition, poly-L-lysine does not have the impurities that are commonly present in natural polymers [85].

The SAM of cysteamine and the poly-L-lysine layers on gold coated coverslips had a thickness of 15±2 Å and 178±16 Å respectively using an ellipsometer (Ellipsometer SE400, SENTECH, Berlin, Germany). Ellipsometry measurements of these layers were done only for gold coated coverslips. Three random measurements of cysteamine and poly-L-lysine layer were performed. The mean and standard errors of the measurements were than calculated to determine the average thickness of the respective layers.

Aim 1 & Task 3: Cell Culture

Cells from a rat pheochromocytoma (PC12) cell line were seeded and cultured in a stock dish and allowed to reach confluence in an undifferentiated state (without NGF) and were split every 3-4 days. These cells will differentiate into sympathetic-neuron like form when exposed to nerve growth factor (NGF) [86], thus neurite development in PC12 cells upon NGF exposure was investigated. Cells were cultured in RPMI-1640 culture medium (Sigma, St. Louis, MO)

supplemented with 10% horse serum (JRH Biosciences, Lenexa, KS), 5% fetal calf serum (Atlanta Biological, Norcross, GA), and 2% v/v penicillin-streptomycin (Sigma, St. Louis, MO). NGF (Alomone Laboratories, Jerusalem, Israel) at 100 ng/ml was added to elicit neurite growth in all experiments. NGF was added at the time of plating on substrates and at 48 hours when the culture media was changed. Cell cultures were maintained at 37° C in a humidified atmosphere of 5% CO_2 /95% air for four days in all experimental studies. Cells were counted using a hemacytometer before seeding them in all the experimental groups. A detailed method of counting cells using the hemacytometer is described in Appendix-C [87].

Cell Culture in Topography Studies: Cells were seeded in triplicates at a seeding density of 5,000 cells/cm^2 on all substrates for SEM and FM analysis of neurite development. The different types of substrates for both types of analysis were set up in parallel and maintained in the same culture dish and hence received the same culture conditions. Any differences in culture media, NGF addition and incubator conditions hence were not a factor that might influence the measured neurite development and cell density response after 4 days of culture. The cells were maintained in culture as mentioned in Aim 1 & Task 3 (Cell Culture).

Cell Culture in Mechanical Strain Studies: Cells were seeded in triplicates at a seeding density of 5,000 cells/cm^2 on smooth and micro-textured PDMS substrates in static (non-stretched) and dynamic (cyclic uniaxial stretch) setups for SEM and FM analysis of neurite development. Cells on smooth and micro-textured substrates in the static conditions were setup in parallel and maintained in the same culture dish. Cells on smooth and micro-textured substrates in the dynamic set ups were maintained in the cell stretcher chamber in a non-stretched state for 72 hours for reaching confluence, after which the cells were subjected to cyclic stretching for additional 24 hours. In the dynamic groups, a uniaxial strain at a level of either 4%, 8% or 16%

was applied under three different strain rates: 0.1Hz, 0.5Hz and 1.0Hz. Cell cultures in all groups were maintained for a total of 96 hours. Note that the experiments for the different setups and types of analysis were conducted sequentially using cells from increasing passage numbers. As only six increasing generation of the same cell population were used in these studies, no major influence of culture passages on growth kinetics, xenobiotic metabolism, chromosomal stability and transformation is expected. The cells were maintained in culture as mentioned in Aim 1 & Task 3 (Cell Culture).

Cell Stretching Apparatus: For mechanical stretching of the deformable substrates, a stretching apparatus was developed as shown in Figure 4. The apparatus consists of a DC motor (Oriental Motors, Torrance, CA.), a cam drive, and a culture chamber with a transparent lid for monitoring without risk of desiccation or contamination (Figure 4a). Inside the culture chamber there are two clamps for fastening the substrates: a fixed clamp and a mobile clamp that is attached to the cam piston. The apparatus is compact enough to be housed inside an incubator (Figure 4b) and an autoclave for sterilization.

The cell-stretching device used in this study was designed to provide controlled strain levels and strain rates. The BX series brushless DC speed control system offered high performance and simple operation from a compact driver and motor (Oriental Motors USA Corp., Torrance, CA). A movable pushing rod fixed above the eccentric disc follows the alteration of the radii and lifts and drops regularly during a revolution of the crank. The extent of the movement of the pushing rod corresponds to the stroke. So a cam in connection with a pushing rod transformed a rotary motion into a linear back and forth movement. This results in a simple harmonic motion which was used for the uniaxial stretching of the smooth and micro-textured PDMS membrane at different strain levels and strain rates.

(a)

(b)

Figure 4. Pictures of the cell stretching apparatus developed to deform flexible substrates. A close-up view of the apparatus (a) and a view of the apparatus placed in an incubator (b).

Aim 1 & Task 4: Cell Density Analysis

After 4 days of culture, cell density in all the setups and analysis was enumerated using areal count method in conjunction with trypan blue (Erythrosin B, Nigrosin) solution to count viable cells. Nuclei of damaged or dead cells take up the trypan blue stain and these apoptotic cells were not counted. The trypan blue solution was mixed 1:1 with the cell's cultures media solution and incubated for 5 minutes. An areal counting method was then performed under an inverted light microscope (Nikon Eclipse ME600, Nikon Inc., Melville, NY) by counting the total number of adherent viable cells in three randomly chosen microscopic fields (with the same area of 1.0 mm^2) in each replicate for all the setups and analysis. After having determined the cell count, the cultures were washed twice with PBS and prepared for neurite development analysis by SEM and FM.

Aim 1 & Task 5: Neurite Development Analysis

Scanning Electron Microscope (SEM): Scanning electron microscope (SEM) (LEO 982 FESEM, Leo Electron Microscopy Inc., Thornwood, NY) was used for the quantitative characterization of cellular morphology such as neurite length, neurite density and angle of neurite orientation (in mechanical strain studies). SEM was useful in distinguishing very detailed 3-D images at much higher magnifications than is possible with a light microscope. SEM images have a great depth of field permitted a large amount of the sample to focus at one time. A procedure for preparation of biological specimens for SEM analysis is described here.

After 96 hours of culture, cells were fixed in 0.25% glutaraldehyde and 4% formaldehyde. The fixed cells were examined by scanning electron microscopy (SEM) for quantitative characterization of cell development such as neurite length, neurite density and

angle of neurite orientation. To prepare cells for SEM analysis, cells with substrates were immersed in 1% osmium tetroxide (OsO4) for 15 minutes, washed in buffered solution, and dehydrated by successive immersion in 10%, 30%, 50%, 70%, 90% and 100% ethanol for five minutes each. Subsequently, cells with substrates were dried in a critical point drier (Samdri model 780-A, Tousimis Research, Rockville, MD). Prior to SEM analysis, a thin layer of gold (about 14 nm) was sputter-coated (Structure Probe Inc., West Chester, PA) on the cells. Quantitative characterization of the neurite morphology (neurite length, neurite density and angle of neurite orientation) for PC12 cells in all experimental groups was performed based on the SEM images.

Fluorescent Microscopy (FM): An upright Fluorescence microscope (Zeiss Axioskop 40, Carl Zeiss Inc., Thornwood, NY) was used to image and characterize the structural proteins, actin and microtubule filaments in the developing neurites. Immuno-fluorescent imaging of biological specimens is an important tool in the analysis of intracellular epitopes. The co-staining of these structural proteins helps discern the cytoskeletal morphology of neurites and filopodia as they stand out very well against the dark background. The actin bundling and microtubule assembly in extending neurites can be used to explain neurite development in response to different types of substrate topographies and strain conditions. This form of microscopy was especially useful in lending support to the quantitative analysis of neurite development under SEM analysis.

The fluorescent analysis of neurite development was done after four days of culture by fixing the cells in 3.7% formaldehyde for 30 minutes in the dark and co-staining the cultures for actin and microtubule specific antibodies. The fixed cells were washed twice in phosphate buffer solution (PBS) and then treated with a 0.1% Triton X-100 in PBS for 10 min (to permeabilize the cell membrane) followed by two PBS washes. The permeabilized cells were then stained for

actin with rhodamine phallodin (Sigma, St. Louis, MO) and tubulin with anti-tubulin (DM1a, Sigma, St. Louis, MO) by diluting at 1:200 in PBS and at 1:100 in PBS, respectively. The stained cultures were then swirled to evenly distribute the contents and kept in the dark at room temperature for 20 minutes (to incubate the antibodies). The specimens were then washed again twice in PBS and the microtubule specific secondary antibody, fluorescein isothiocyanate (FITC) goat anti-mouse antibody (Sigma, St. Louis, MO) diluted at 1/100 in PBS was added to the cultures. The cultures were swirled and kept in the dark at room temperature for 30 minutes to incubate the secondary antibody. The stained cells on the substrates were then prepared for fluorescent microscopy analysis by covering with a coverslip using a 1:1 mounting solution of PBS and glycerol. The coverslips were sealed by paraffin to prevent desiccation of the mounted cells. The cells were observed using fluorescent microscopy (Zeiss Axioskop 40, Carl Zeiss Inc., Thornwood, NY). The stained tubulin and actin were observed using fluorescein (488 nm excitation and 510-520 nm emission wavelength) and rhodamine (546 nm excitation and 560-580 nm emission wavelength) respectively. Quantitative characterization of the neurite morphology (neurite length, and neurite density) for PC12 cells in all experimental groups was performed based on the FM images.

Aim 2: Plating Efficiency

A separate setup was used to determine the plating efficiency of PC12 cells on different types of substrates. The cells were seeded in triplicates and at the same seeding cell density as mentioned in Aim 1 & Task 3 (at 5,000 cells/cm^2). The cell count of adherent viable cells was performed six hours after cell seeding by staining the cultures with trpyan blue (as mentioned in Aim 1 & Task 4, Cell Density Analysis) and using the areal count method under an optical

microscope (Nikon TE 300, Nikon Inc., Melville, NY). Apoptotic and damaged cells that took up the blue stain were not included in the count. The trypan blue solution was added in a 1:1 with the cell's cultures media solution and incubated for 5 minutes. The number of adherent viable cells was then counted on all types of substrates in randomly chosen microscopic fields (with the same area of 1.0 mm^2) per replicate in all types of substrates. After that the percentage of the adhered viable cells out of the total plated cells was calculated as the plating efficiency.

Aim 3 & Task 1: Quantifying Neurite Development and Cell Density

To quantify the neurite development and cell density of the cells subjected to the experimental conditions, the neurite length, neurite density (number of neurites per cell) and cell count in each setup were measured. The neurite length and neurite density of PC12 cells on all types of substrates were measured and served as a quantitative analysis of neurite development both by SEM and FM. Only cells that had neurites were measured. A total of 60 cells were counted in each group (20 from each replicate). Manual tracing method was used to measure the neurite lengths. To do that the length of the scale bar specifying the scale (in microns) of the field of view was first measured in millimeters using a ruler and the corresponding conversion factor was determined. Then the respective neurite lengths were measured in millimeters and converted back to microns using the calculated conversion factor. Neurite lengths were measured from their base along the usually curved neurites to the tip of the leading edge of growth cones. Neurite density was counted as the number of neurites extending from a single cell body. Cell density in all the setups was enumerated using an areal counting method under a light microscope (Nikon Eclipse ME600, Nikon Inc., Melville, NY) by counting the total number of

cells in three randomly chosen microscopic fields in each replicate for all setups and analysis. Cell multiplication was used as a measure of cell density.

In topographical studies, the number of filopodia per cell was counted and its correlation with neurite density in cells on substrates with different size and shape features was determined from a total of 60 cells in the triplicate setups for the SEM analysis. In mechanical strain studies, the neurite orientation response to dynamic uniaxial strain was also measured from a total of 60 cells in each group (20 from each replicate). The angle of neurite orientation was measured manually from the SEM images using a protractor having 0°-180° divisions. The angle of neurite orientation was taken as the angle between the secant line from the root to the tip of a neurite extension and the direction of the applied strain (dynamic setups) and randomly marked axis (static setups). The measured angles were grouped into three angular ranges: 0°-30°, 31°-60° and 61°-90° and the percentage of neurites aligning in a particular angular range was calculated. Also, in the mechanical strain studies, the product of the applied strain level and strain rate was defined as mechanical energy and it was used to determine its effect on neurite length and neurite density. The relationship between the development of the length and number of neurites and the mechanical energy was determined.

Aim 3 & Task 2: Statistical Analysis

Statistical means and standard errors for the dimensions of the substrate topography features were calculated based on three random readings. The statistical means and standard errors for plating efficiency of cells on different types of substrates was calculated based on the data from the triplicate culture setups. Regular two-sample *t*-tests were performed for the

difference in plating efficiency and a *p*-value of less than 0.05 was considered to be significantly different.

Statistical Analysis in Topography Studies: Statistical means and standard errors for the neurite length, neurite density, and cell density were calculated based on the data obtained from the triplicate cultures setups. Weighted two-sample *t*-tests were performed to determine the statistical difference between types of substrates for the neurite length and neurite density because these measurements were concomitant variables with uneven number of samples. The enumerated cell densities for each type of substrate from the SEM and FM analysis were pooled together for statistical analysis. Regular two-sample *t*-tests were performed for the difference in cell density. A *p*-value of less than 0.05 was considered to be significantly different.

A correlation between the number of filopodia and neurites was performed by analyzing the correlation coefficient (R). The R value was determined using Excel as the strength of the linear association between the number of neurites and the number of filopodia. The degree of correlation between two variables was found by comparing the sum of the products of the deviations of the two distributions; i.e. with a measure that combines the sum of squared deviations of the development of the length and the number of neurites distribution and the mechanical energy distribution. The result was a ratio that is a statistical measure called the correlation coefficient. Correlation coefficients range from -1.00 to +1.00. The value of -1.00 represents a perfect negative correlation while a value of +1.00 represents a perfect positive correlation. A value of 0.00 represents a lack of correlation. The statistical significance of the R value was also calculated to determine whether the results obtained are due to the variables being studied and not due to chance. The statistical significance was determined by comparing the

critical value of R from the Pearson-R-Table (p = 0.05) with the calculated value of R. If the calculated value is higher than the tabulated value, R is considered statistically significant.

Statistical Analysis in Mechanical Strain Studies: A 3-factorial design (4×4×2) was used with three fixed effects: strain level (static, 4%, 8% and 16%), strain rate (static, 0.1Hz, 0.5Hz and 1.0Hz) and topography (smooth and micro-textured). Statistical means and standard errors for the neurite length, neurite density, cell density, and percentage of neurites aligning in a particular angular range were then calculated based on the data from the triplicate cultures setups. Note, unlike the topography studies the experiments in mechanical strain studies were set up separately for the SEM and FM analysis. Hence, the cell density readings for the different setup in the SEM and FM analysis were enumerated and are reported separately. Also, the percentage of neurites aligning in a particular angular range was only measured from the triplicate culture setup for SEM analysis.

Comparisons were made between cells on smooth and micro-textured substrates at each strain condition to determine the combined effect of applied strain and topography and the combined effect of strain level and strain rate on neurite development. Note that for the data analysis, a series of images from each condition to determine neurite numbers and lengths were used. The relatively large number of cells in our data analysis provided us with a statistically valid way to quantify the differences in neurite development. But due to limited space, only a few representative images are shown here. Tukey tests were performed to compare the different groups with a p-value <0.05 being considered as statistically different. Tukey tests allow for comparisons of unequal samples as the responses were concomitant variables with uneven number of samples. Statistical analysis system (SAS) software was used to perform statistical

analysis. A correlation between the development of the length and number of neurites and the mechanical energy was performed by analyzing the correlation coefficient (R).

Aim 4: Biochemical Assay

The biochemical assay was performed to determine the differentiated state of the neurons for cells on nano-, micro- and smooth substrates. The acetylcholinesterase assay measured the level of acetylcholinesterase (AChE), which has been reported to increase on differentiation of PC12. To investigate the state of cell differentiation in PC12 cells, another set of cultures with nano-, micro- (shallow micro-substrate) and smooth substrates was setup. The cells were seeded in triplicates and at the same seeding cell density and as mentioned in Aim 1 & Task 3 (at 5,000 cells/cm^2). All the setups were cultured and maintained under identical culture conditions as mentioned in Aim 1 & Task 3.

After 4 days of culture, an acetylcholinesterase assay based on Ellman's method [88] was performed to cells removed from the substrates by trypsin-EDTA (Sigma-Aldrich Corp., St. Louis, MO). 10,000 cells/ml pooled together from the triplicates from each type of substrate were used in the biochemical assay. For the enzyme source, PC12 cell cultures were homogenized in a homogenation buffer 910 mM Tris-HCl (pH 7.2), which contained 1 M NaCl, 50 mM $MgCl_2$ and 1% Triton X-1000 and centrifuged at 10,000 ´ g for 30 minutes. The resulting supernatant was used as an enzyme source. All of the extraction steps were carried out at 4°C.

Acetylcholinesterase enzyme concentration was determined using a colorimetric assay kit (ADVIA Chemistry Systems, Bayer Corp., Tarrytown, NY) based on the hydrolysis of acetylthiocholine iodide (ATChI) to thiocholine and acetate (Eq. 1) by AChE. The thiocholine then reacted with dithiobisnitrobenzoate (DTNB) to produce a yellow color (Eq. 2). The quantity

of yellow color which develops over time is a measure of the activity of AChE and the differentiated state of the neurons and was measured using a spectrophotometer at a wavelength of 412 nm. Absorbance was read immediately after adding an Ellman's reaction mixture [70 ml; 0.5 mM acetylthiocholine, 1 mM 5, 5-dithio-bis (2-nitro benzoic acid)] in a 50 mM sodium phosphate buffer (pH 8.0) to the above reaction mixture. Readings were monitored for 90 seconds at 20 second intervals to verify that the reaction had reached completion (plateau region). A reference setup with no cells was used as a negative control and measured by substituting saline solution for the enzyme.

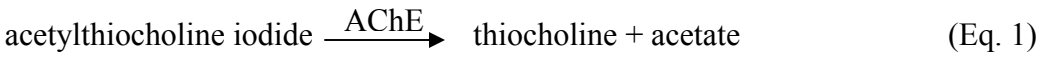

(Eq. 1)

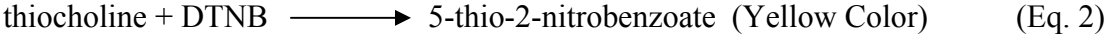

(Eq. 2)

CHAPTER 5

RESULTS AND DISCUSSION

Effect of Size and Shape of the Substrate Topography Feature on Neurite Development

Characterizing Cell Morphology Response to Substrate Topography. First the dimensions of the different types of substrate topography features were characterized. Then the cell morphology on these different types of substrates was characterized both by SEM and FM. Specifically, by comparing neurite development on nano and micro-structured substrates and on nanopillars and nanopores substrates.

Figure 5 shows images of the different size substrate topographies on silicon wafers. A SEM image of the nano-featured substrate with dimensions of 890±43 nm in height, 103±14 nm in diameter and 131±20 nm in separation is shown in Figure 5a (nano-substrate). A top-view stereo-microscope image of a micro-substrate with dimensions of 4.0±0.5 μm in height, 5.0±0.6 μm in diameter, and 40.0±1.7 μm in separation is shown in Figure 5b (high micro-substrate). A top-view stereo-microscope image of a micro-substrate with dimensions of 1.5±0.2 μm in height, 15.0±0.8 μm in diameter, and 30.0±0.9 μm in separation is shown in Figure 5c (shallow micro-substrate). Figure 6 shows SEM images of different nano-featured substrate topographies. A top-view of the nanopillars substrate along with a cross-section view in the inset is shown in Figure 6a. The nanopillars had dimensions of 229±28 nm in diameter, 69±32 nm in separation and 2123±84 nm in height. A top-view of the nanopore substrates with the cross-sectional view in the inset is shown in Figure 6b. The pores had dimensions of 206±42 nm in diameter and 41±17 nm in separation. The pores are through holes approximately 35 μm deep.

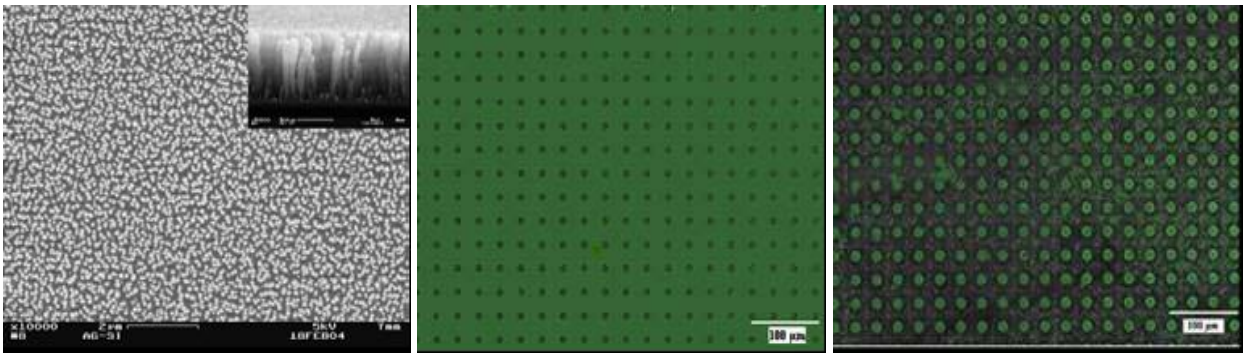

(a) (b) (c)

Figure 5. Images show the different size substrate topographies on silicon wafers. A top-view of: (a) a SEM image of a nano-substrate with standing silicon nano-pillar arrays and a cross-section view is shown in the inset; (b) stereo-microscopic image of micro-substrates with an arrays of higher micro-islands (4.0 μm in height); (c) stereo-microscopic image of micro-substrates with an arrays of shallow micro-islands (1.5 μm in height).

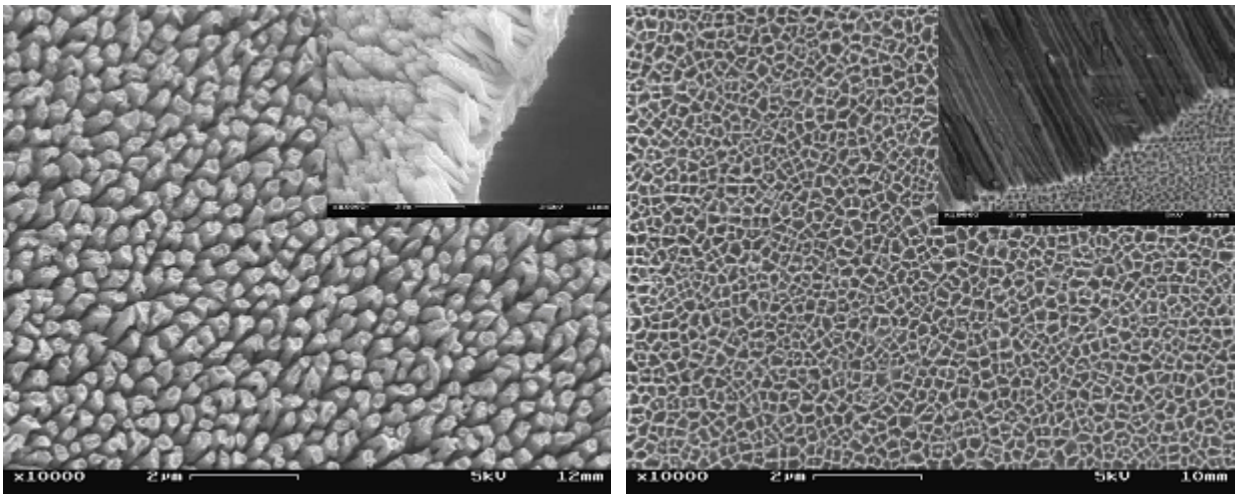

(a) (b)

Figure 6. SEM images of nano-featured substrates. A top-view along with a cross-section view of the nano-featured substrate with nanopillars (a) and nanopores (b) is shown.

In Figure 7, four SEM images of PC12 cells cultured on nano-, high micro-, shallow micro- and smooth substrates, respectively, are given. Figure 7a shows a dense culture on nano-substrates, Figure 7b and 7c shows cells on high and shallow micro-substrates, and Figure 7d shows cells on a smooth substrate. The cells on nano-substrate had shorter and fewer neurites compared to smooth substrates. As compared with cells on smooth substrates, cells on both micro-substrates had longer and multiple neurites. In Figure 8, four SEM image, at a higher magnification, of cells on nano-, high micro-, shallow micro- and smooth substrates, respectively, are shown. The cell on nano-substrate (Figure 8a) had numerous filopodia all around the cell body without any active lamellopodia following them, and the cell body was well spread and had an amoeboid-like shape. The cells on high micro-substrate (Figure 8b) and shallow micro-substrate (Figure 8c) had only a few filopodia at the tip of the extending neurite. Smooth substrate (Figure 8d) had only few filopodia around the cell body and at the tip of the extending neurite.

Figure 9 shows four SEM images of PC12 cells cultured on four different types of substrates. Figure 9a shows a dense culture of cells on nanopillars with short and few neurites per cell, Figure 9b shows cells cultured on nanopores with intermediate length and number of neurites per cell, and Figures 9c and 9d show cells on gold coated coverslips and bare coverslips with long and multiple neurites per cell. Figure 10 shows four SEM images at a higher magnification, of cells on different types of substrates. Figure 10a and 10b shows filopodia interactions with the nano-pillared and nanoporous substrate, respectively. Figure 10c and 10d shows filopodia interactions with the gold coated coverslips and bare coverslips, respectively.

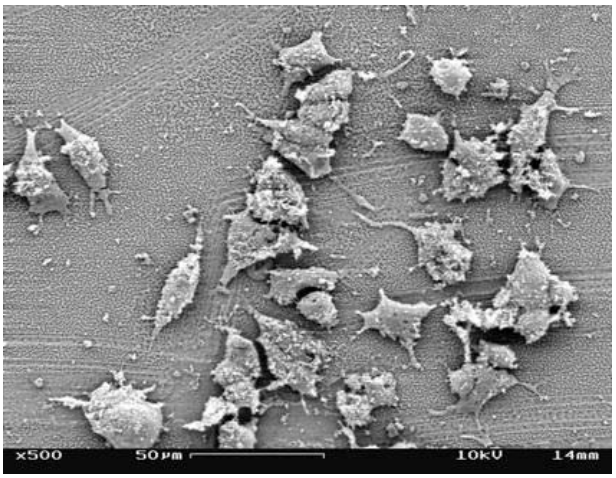

(a)

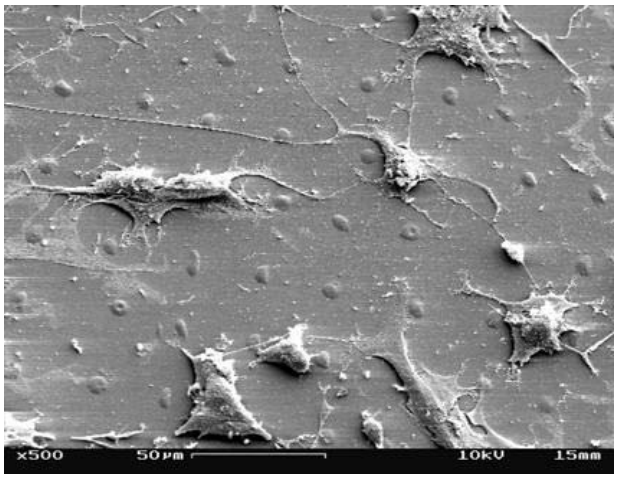

(b)

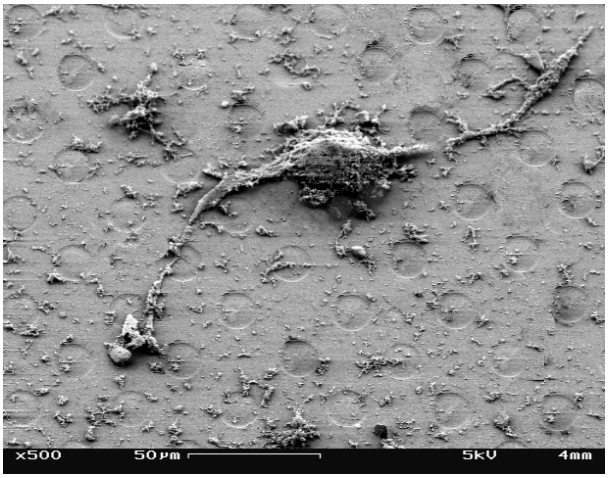

(c)

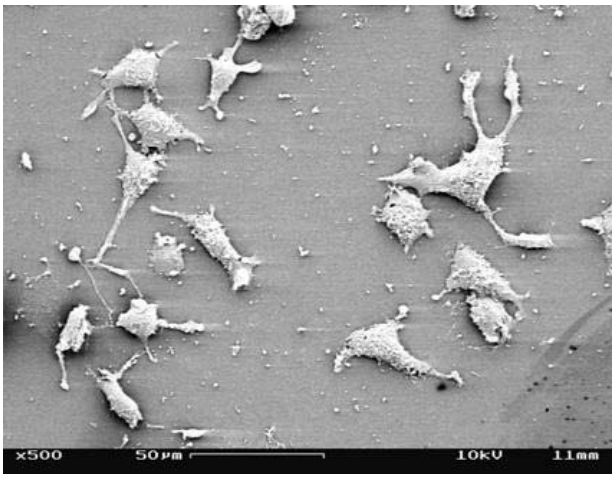

(d)

Figure 7. SEM images of cells cultured on substrates with different size topographic features. Cells cultured on: (a) nano-substrates had a relatively dense culture and cells with short and few neurites; (b) high micro-substrates had long and multiple neurites; (c) shallow micro-substrates also had long and multiple neurites; (d) smooth substrates had intermediate length and number of neurites.

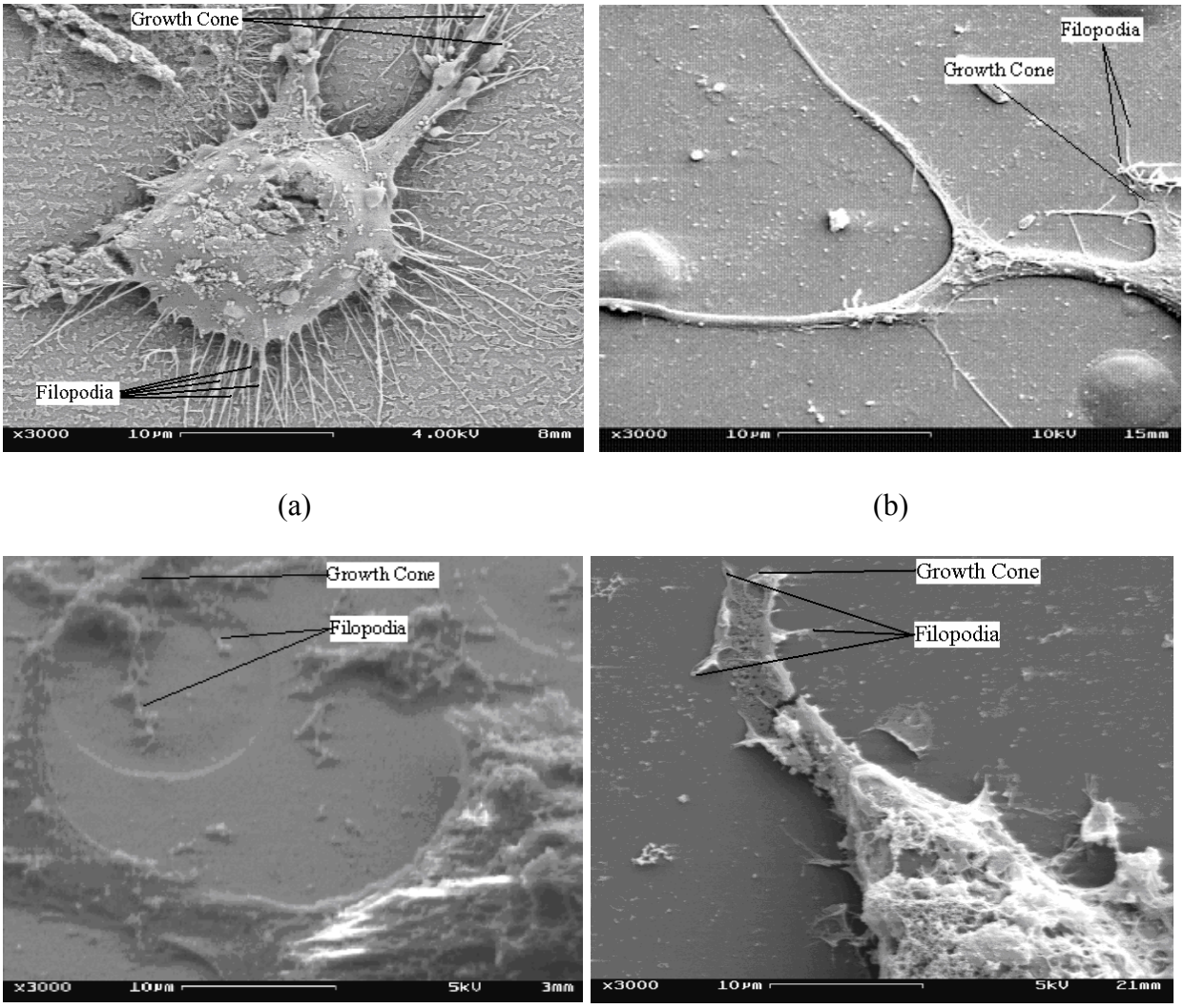

Figure 8. A higher magnification SEM images of cells cultured on substrates with different size topographic features. Cell on: (a) nano-substrate had numerous filopodia all around the cell body; (b) high micro-substrate had a few filopodia mostly concentrated at the tip of the growth cone; (c) shallow micro-substrate also had a few filopodia mostly concentrated at the tip of the growth cone; (d) smooth substrate had a few filopodia around the cell body and growth cone.

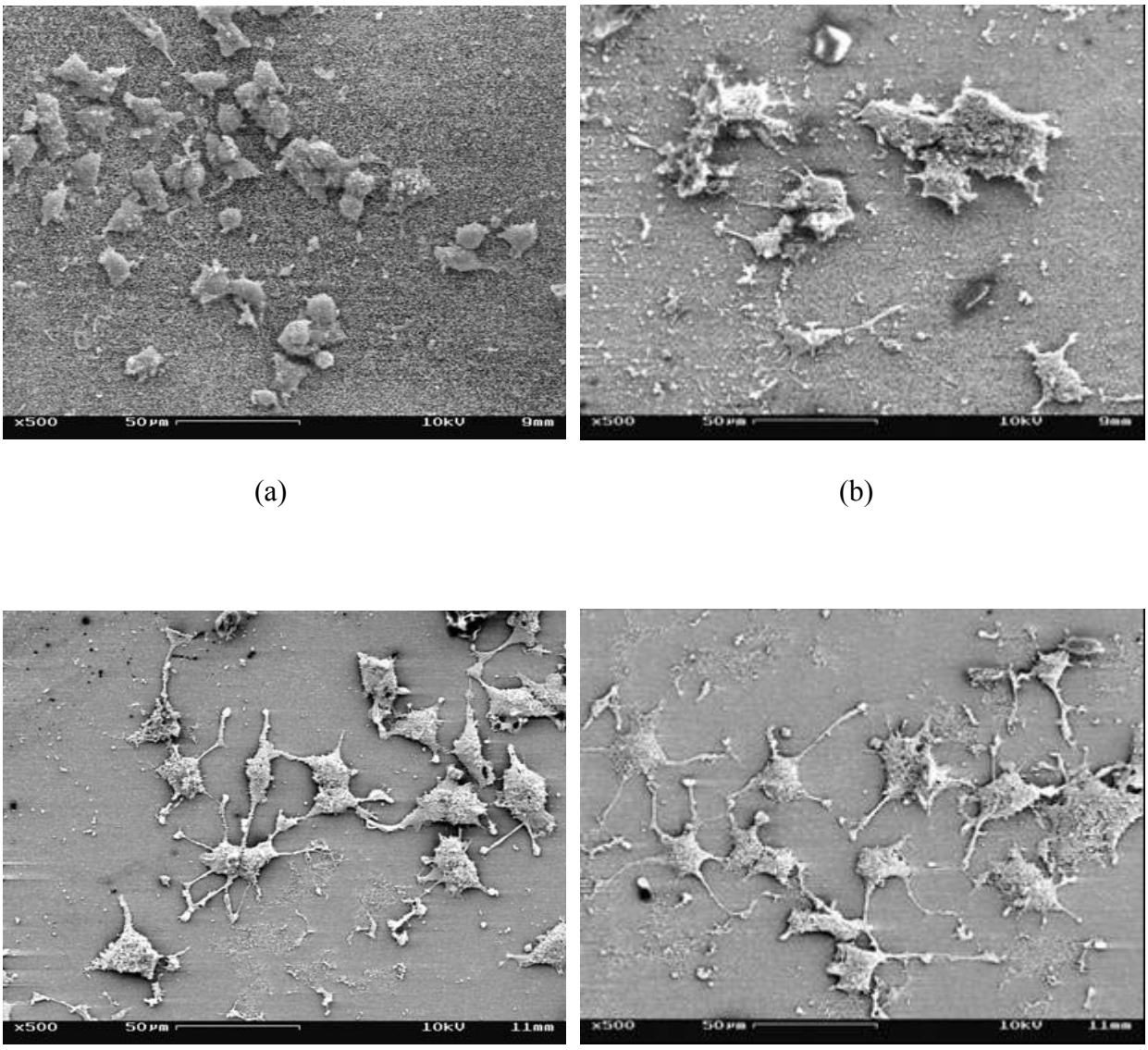

(a) (b)

(c) (d)

Figure 9. SEM images of cells cultured on substrates with different shape topographic features. Cells cultured on: (a) nanopillars had short and few neurites and these cells had a relatively high cell density; (b) nanopores had intermediate length and number of neurites; (c) gold coated coverslips had long and multiple neurites; (d) bare coverslips also had long and multiple neurites.

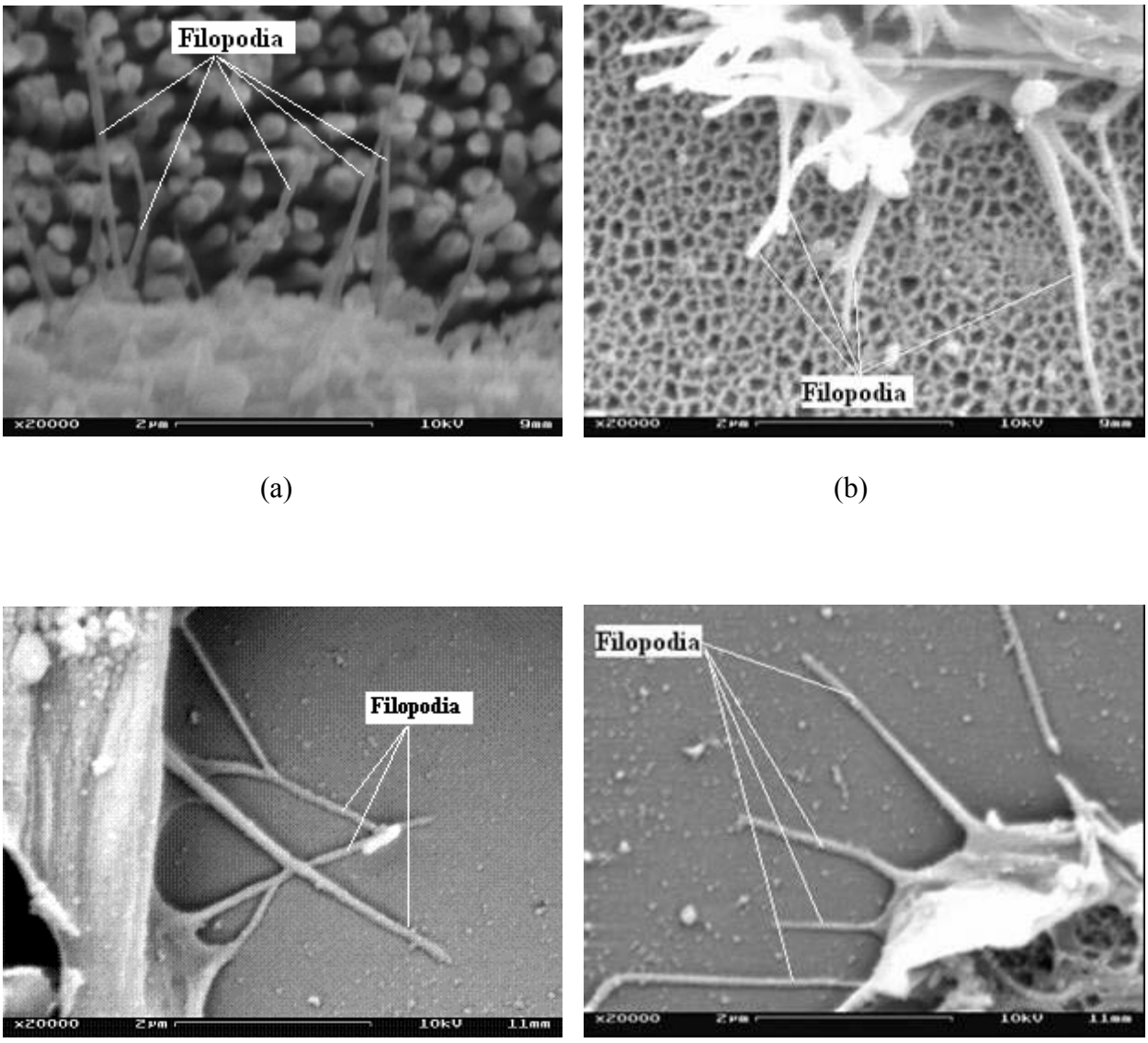

Figure 10. A higher magnification SEM images of cells cultured on substrates with different shape topographic features. Cell on: (a) nanopillars interacted with the nano-pillared substrate through the tip of the filopodia; (b) nanopores interacted with the nanoporous substrate through the tip of the filopodia; (c) gold coated coverslips interacted with the substrate through flat lying filopodia; (d) bare coverslips interacted with the substrate through flat lying filopodia.

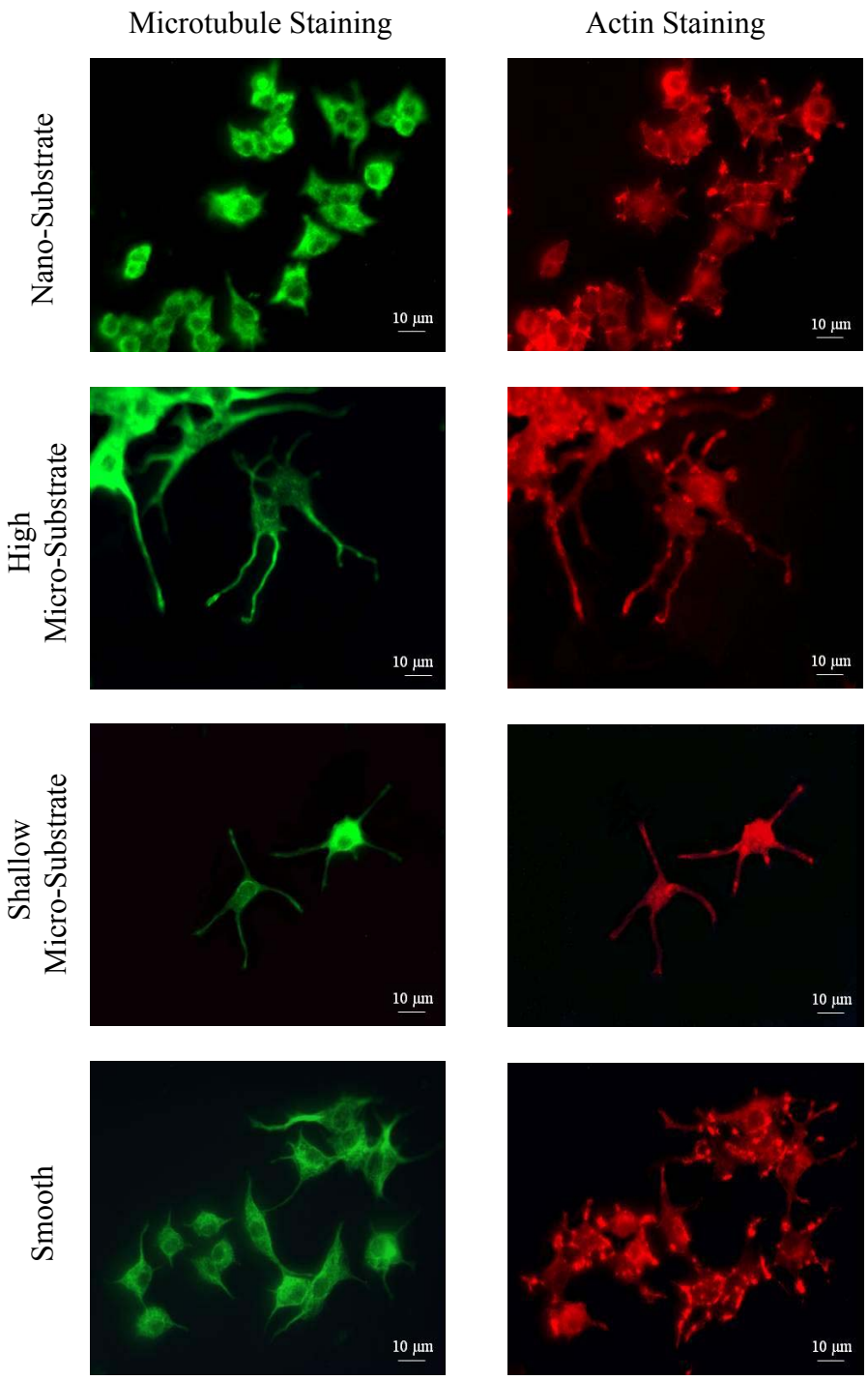

Figure 11. Fluorescent images of stained microtubules and actin in PC12 cells cultured on substrates with different size topographic features. Cells cultured on nano-substrates had a few and short neurites. Cells cultured on high micro-substrates had longer and multiple neurites. Cells cultured on shallow micro-substrates also had longer and multiple neurites. Cells cultured on smooth substrates had intermediate length and number of neurites.

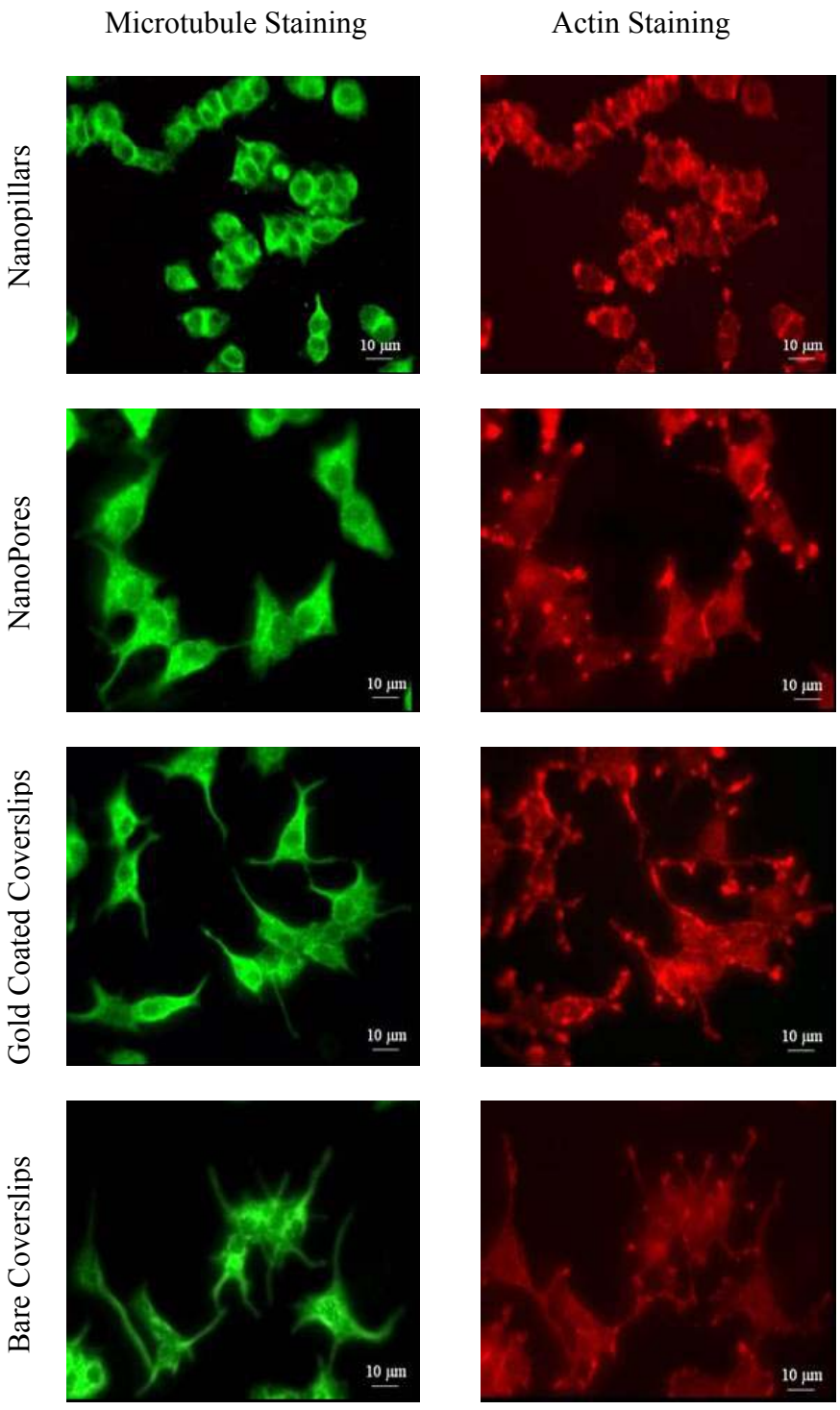

Figure 12. Fluorescent images of stained microtubules and actin in PC12 cells cultured on substrates with different shape topographic features. Cells cultured on nanopillars had a dense culture and these cells had few short neurites per cell. Cells cultured on nanopores had neurites of intermediate length and neurite density. Cells cultured on gold coated coverslips had longer and multiple neurites. Cells cultured on bare coverslips also had longer and multiple neurites.

The SEM analysis of cells on different types of substrates shows that the shape of growth cones is different on nano and micro-featured from that on smooth substrates. The growth cones of cells on smooth substrates were spread out and had ruffled lamellopodia (leading edge). The growth cones of cells on substrates with nanopillars, nanopores and micro-islands were bi-furcated (branched). Changes in growth cone morphology on patterned substrate topography have also been reported by others. Clark et al. [89] observed that growth cones of mice dorsal root ganglion neurons on smooth substrates were wide with lamellar structures while that on laminin patterned micro tracks (4-50 μm) had narrower growth cone and lamellopodia. These findings support our results in that substrate topography affects the shape of the growth cones. These differences in the shape of the growth cone could lead to different responses in neurite development [89].

Figure 11 shows the fluorescent images of the microtubule and actin co-staining in PC12 cells seeded on substrates with different size topographic features. Cells on nano-substrates (Figure 11a) had short and few neurites per cell. The morphology of the neurites on both the micro-substrates was totally different from that observed on nano-substrates Cells on high micro-substrates (Figure 11b) and shallow micro-substrates (Figure 11c) had long and multiple neurites per cell. Cells on smooth-substrate (Figure 11d) had intermediate length and number of neurites per cell. Figure 12 shows the fluorescent images of the actin and microtubule co-staining in PC12 cells seeded on substrates with different shape topographic features. Cells cultured on nanopillars (Figure 12a) had short and few neurites per cell, while cells cultured on nanopores (Figure 12b) had intermediate length and number of neurites. Cells cultured on gold coated coverslips (Figure 12c) and bare coverslips (Figure 12d) had long and multiple neurites per cell.

A similar trend was observed for the neurite development in cells on different types of substrates when comparing between SEM and FM analyses. Pillars on the nano-substrates with dimensions (103 nm in diameter and 131 nm in separation) comparable to those of filopodia (100-120 nm in diameter) inhibited neurite development in PC12 cells. By contrast, islands on the high micro-substrates (5 μm in diameter and 40 μm in separation) and shallow micro-substrates (15 μm in diameter and 30 μm in separation) with dimensions comparable to neuron cell-body (10-20 μm in diameter) and neurites (1-5 μm in thickness) promoted neurite development in PC12 cells. It is possible that these patterned islands offer the cells a 3D environment for neurite development by initiating an enhanced cell spreading and attachment over these dome-shaped islands. Nanopillars with dimensions (229±28 nm in diameter and 69±32 nm in separation) comparable to those of filopodia (100-120 nm in diameter) inhibited neurite outgrowth in PC12 cells. By contrast, nanopores with similar dimensions (206±42 μm in diameter and 41±17 μm in separation) promoted longer and multiple neurites in PC12 cells. However, the gold coated coverslips and bare coverslips enhanced neurite development the most.

Determining the Plating Efficiency on Different Types of Substrates. The plating efficiency of cells on different types of substrates was calculated as the percentage of the adhered viable cells out of the total plated cells six hours after seeding using the trypan blue assay. The means and standard errors of the percentage plating efficiency were calculated and comparisons were made between the plating efficiency on different types of substrates. Specifically, comparisons were made between the plating efficiency on nano-, high micro-, shallow micro- and smooth substrates and between the nanopillars, nanopores, gold coated coverslips and bare coverslips. Figure 13 shows the plating efficiency of cells on different types of substrates. Figure 13a, shows

the mean plating efficiency was 86.3±2.9%, 90.5±3.3%, 88.0±2.6%and 87.0±2.6% for nano-, high micro-, shallow micro- and smooth substrates, respectively. Figure 13b, shows the mean plating efficiency was 83.4±2.2%, 85.8±2.0%, 86.9±2.4% and 90.1±2.5% for cells on nanopillars, nanopores, gold coated coverslips and bare coverslips, respectively. The plating efficiency was very high (>80%) on all types of substrates. Furthermore there was no significant difference in the plating efficiency on different types of substrates. These findings suggest that cell adhesion was not a significant contributing factor to the differences observed in neurite development and cell density on different types of substrates.

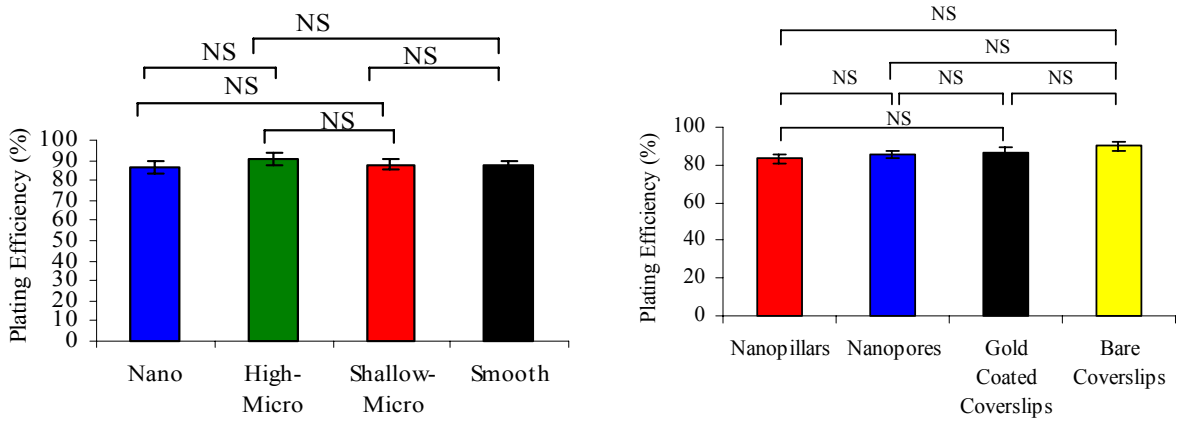

(a) (b)

Figure 13. Bar graphs show the mean plating efficiency of cells on different types of substrates. Plating efficiency on: (a) substrates with different size topographic features; (b) substrates with different shape topographic features. NS = Not Significant.

Quantification of Neurite Development and Cell Density. To perform a quantitative analysis of neurite development the number of neurites was counted and their lengths were measured in each of the 60 cells from three replicates for each type of substrate from both types of analyses. With all the measurements pooled together from the triplicate cultures for each type of substrate,

the means and standard errors of the neurite length and neurite density for each type of substrate were calculated. Comparisons were made between the neurite length and neurite density on different types of substrates to determine neurite development. To perform the quantitative analysis of cell density, three random counts of cells in 1 mm^2 area from three replicates for each type of substrate in both analyses were taken. With all the measurements pooled together from the triplicate cultures for each type of substrate, the means and standard errors of the cell density for each type of substrate from both analyses were calculated. Comparisons were made between the cell counts on different types of substrates to determine cell density.

The quantitative analysis of neurite length, neurite density and cell density for cells on nano-, high micro-, shallow micro- and smooth substrates are shown in Figure 14. Figure 14a shows that the mean neurite length was 38.7±1.4 μm, 90.5±2.7 μm, 79.9±2.1 μm and 47.7±1.4 μm for cells on nano-, high micro-, shallow micro- and smooth substrates, respectively by SEM analysis. Similarly, the mean neurite density was 19.5±3.3 μm, 73.8±0.8 μm, 67.1±2.8 μm and 38.1±3.0 μm for cells on nano-, high micro-, shallow micro- and smooth substrates, respectively by FM analysis. A similar trend was found in the neurite lengths when comparing between the cells on the different types of substrates by both SEM and FM analysis. Comparing with cells on smooth substrates, cells on nano-substrates had significantly (#$p<0.05$) shorter neurites, while cells on high micro-substrates (@$p<0.05$) and shallow micro-substrates (*$p<0.05$) had significantly longer neurites. Cells on high micro-substrates had significantly ($p<0.05$) longer neurites as compared with cells on shallow micro-substrates.

Figure 14b shows that the mean neurite density was 2.8±0.1, 5.1±0.2, 4.5±0.1 and 3.4±0.1 (neurites/cell) for cells on nano-, high micro-, shallow micro- and smooth substrates, respectively by SEM analysis. Similarly, the mean neurite density was 2.8±0.1, 5.1±0.1, 4.7±0.1

and 3.8±0.1 (neurites/cell) for cells on nano, high-micro, shallow-micro and smooth substrates, respectively by FM analysis. A similar trend was observed in the neurite length when comparing between the cells on the different types of substrates by both SEM and FM analysis. In comparison with cells on smooth substrates, cells on nano-substrates had a significantly (#p<0.05) lower neurite density, while cells on high micro-substrates (@p<0.05) and shallow micro-substrates (*p<0.05) had significantly greater neurite density. Cells on high micro-substrates had significantly ($$p$<0.05) greater neurite density as compared with cells on shallow micro-substrates.

Figure 14c shows that the mean cell density was 20.9±0.7, 10.3±0.2, 11.7±0.3 and 16.3±0.3 ($\times 10^3$-cells/cm^2) for nano, high-micro, shallow-micro and smooth substrates, respectively after 4 days of culture. In comparison with cells on smooth substrates, cells on nano-substrates had significantly (#p<0.05) greater cell density, and cells on high micro-substrates (@p<0.05) and shallow micro-substrates (*p<0.05) had significantly lower cell density. Cells on high micro-substrates had significantly ($$p$<0.05) lower cell density as compared with cells on shallow micro-substrates.

The findings of this study address the objectives of the Research Question 1 by elucidating the effect of nano and micro-substrates on neurite development. Under an identical culture condition PC12 cells exhibited different activities on different types of substrates. On micro-substrates, cultures had a relatively low cell density but cells developed numerous long neurites. Interestingly, the comparison between the different types of micro-substrates revealed that the dimensions of the micro-islands had an effect on the neurite development in PC12 cells. Cells on high micro-substrates (4.0 μm height) had longer and multiple neurites as compared with cells on shallow micro-substrates (1.5 μm height). This suggests that even within the same

scale range (micron) differences in feature dimensions can have a significant effect on neurite development. On nano-substrates, cultures had a significantly high cell density and cells developed a large number of filopodia. But these cells had short neurite extensions, suggesting that the nano-substrates inhibit the conversion of filopodia into neurites, or there is an increase in cell proliferation which increases cell density, which leads to altered cell morphology.

That cells cultured on nano-featured substrates developed a large number of filopodia was also reported by others. With fibroblast cells cultured on nano-featured substrates, Dalby et. al. [36] observed a similar development of extensive filopodia around the cells. They attributed this phenomenon to that cells were spatially aware of their nano-featured surroundings, and that the cells may be actively preparing for their down-stream activities. For a cell, the main function of filopodia is to probe the physical and chemical environments of its surrounding for attachment and growth purpose [90]. In the case of PC12 cells, extension of filopodia is a key up-stream event for guiding the formation of growth cones in extending neurites. Thus the development of such a large number of filopodia in cells cultured on nano-substrates is clearly a sign that the cells are spatially aware of their nano featured surroundings. But in terms of down-stream neurite outgrowth activities, the parallel study with both the nano-substrates and micro-substrates suggests that filopodia extensions do not necessarily lead to neurite outgrowth. Based on the fact that cells on micro-substrates had exhibited significant neurite outgrowth under the same culture condition and duration, I speculate that the cells on nano-substrates may be still busy probing and sensing their surroundings. It is possible that the small diameter and spacing of the vertically aligned nanopillars in these nano-substrates may impose certain difficulty for filopodia as well as lamellopodia to move about for guiding neurite outgrowth, thus leading to the inhibition of differentiation and enhancement of proliferation.

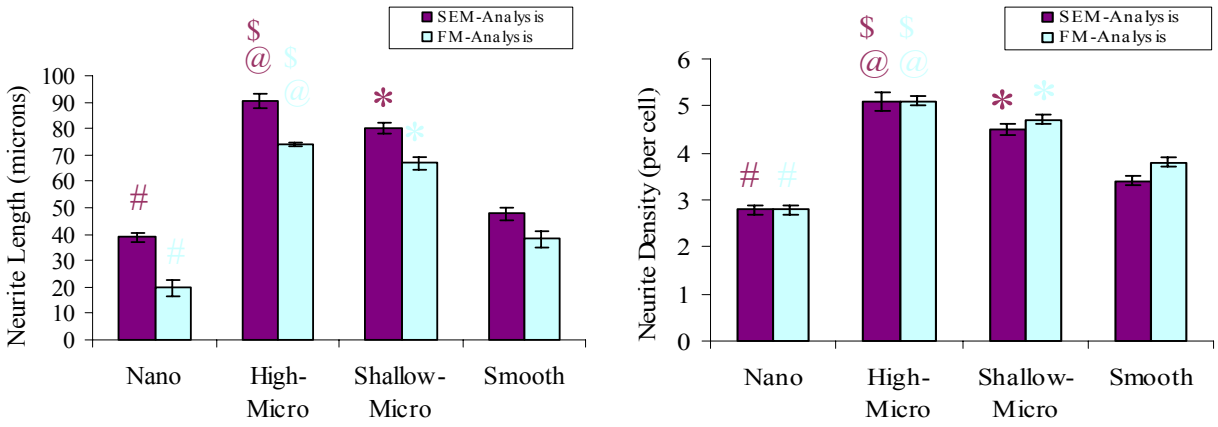

(a) (b)

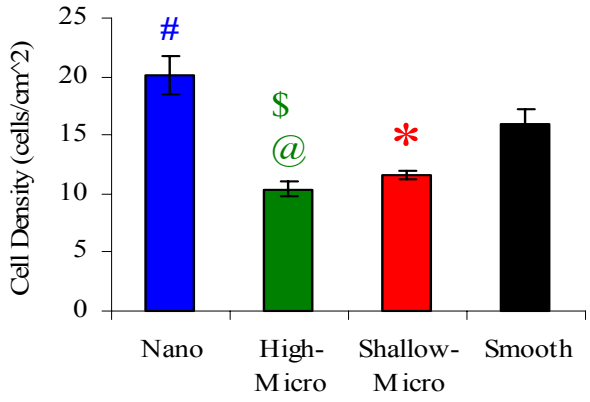

(c)

Figure 14. Bar graphs show the quantitative analysis of different cellular activities on substrates with different size topographic features. The mean: (a) neurite length; (b) neurite density; (c) cell density. Values reported are mean ± standard error; n = 3; # $p < 0.05$ (nano-substrates compared with smooth substrates), @$p < 0.05$ (high micro-substrates compared with smooth substrates), *$p < 0.05$ (shallow micro-substrates compared with smooth substrates), \$$p < 0.05$ (high micro-substrates compared with shallow micro-substrates); NS = Not Significant.

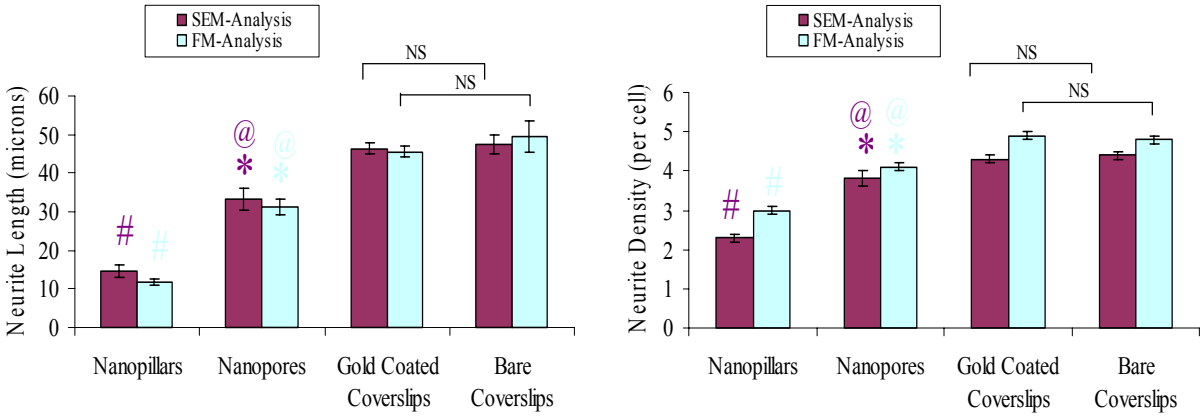

(a)

(b)

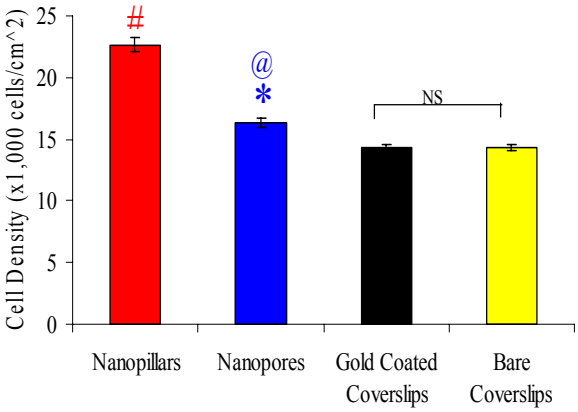

(c)

Figure 15. Bar graphs show the quantitative analysis of different cellular activities on substrates with different shape topographic features. The mean: (a) neurite length (b) neurite density (c) cell density. Values reported are mean ± standard error; $n = 3$; # $p < 0.05$ (nanopillars compared with controls); *$p < 0.05$ (nanopores compared with controls); @$p < 0.05$ (nanopores compared with nanopillars); NS = Not Significant.

In Figure 15, three bar graphs of different cellular activities on nanopillars, nanopores, gold coated coverslips and bare coverslips are shown. As shown in Figure 15a, the mean neurite length was determined to be 14.5±1.6 μm, 33.2±2.9 μm, 46.3±1.5 μm and 47.4±2.5 μm for cells on nanopillars, nanopores, gold coated coverslips and bare coverslips, respectively by SEM analysis. Similarly, the mean neurite density was 11.9±0.8 μm, 31.3±2.1 μm, 45.5±1.4 μm and 49.4±4.0 μm for cells on nanopillars, nanopores, gold coated coverslips and bare coverslips, respectively by FM analysis. Cells on nanopillars (#p<0.05) and nanopores (*p<0.05) had significantly shorter neurites as compared with cells on smooth coverslips in both analyses. Furthermore, cells on nanopores (@p<0.05) had significantly longer neurites as compared with cells on nanopillars in both analyses. There was no significant (NS) difference in neurite length between the cells on gold coated and bare coverslips in both analyses.

As shown in Figure 15b, the mean neurite density was 2.3±0.1, 3.8±0.2, 4.3±0.1 and 4.4±0.1 (neurites/cell) for cells on nanopillars, nanopores, gold coated coverslips and bare coverslips, respectively by SEM analysis. Similarly, the mean neurite density was 3.0±0.1, 4.1±0.1, 4.9±0.1 and 4.8±0.1 (neurites/cell), for cells on nanopillars, nanopores, gold coated coverslips and bare coverslips, respectively by FM analysis. Cells on nanopillars (#p<0.05) and nanopores (*p<0.05) had significantly fewer neurites per cell as compared with cells on smooth coverslips in both analyses. Furthermore, cells on nanopores (@p<0.05) had significantly greater number of neurites per cell as compared with cells on nanopillars in both analyses. There was no significant (NS) difference in number of neurites per cell between the cells on gold coated coverslips and bare coverslips in both analyses.

As shown in Figure 15c, the mean cell density was 22.6±0.6, 16.4±0.4, 14.3±0.3 and 14.3±0.3 ($\times 10^3$-cells/cm^2) for cells on nanopillars, nanopores, gold coated coverslips and bare

coverslips, respectively (note that cells were seeded at a density of 5,000 cells/cm^2). Cells on nanopillars (#p<0.05) and nanopores (*p<0.05) had a significantly higher cell density as compared with cells on smooth coverslips. Furthermore, cells on nanopores (@p<0.05) had significantly lower cell density as compared with cells on nanopillars. There was no significant (NS) difference in cell density between the cells on gold coated coverslips and bare coverslips.

These findings addressed the objectives of the Research Question 1 by elucidating the effect of nano-pillared and nano-pored substrates on neurite development. PC12 cells cultured under identical conditions on different types of substrates exhibited different cell morphology. These results showed that the nanopillars restrict the motility of the growth cone and neurite outgrowth, thus leading to a higher count of cell proliferation while nanopores enhanced cell differentiation activity. These observations are consistent with the findings of cellular activities on nano-substrates where cells on silicon nanopillars also had a high cell density and short neurites showed high cell proliferation. The different neurite development seen in cells cultured on smooth and nano-featured substrates is clearly a sign that topographical features influence the development of neurite outgrowth.

In terms of proliferation, our findings show that on nanopillars, cells continued to proliferate as is evidenced by the high cell density on these substrates and these cells developed short and few neurites. On smooth substrates – gold coated and bare coverslips, by contrast, cells continued to differentiate and ceased to proliferate. On nanopores, cells had intermediate cell differentiation and proliferation. I speculate that the small diameter and spacing of the vertically aligned nanopillars might impose certain difficulty in the movement of the growth cone for guiding neurite outgrowth, thus leading to the inhibition of differentiation and enhancement of

proliferation. In the case of nanopores, the substrates provide a connected ridge network for the attachment of the growth cone to guide the neurite development.

Others have also reported that neuron cells cultured on nano-featured substrates had different cell morphology and neurite development as compared with smooth substrates. With PC12 cells cultured on ridges with widths in the nanoscale (70 nm to 1900 nm), Foley et al. [91] observed a similar neurite development. The grooves and ridges constrained the number of neurites that the cells could extend, thus promoting a bipolar rather than branching phenotype typical of these cells when cultured on flat surfaces. They attributed this phenomenon to that the cells were spatially aware of their nano-featured surroundings, and that the developing growth cones alter their direction of migration in an attempt to minimize the number of discontinuities encountered. These findings are consistent with our results in that the average number of neurites produced by cells is reduced when cells are cultured on nanoscale featured substrates.

To perform a quantitative analysis for the effect of filopodia extension on neurite development, the number of neurites and the filopodia were counted in each of the 60 cells from three replicates for each type of substrate from the SEM analysis. With all the measurements pooled together from the triplicate cultures for each type of substrate, the respective means were calculated and the correlation between the number of filopodia extensions and number of neurites per cell was then determined. Figure 16 shows the variation of the number of filopodia with the number of neurites in cells on different types of substrate topographies. It was determined that there is a significantly ($p < 0.05$) strong correlation (all $R < -0.9$) between filopodia extensions and the number of neurites on all substrates. This suggests that the number of filopodia decreases with the increase of the number of neurites.

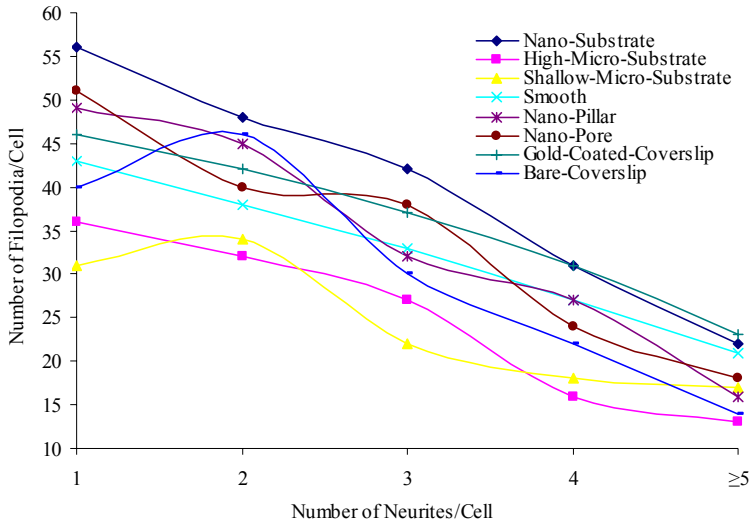

Figure 16. Variation of the number of filopodia with the number of neurites in cells on different types of substrates.

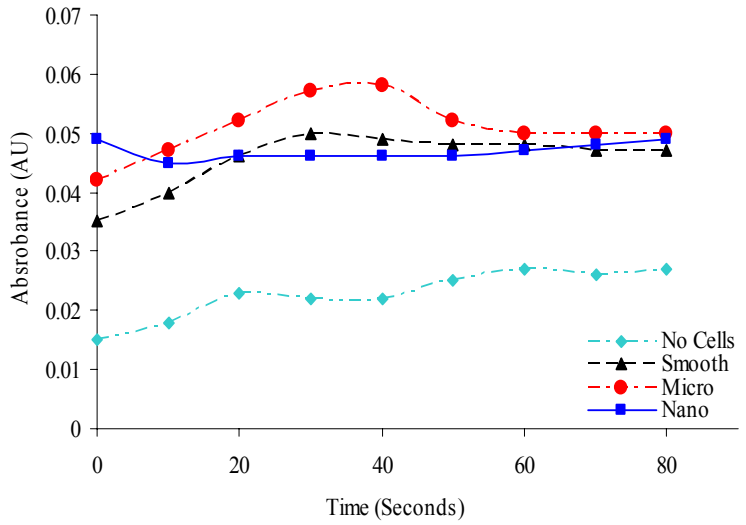

Figure 17. Color absorbance activities obtained from the acetylcholinesterase assay. The slope of the curves describes the differentiation activity in PC12 cells. A higher differentiation activity is seen initially in cells on micro-substrates than in cells on nano-substrates. The blank absorbance curve is from the negative control setup with no cells, and it represents the background absorbance signal (this background signal can be subtracted from the absorbance readings).

Biochemical Verification of Differentiation and Proliferation. The measurements of color absorbance activities obtained from the acetylcholinesterase assay were used to quantify cell differentiation. Specifically, the slope of the absorbance curves was calculated; a steeper slope defines greater differentiation. Figures 17 shows the results of the acetylcholinesterase assay for the cells on nano-, micro- (shallow micro-substrate) and smooth substrates, where the absorbance of the colored product from the breakdown of ATChI over time was plotted. The data show that the initial rate of ATChI hydrolysis (during the time period in which most of the ATChI is hydrolyzed) is comparable for cells on smooth and micro-substrates, and it is much lower for cells on nano-substrates. The results of the acetylcholinesterase assay showed increased PC12 differentiation activity in cells on micro-substrates. Thus, cells on nano-substrates had more proliferation activity, and cells on micro-substrates had more differentiation activity. This result agrees with the morphological data, thus confirming that nano-substrates inhibit differentiation of PC12 cells. The results of this study provided a morphological and biochemical understanding of neurite development in response to different scale substrate topography features.

The Combined Effect of Substrate Topography and Mechanical Strain on Neurite Development in PC12 Cells

Characterizing Cell Morphology Response to Substrate Topography. The dimensions of the micro-textured substrate were characterized. After that, the cell morphology on these micro-textured and smooth substrates subjected to a range of strain levels and strain rates was characterized by SEM and FM analysis. Figure 18 shows a top-view of the micro-islands on parylene (Figure 18a) and PDMS (Figure 18b). The dimensions of the micro-islands on parylene were 16.8±2.5 μm in diameter, 29.4±3.3 μm in separation and 1.6±0.2 μm in height and arranged

in a 2-D square array pattern. The PDMS substrate had micro-islands of 15.7±1.8 μm in diameter, 30.8±2.6 μm in separation and 1.5±0.3 μm in height and arranged in a 2-D square array pattern.

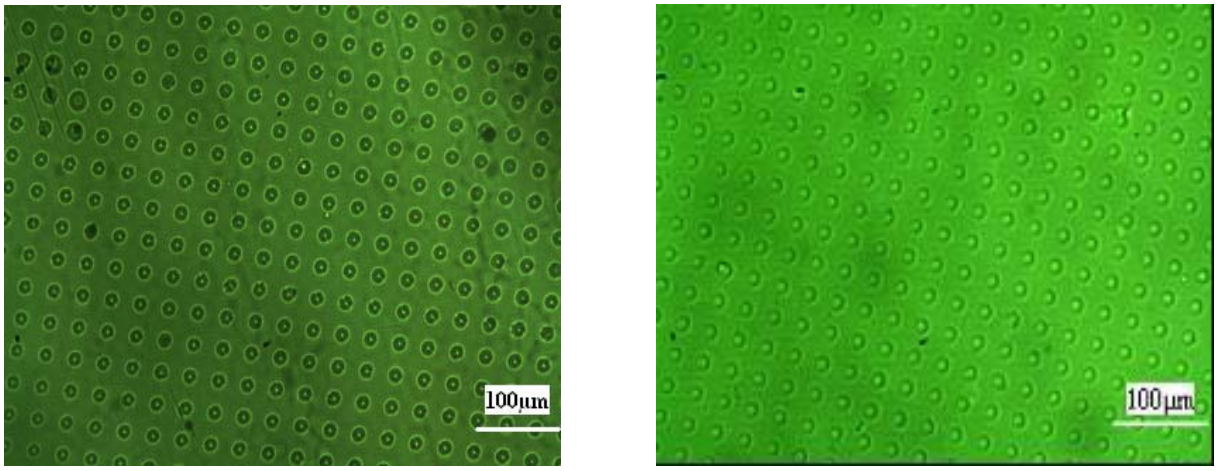

(a) (b)

Figure 18. Stereo-microscopic image shows a top view of micro-islands arranged in a square array pattern. The micro-pattern on: (a) parylene; (b) PDMS.

Figure 19 shows representative SEM images of cells in the static condition on smooth substrates and micro-textured substrates. In the static condition, cells on smooth substrates had shorter and fewer neurites while cells on micro-textured substrates had longer and multiple neurites. Figure 20 shows six representative SEM images of cells on smooth and micro-textured substrates for the 4% at 0.1Hz, 0.5Hz and 1.0Hz conditions. In the 4% at 0.1Hz condition, smooth substrate elicited short and few neurites development while on micro-textured substrates elicited longer and multiple neurites outgrowth. At a lower strain level of 4%, the length and the number of neurites per cell increased with increasing strain rate. Cells on smooth exhibited

similar neurite length and neurite density morphology as there counterparts on micro-textured substrates at 0.5Hz and 1.0Hz frequencies. Figure 21 shows six representative SEM images of cells on smooth and micro-textured substrates for the 8% at 0.1Hz, 0.5Hz and 1.0Hz conditions. It is seen that at an intermediate strain level of 8%, neurite length and neurite density decreased with increasing strain rate for cells on smooth and micro-textured substrates. In these setups, the neurite length and neurite density of cells on smooth substrates was similar to there counterparts on micro-textured substrates. Figure 22 shows six representative SEM images of cells on smooth substrates for the 16% at 0.1Hz, 0.5Hz and 1.0Hz conditions. These images show that at a high strain level of 16%, the neurite length and neurite density also decreased with increasing strain rate for cells on smooth and micro-textured substrates. Cells in these setups also exhibited similar neurite length and neurite density morphology on smooth and micro-textured substrate.

Note that the critical point dehydration used to dehydrate the sample for SEM analysis caused the wrinkled pattern and also the flattening deformation of the micro-structures (thus the micro-islands are not visible) on PDMS substrates in Figures 19-22.

Smooth Micro-textured

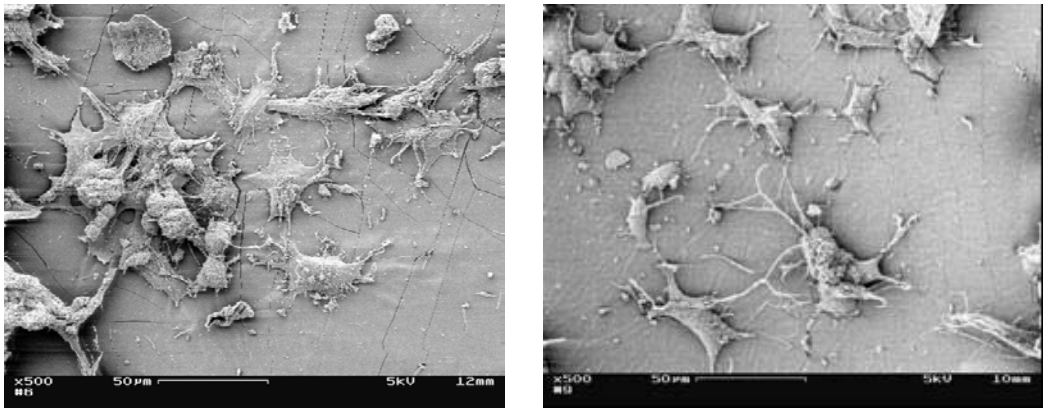

Figure 19. SEM images of cells on smooth and micro-textured in the static conditions (no stretching). The applied strain is along the vertical direction.

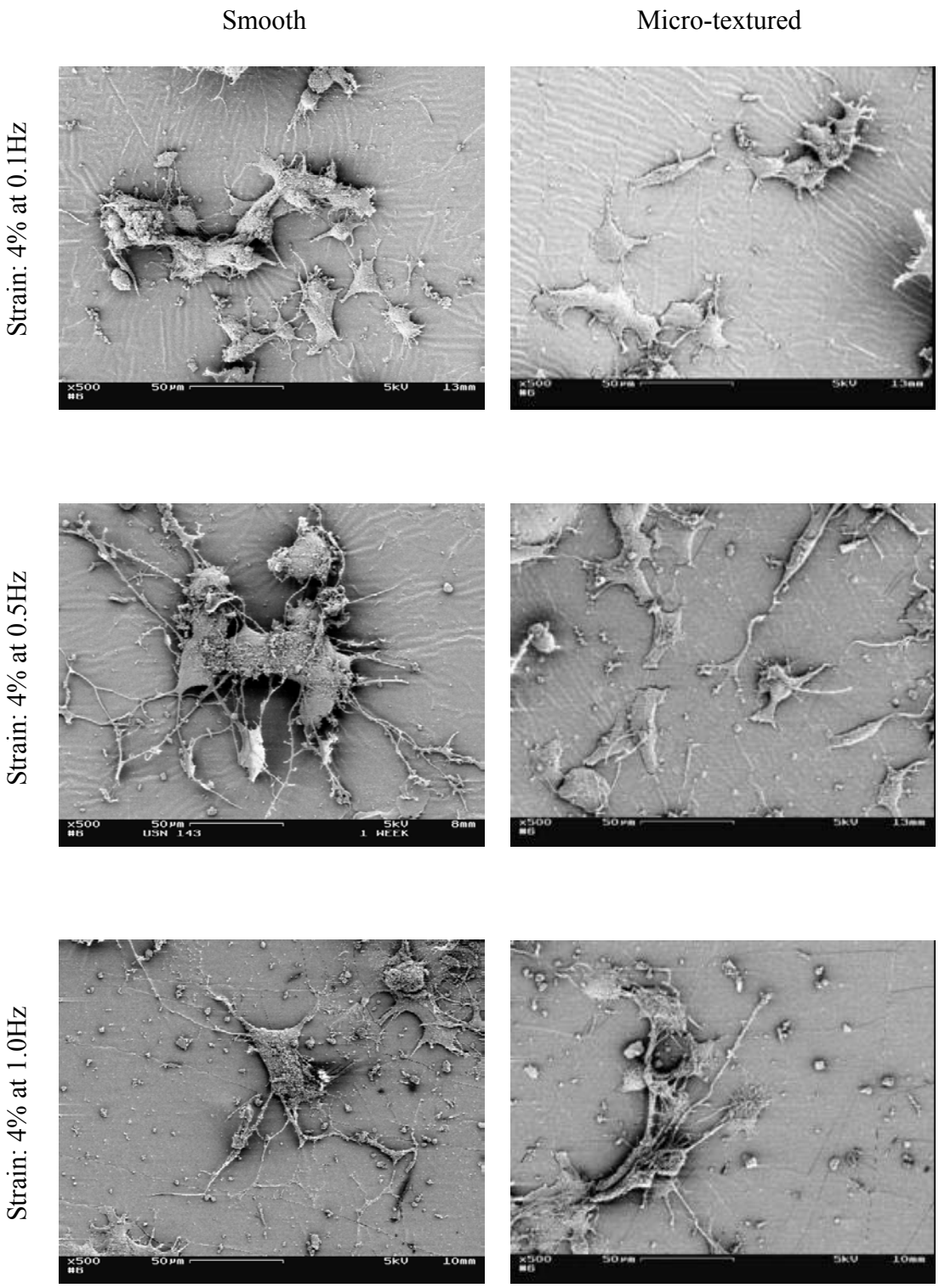

Figure 20. SEM images of cells on smooth and micro-textured substrates in the 4% strain at 0.1Hz, 0.5Hz, and 1.0Hz conditions. The applied strain is along the vertical direction.

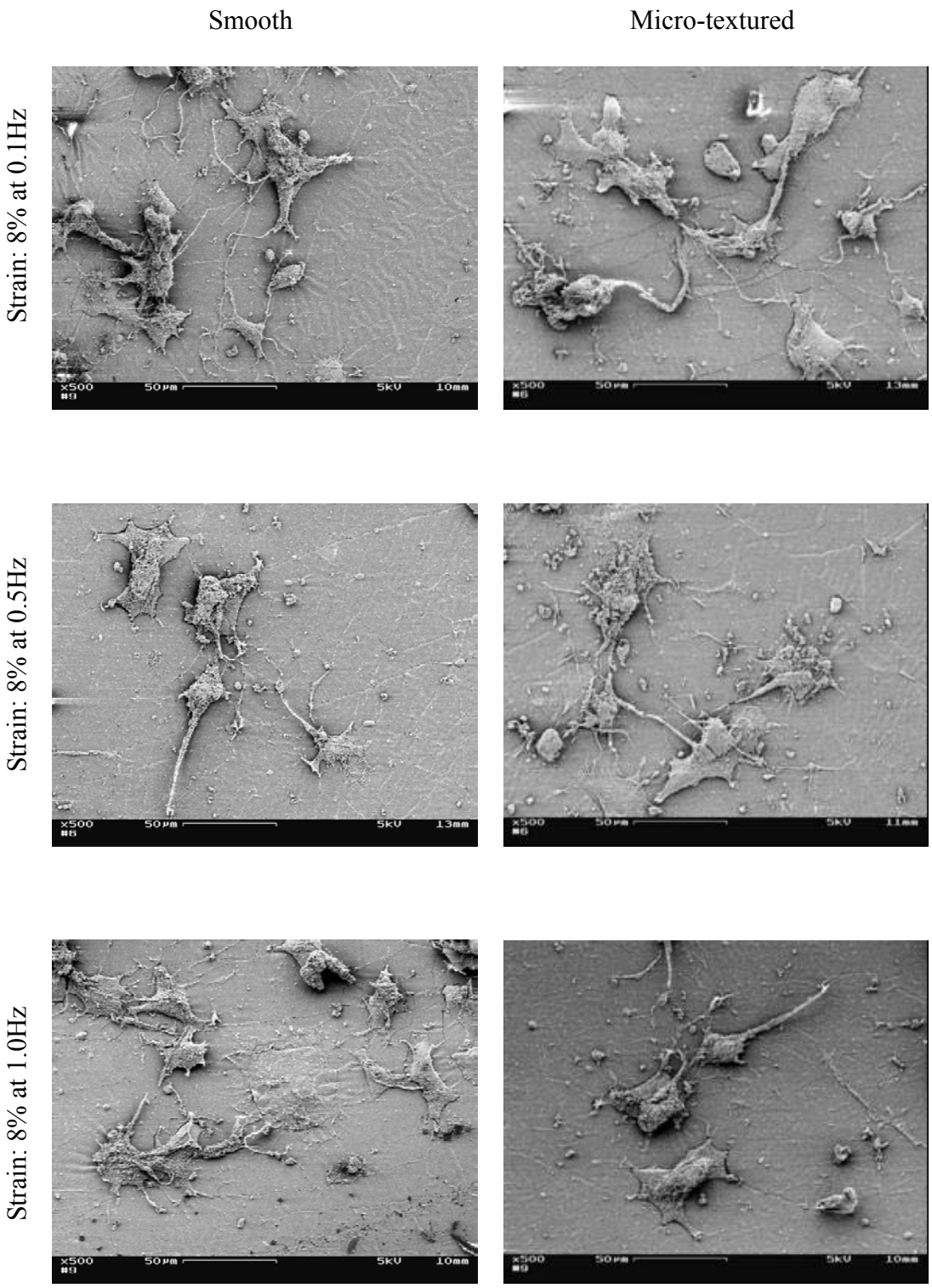

Figure 21. SEM images of cells on smooth and micro-textured substrates in the 8% strain at 0.1Hz, 0.5Hz and 1.0Hz conditions. The applied strain is along the vertical direction.

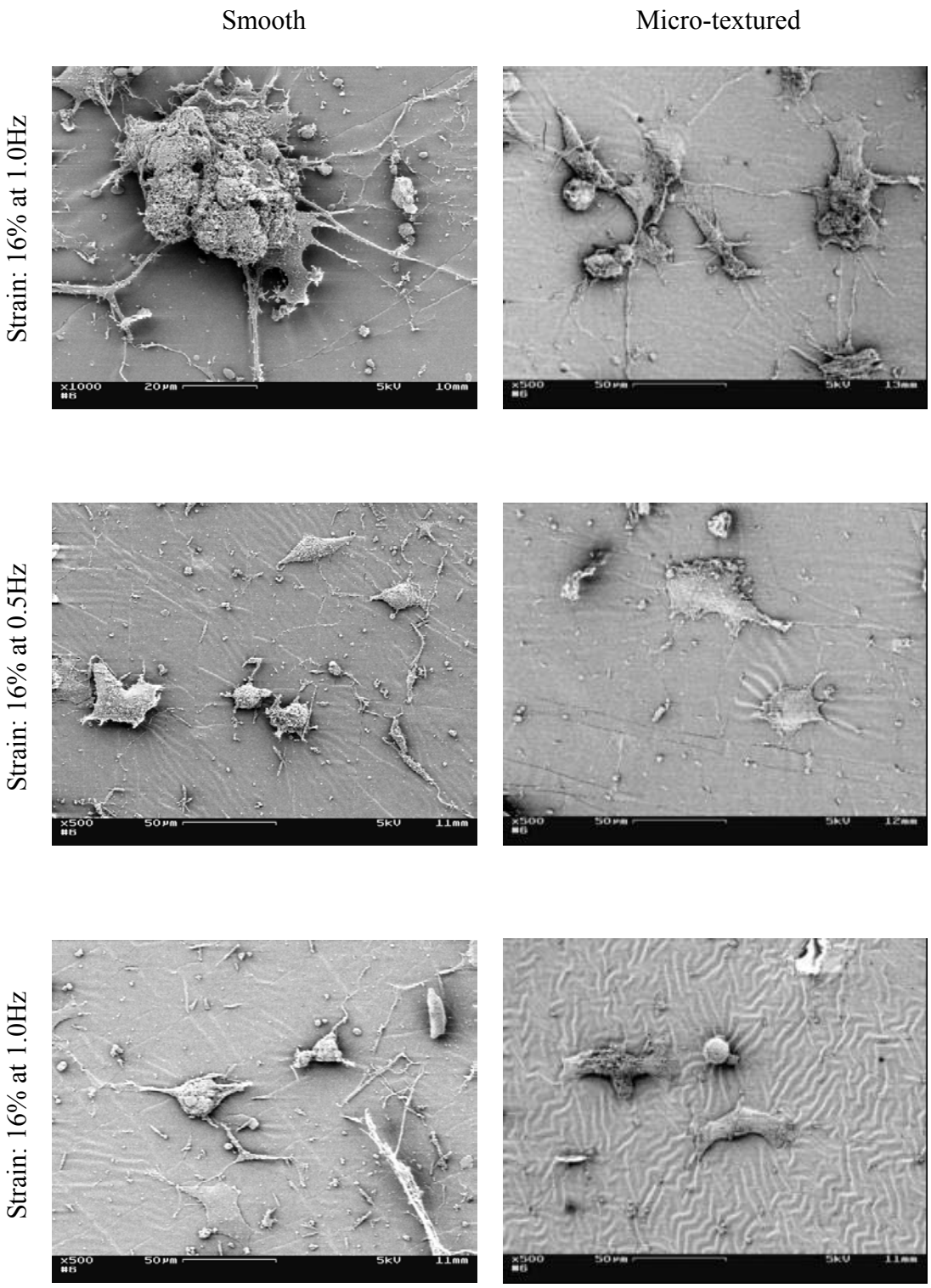

Figure 22. SEM images of cells on smooth and micro-textured substrates in the 16% strain at 0.1Hz, 0.5Hz and 1.0Hz conditions. The applied strain is along the vertical direction.

As shown in Figure 23, four representative fluorescent images of stained actin and microtubules show neurite development in the static condition. In the static setups, cells on smooth substrate had short and few neurites while cells on micro-textured substrates had longer and multiple neurites per cell. As shown in Figure 24, twelve representative fluorescent images of cells on smooth and micro-textured substrates for the 4% at 0.1Hz, 0.5Hz and 1.0Hz conditions. In the 4% at 0.1Hz condition, cells on smooth substrate developed shorter and fewer neurites while cells on micro-textured substrates developed longer and multiple neurites. At a lower strain level of 4% and 0.5Hz and 1.0Hz frequencies, cells on smooth substrates exhibited similar neurite length and neurite density as their counterparts on micro-textured substrates. Furthermore, in these setups the length and the number of neurites per cell increased with increasing strain rate on smooth and micro-textured substrates. As shown in Figure 25, twelve fluorescent images of cells on smooth and micro-textured substrates for the 8% at 0.1Hz, 0.5Hz and 1.0Hz conditions. At an intermediate strain level of 8%, neurite length and neurite density of cells on smooth substrates was similar to their counterparts on micro-textured substrates at 0.1Hz, 0.5Hz, and 1.0Hz frequencies. Also, in these setups, the neurite length and neurite density decreased with increasing strain rate for cells on both the smooth and micro-textured substrates. As shown in Figure 26, twelve fluorescent images of cells on smooth and micro-textured substrates for the 16% at 0.1Hz, 0.5Hz and 1.0Hz conditions. These images show that at a high strain level of 16%, cells on smooth substrates also had similar neurite length and neurite density to their counterparts on micro-textured substrates at 0.1Hz, 0.5Hz, and 1.0Hz frequencies. In these setups, the neurite length and neurite density also decreased with increasing strain rate. Note that the neurite orientation was not measured due to the inability to mark the substrates during specimen preparation for FM analysis.

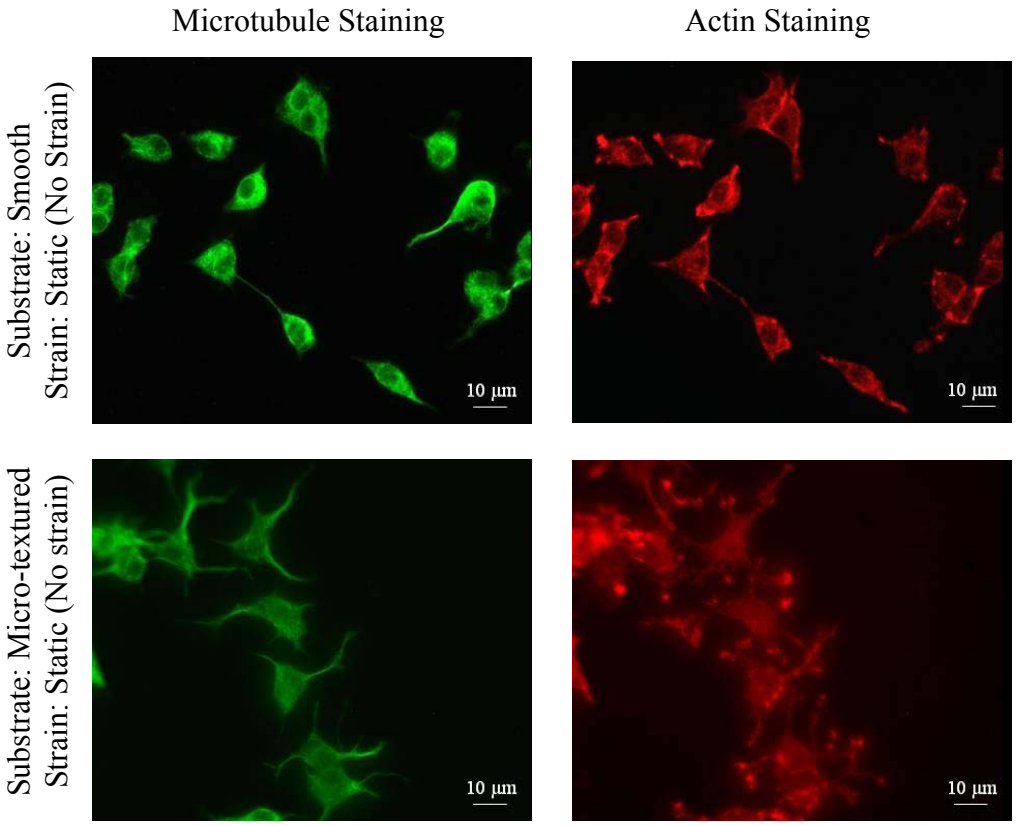

Figure 23. Images of PC12 cells co-stained for microtubules and actin in static conditions (no strain) on smooth and micro-textured substrates.

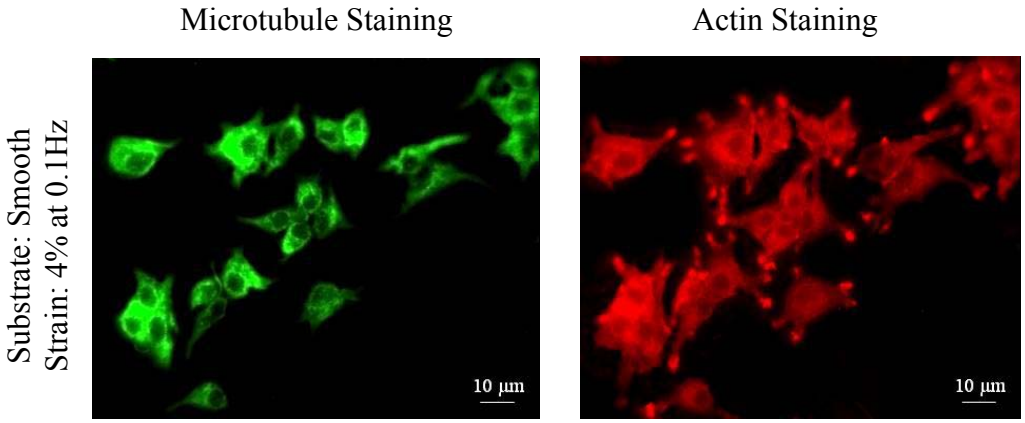

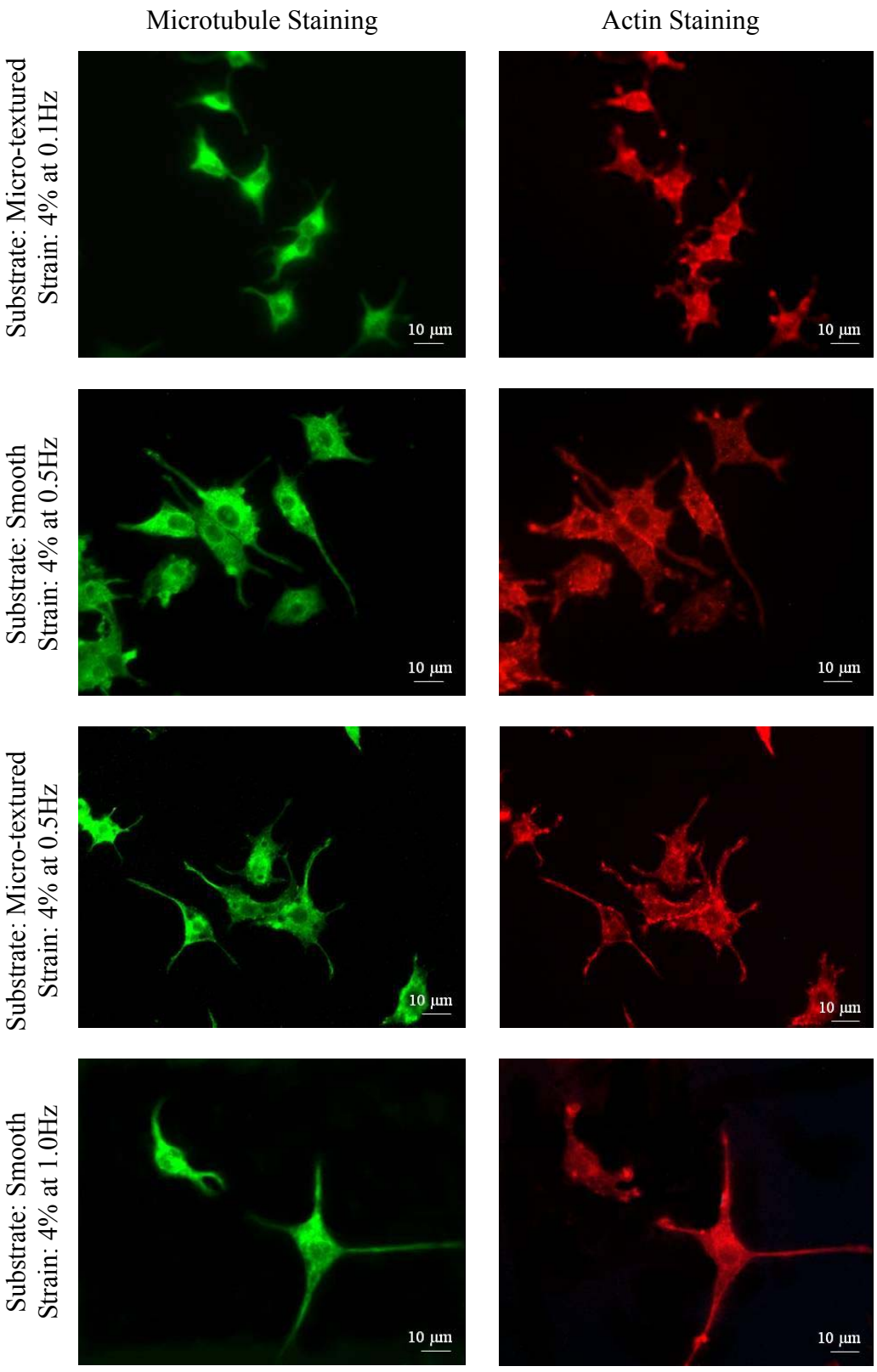
Microtubule Staining
Actin Staining
Substrate: Micro-textured
Strain: 4% at 0.1Hz
Substrate: Smooth
Strain: 4% at 0.5Hz
Substrate: Micro-textured
Strain: 4% at 0.5Hz
Substrate: Smooth
Strain: 4% at 1.0Hz
10 μm

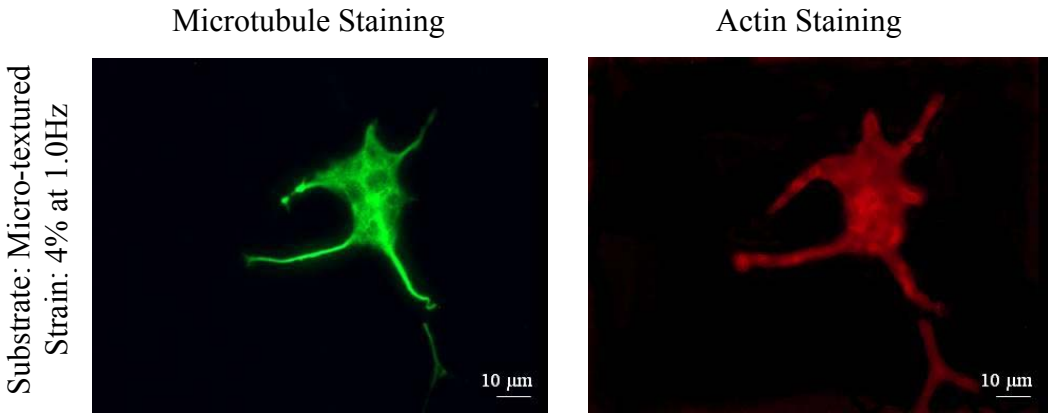

Figure 24. Images of PC12 cells co-stained for microtubules and actin in 4% at 0.1Hz, 0.5Hz, and 1.0Hz conditions on smooth and micro-textured substrates.

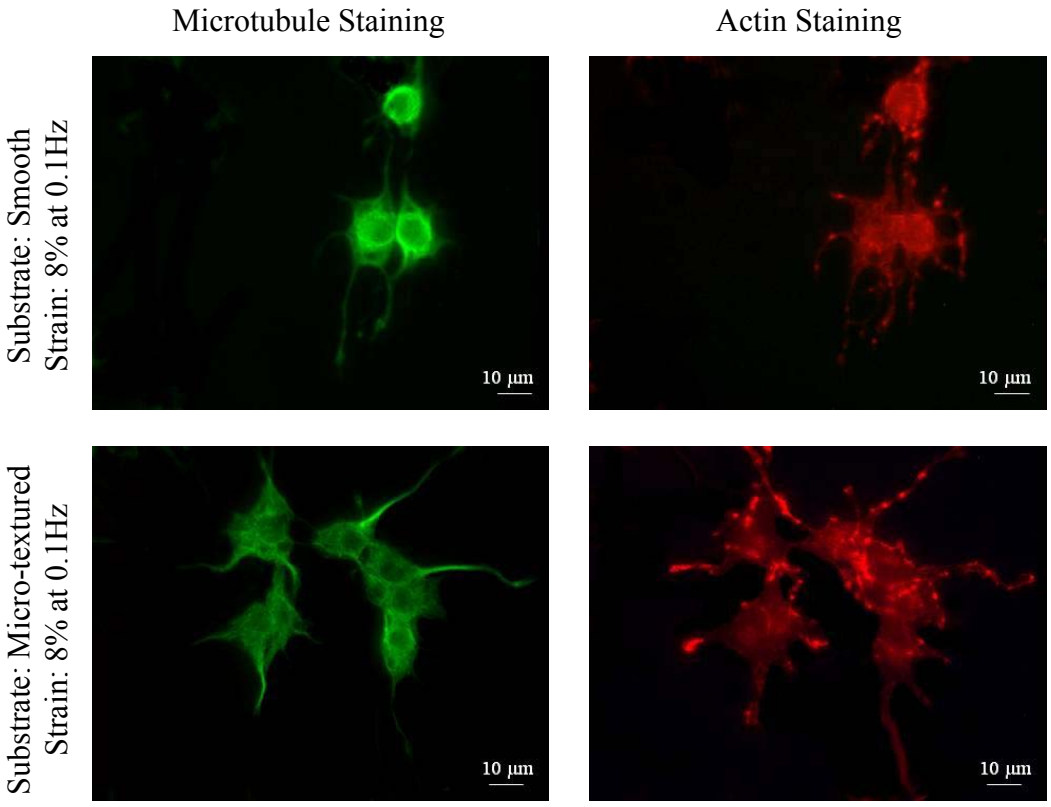

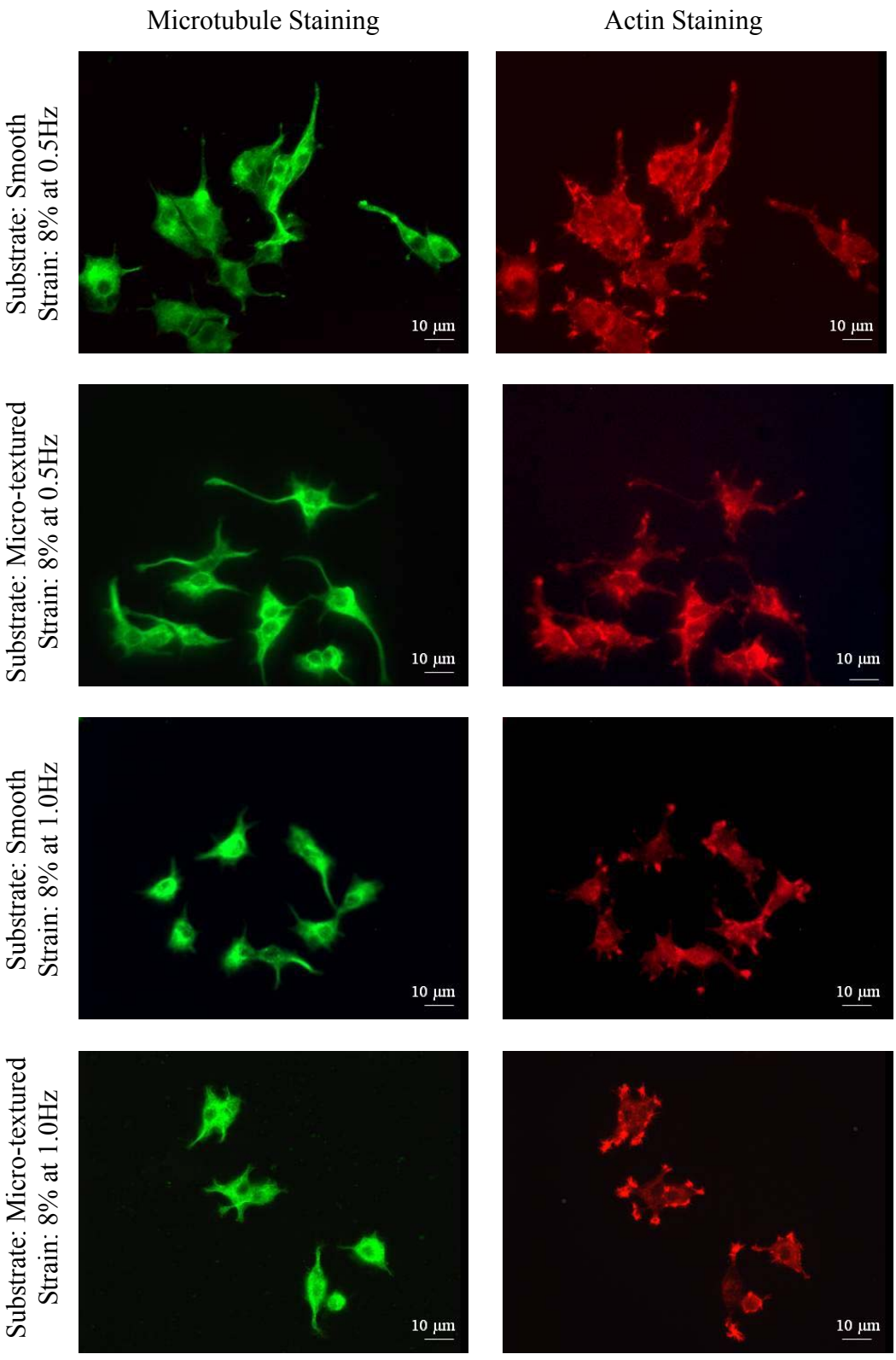

Figure 25. Images of PC12 cells co-stained for microtubules and actin in 8% at 0.1Hz, 0.5Hz, and 1.0Hz conditions on smooth and micro-textured substrates.

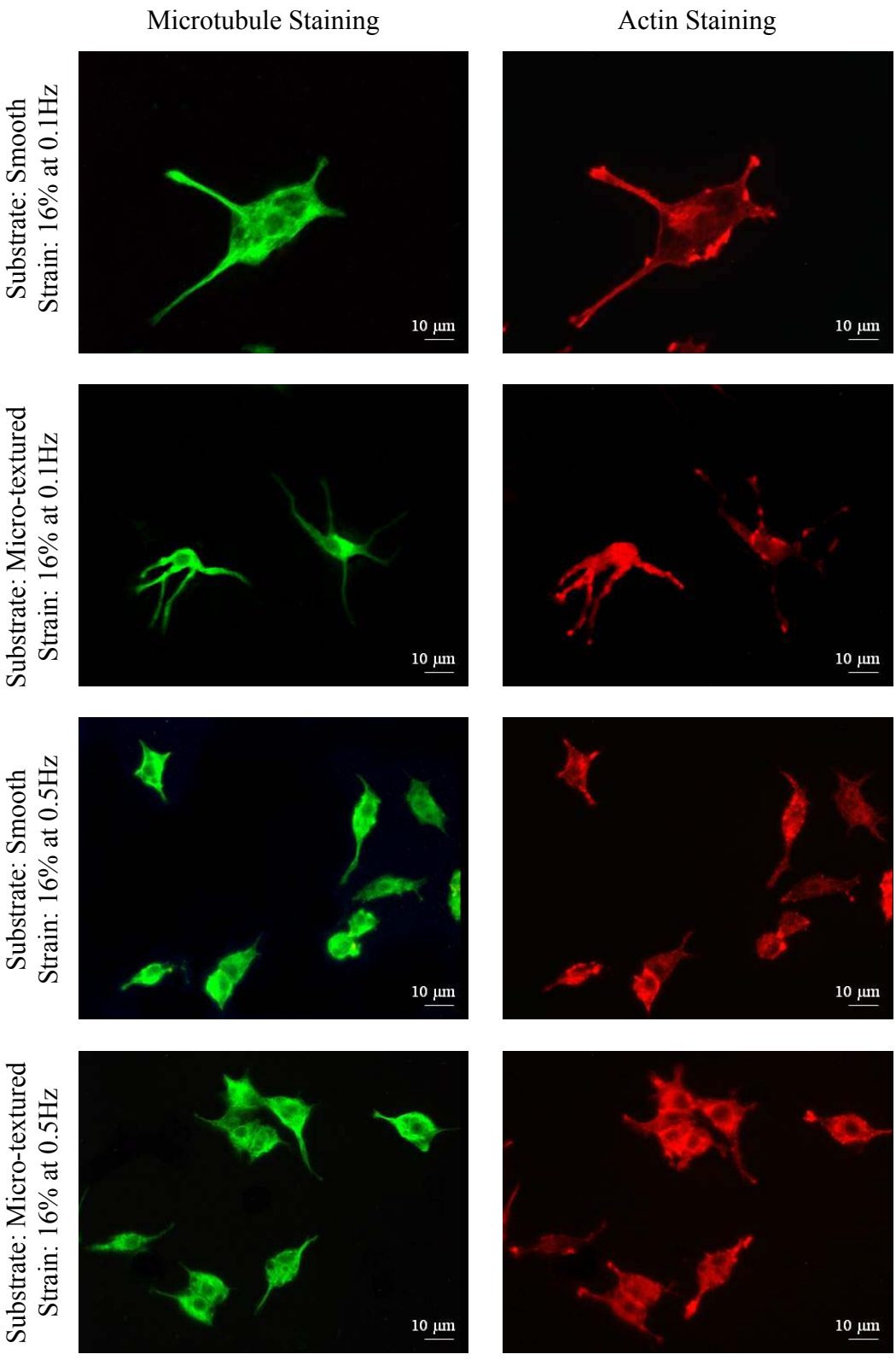
Microtubule Staining
Actin Staining
Substrate: Smooth
Strain: 16% at 0.1Hz
Substrate: Micro-textured
Strain: 16% at 0.1Hz
Substrate: Smooth
Strain: 16% at 0.5Hz
Substrate: Micro-textured
Strain: 16% at 0.5Hz
10 μm

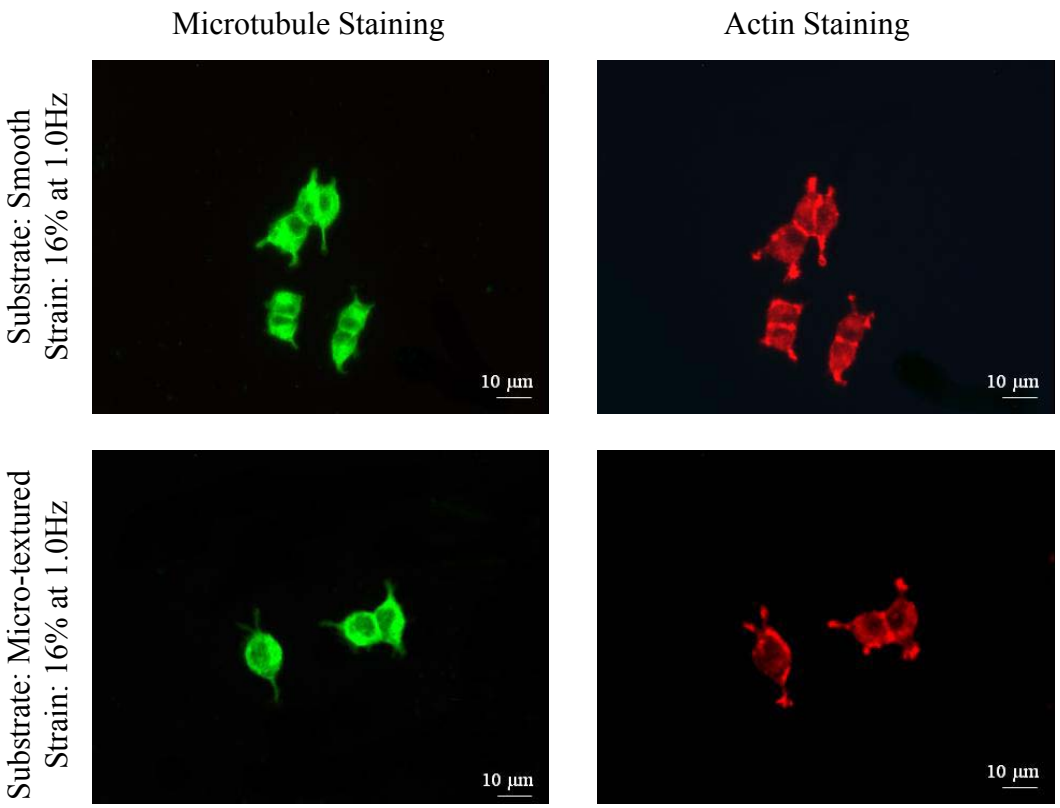

Figure 26. Images of PC12 cells co-stained for microtubules and actin in 16% at 0.1Hz, 0.5Hz, and 1.0Hz conditions on smooth and micro-textured substrates.

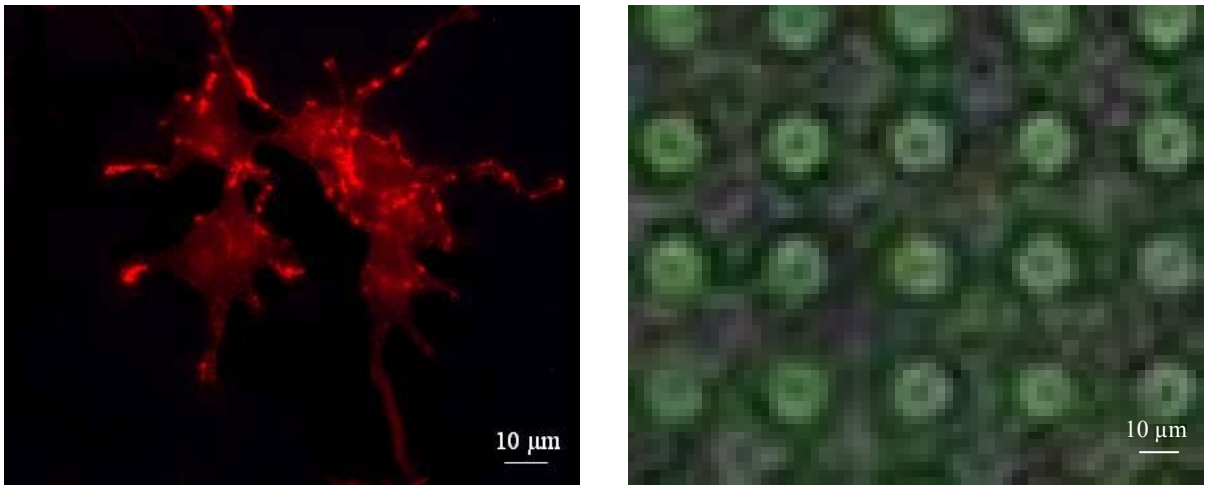

Figure 27. Shows bright actin staining spots along the length of the neurites (a) the underlying micro-textured substrate (b).

Figure 27a shows bright actin staining spots along the length of the neurites and Figure 27b shows the underlying micro-texture substrates. Cells on the micro-textured substrates in the 8% and 16% at 0.1Hz conditions were observed to have a bright actin-stain spots along the length of their neurites. The bright spots were spaced 5-15 μm apart. The underlying substrate had micro-islands with 15 μm in diameter and 30 μm in spacing. Even though the observed staining spots on the neurites were within the corresponding range of the substrate feature dimensions, the arrangements of these did not follow the underlying pattern (when superimposing the bright actin spots over the underlying micro-textured substrates we did see a clear overlapping between the two patterns). Hence, the observed actin staining spots can not be interpreted as actin-rich focal adhesion contacts with the substrate features.

In the static and 4% at 0.1Hz conditions, cells on micro-textured substrates had greater neurite development and lower cell density as compared with cells on smooth substrates. In the 4% at 0.5Hz and 1.0Hz, 8% and 16% at 0.1Hz, 0.5Hz and 1.0Hz conditions, cells showed similar neurite development and cell density on both types of substrates. These facts suggest that under the static and small strain conditions, micro-texture had a significant effect on neurite extension. These observations are consistent with the findings of cells cultured on micro-substrates with an array of micro-islands (Research Question 1). Cells on these micro-substrates also had longer and multiple neurites as compared with cells on smooth substrates under no strain conditions.

Under dynamic conditions, the magnitude of the strain level and strain rate determined the neurite development and cell density on smooth and micro-textured substrates. Specifically, at the strain level of 4%, a higher strain rate enhanced the neurite development, while at the strain levels of 8% or 16% a lower strain rate induced a similar stimulatory effect on neurite development. But the highest strain condition (16% at 1.0Hz) in this study had limited neurite

development. These facts suggest that there is an interrelated relationship between strain rate and strain level. Specifically, at high strain levels, increasing strain rate decreases the development of neurite extensions, while at low strain rates, increasing strain rate increases the development of neurites.

Determining the Plating Efficiency on Smooth and Micro-Textured Substrates. The percentage plating efficiency of cells on smooth and micro-textured PDMS substrates was determined by counting the adhered viable cells out of the total plated cells six hours after seeding. The means and standard errors of the percentage plating efficiency were calculated and comparisons were made between the plating efficiency on smooth and micro-textured substrates.

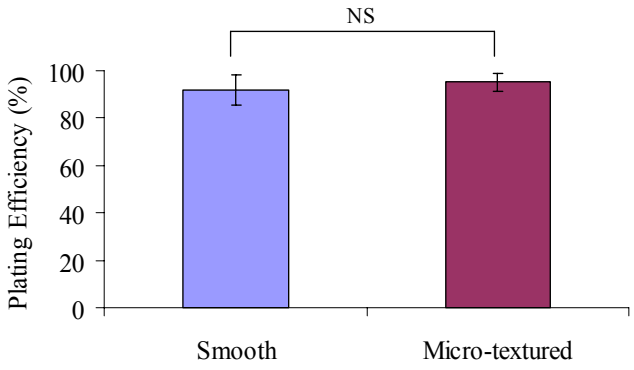

Figure 28. Bar graphs showing the mean plating efficiency on smooth and micro-textured PDMS substrates. NS = Not Significant.

Figure 28 shows the bar graphs for the mean plating efficiency on smooth and micro-textured PDMS substrates being 91.7±6.4% and 95.3±3.7% respectively. The trypan blue assay showed that the plating efficiency on both smooth and micro-textured substrates was very high (>90%). Furthermore, there is no significant difference in the plating efficiency between the smooth and micro-textured substrates. These findings suggest that differences in plating efficiency on smooth and micro-textured did not influence the observed neurite development and cell density on these different types of substrates.

Quantification of Neurite Development and Cell Density. The measured neurite lengths, neurite density and cell density were quantified in a similar manner to that done in Research Question 1. Furthermore, the neurite orientation response to the applied strain was also measured to determine the influence of applied strain on neurite development. A quantitative analysis of neurite development was performed by counting the number of neurites and their lengths were measured in each of the 60 cells from three replicates for each type of substrate in all setups. Similarly, the angle of neurite orientation angle in respect to the applied strain in the dynamic setups and a randomly marked axis in the static setups were measured in each of the 60 cells from three replicates for each type of substrate in all setups. The measured angles were grouped into three angular ranges: 0°-30°, 31°-60° and 61°-90° and the percentage of neurites in a specific group was calculated. The means and standard errors of the neurite length, neurite density and neurite orientation measurements were calculated by pooling together the triplicate cultures for each type of substrate. Comparative analyses were made between the neurite length and neurite density to determine neurite development. A quantitative analysis of cell density was performed by enumerating cells in 1 mm^2 area from three replicates for each type of substrate in

both analyses. The means and standard errors of the cell density were calculated by pooling together the triplicate cultures for each type of substrate from both analyses. Comparisons were made between the cell counts on different types of substrates to determine cell density.

The results of a quantitative evaluation of neurite length, neurite density, cell density and neurite alignment for all cultures obtained directly under SEM are listed in Table 1. Similarly, the results of the quantitative evaluation of neurite length, neurite density and cell density for all cultures obtained through FM are shown in Table 2.

Table 1. Results of the SEM quantitative analysis of cellular activities in PC12 cells seeded on smooth and micro-textured substrates in static and dynamic conditions.

Strain condition and Type of Substrate [Smooth (S) and micro-textured (T)]	Mean neurite development		Mean Cell Density (cells/cm^2)	Mean percentage of neurites in a specified neurite orientation		
	Length (μm)	Neurites per cell		0°-30°	31°-60°	61°-90°
Static (S)	22.7±0.4	2.0±0.1	13.6±0.1K	33.0±1.5	34.3±2.5	32.7±0.3
Static (T)	41.4±0.3	2.7±0.1	9.8±0.2K	38.3±2.1	25.0±0.6	36.7±0.9
4% at 0.1Hz (S)	21.9±0.8	2.2±0.1	13.4±0.1K	32.3±1.2	34.0±3.0	33.7±0.9
4% at 0.1Hz (T)	42.7±1.4	2.8±0.1	9.5±0.2K	39.0±2.1	25.0±1.2	36.0±1.0
4% at 0.5Hz (S)	47.8±1.5	3.0±0.1	10.2±0.2K	44.0±1.5	35.3±1.2	20.7±1.5
4% at 0.5Hz (T)	49.4±2.0	3.0±0.1	10.1±0.1K	46.0±1.5	34.0±1.2	20.0±1.7
4% at 1.0Hz (S)	69.1±1.0	3.4±0.1	7.1±0.1K	61.0±3.4	27.7±1.2	11.3±2.0
4% at 1.0Hz (T)	69.8±1.0	3.5±0.1	7.0±0.1K	66.3±2.1	25.0±0.9	8.0±1.6
8% at 0.1Hz (S)	60.1±0.8	3.2±0.1	8.8±0.1K	52.2±3.4	33.5±2.0	14.3±2.4
8% at 0.1Hz (T)	61.4±0.6	3.2±0.1	8.7±0.1K	57.3±2.8	32.3±0.9	10.3±1.9
8% at 0.5Hz (S)	37.9±0.9	2.7±0.1	10.6±0.1K	34.3±1.9	42.7±1.2	23.0±1.5
8% at 0.5Hz (T)	38.7±0.6	2.8±0.1	10.6±0.1K	32.0±0.6	43.0±1.2	25.0±1.0
8% at 1.0Hz (S)	32.4±0.5	2.5±0.1	11.1±0.1K	22.0±1.5	32.0±1.2	46.0±2.1
8% at 1.0Hz (T)	34.1±1.3	2.5±0.1	11.0±0.1K	20.0±1.0	32.0±0.6	48.0±0.6
16% at 0.1Hz (S)	67.2±1.1	3.4±0.1	7.3±0.1K	60.7±2.9	27.7±0.9	11.7±1.5
16% at 0.1Hz (T)	67.8±1.1	3.4±0.1	7.2±0.1K	66.0±3.5	26.7±2.0	9.3±1.4
16% at 0.5Hz (S)	26.6±0.2	2.4±0.1	8.0±0.1K	17.7±0.9	35.0±1.2	47.3±0.9
16% at 0.5Hz (T)	27.3±0.4	2.3±0.1	7.9±0.1K	16.7±0.7	34.7±0.7	48.7±1.3
16% at 1.0Hz (S)	20.7±0.5	1.9±0.1	5.9±0.3K	14.3±0.9	30.0±0.6	55.7±0.7
16% at 1.0Hz (T)	20.6±0.4	2.0±0.1	5.5±0.2K	13.3±0.6	30.5±0.6	56.2±1.0

Table 2. Results of the FM quantitative analysis of cellular activities in PC12 cells seeded on smooth and micro-textured substrates in static and dynamic conditions.

Strain condition and Type of Substrate [Smooth (S) and micro-textured (T)]	Mean neurite development		Mean Cell Density (cells/cm^2)
	Length (μm)	Neurites per cell	
Static (S)	30.8±1.5	2.6±0.1	14.2±0.1K
Static (T)	44.7±0.1	3,2±0.1	11.3±0.8K
4% at 0.1Hz (S)	31.3±3.2	2.6±0.1	15.1±1.0K
4% at 0.1Hz (T)	45.6±2.3	3.1±0.1	10.9±1.1K
4% at 0.5Hz (S)	46.6±3.2	3.7±0.1	11.4±1.4K
4% at 0.5Hz (T)	49.6±2.8	3.7±0.1	11.7±1.4K
4% at 1.0Hz (S)	60.5±0.8	4.1±0.1	7.9±0.7K
4% at 1.0Hz (T)	63.8±4.6	4.1±0.1	7.7±0.6K
8% at 0.1Hz (S)	49.8±0.8	3.6±0.1	8.5±0.6K
8% at 0.1Hz (T)	52.5±2.2	3.5±0.1	8.7±0.6K
8% at 0.5Hz (S)	45.8±2.2	3.1±0.1	11.0±0.6K
8% at 0.5Hz (T)	47.1±4.8	3.1±0.1	10.3±1.1K
8% at 1.0Hz (S)	37.3±1.6	2.9±0.1	11.7±0.8K
8% at 1.0Hz (T)	39.1±1.9	2.9±0.1	11.6±0.9K
16% at 0.1Hz (S)	59.8±1.7	3.9±0.1	7.3±1.1K
16% at 0.1Hz (T)	60.5±4.3	4.0±0.1	7.1±0.3K
16% at 0.5Hz (S)	34.4±0.1	2.8±0.1	8.6±0.5K
16% at 0.5Hz (T)	36.6±3.4	2.8±0.1	8.2±0.7K
16% at 1.0Hz (S)	26.3±0.7	2.5±0.1	5.9±0.4K
16% at 1.0Hz (T)	27.2±0.7	2.4±0.1	5.7±0.3K

Note, that the relationship between neurite development and cell density in response to different types of substrate topographies and strain conditions was observed to be the same by both types of analyses. Hence, the statistical comparisons of neurite length, neurite density and cell density between the cultures in different groups represent the observations made by both the SEM and FM analysis. It is seen that on both types of substrates, cells in the conditions of 4% at 1.0Hz and 16% at 0.1Hz had most prominent development in neurite length and neurite density but with the lowest cell densities. Conversely, on smooth substrates, cells in the static and 4% at 0.1Hz conditions had less development in neurite length and neurite density but with the highest

cell densities. The only exception to this was the highest mechanical condition (16% at 1.0Hz) for both types of substrates in which cells had the smallest neurite development and the lowest cell densities. Also, on both types of substrates, cells in the conditions of 4% at 1.0Hz and 16% at 0.1Hz had a dominating number (>50%) of neurites oriented in the 0°-30° angular range. Conversely, on both types of substrates, cells in the condition of 16% at 1.0Hz had a dominant number of neurites oriented in the 61°-90° angular range. Note that a quantitative evaluation of the neurite orientation angle was not performed using the FM due to the inability in making accurate measurements.

Figure 29 shows the results of neurite lengths along with statistical comparisons in various mechanical conditions using the SEM (Figure 29a) and FM (Figure 29b). The bar graph shows that on both types of substrates, cells subjected to 16% at 0.1Hz and 4% at 1.0Hz had significantly (xp and +p<0.05 respectively) longer neurites (68.4±1.2 μm and 61.2±0.9 μm as determined by SEM and FM analysis respectively) as compared with the rest of the groups. Cells on both types of substrates subjected to 16% at 1.0Hz had significantly (#p<0.05) shorter neurites (21±0.2 μm and 26.8±0.5 μm as determined by SEM and FM analysis respectively) as compared with the rest of the groups. In the static condition, cells on micro-textured substrates had significantly (*p <0.05) longer neurites as compared with cells on smooth substrates. But on each type of substrates, cells in the static and 4% at 0.lHz conditions showed similar neurite length. In comparison with cells on smooth substrates in 4% at 0.5Hz and 1.0Hz, 8% and 16% at 0.1Hz, 0.5Hz and 1.0Hz conditions, cells on micro-textured substrates showed no significant difference in neurite length. Figure 30 shows the bar graphs for neurite density along with their statistical comparison in various mechanical conditions using the SEM analysis (Figure 30a) and FM (Figure 30b). Cells on both types of substrates stretched under 4% at 1.0Hz and 16% at

0.1Hz had significantly (xp and +p<0.05 respectively) higher neurite density (3.4±0.1 and 4.0±0.1 neurites per cell as determined by SEM and FM analysis respectively) as compared with the rest of the groups. Cells on both types of substrates subjected to 16% at 1.0Hz strain condition had significantly (#p<0.05) lower neurite density (2.0±0.1 and 2.4±0.1 neurites per cell as determined by SEM and FM analysis respectively) as compared with the rest of the groups. In the static conditions, cells on micro-textured substrates had significantly (*p<0.05) higher neurite density as compared with cells on smooth substrates. Cells on both types of substrates in the 4% at 0.lHz condition showed similar neurite density as their counterparts in the static condition. Cells subjected to strain conditions of 4% at 0.5Hz and 1.0Hz, 8% and 16% at 0.1Hz, 0.5Hz and 1.0Hz had no significant difference in their neurite density on both types of substrates.

The obtained cell density and its statistical comparison between various mechanical conditions are shown in Figure 31. Note that the cell density for both the SEM (Figure 31a) and FM (Figure 31b) analysis were counted using an optical microscope. However, as the cultures for the two microscopy analysis were setup and analyzed at separate times, the cell densities are consequently reported separately (see Table 1 for SEM data and Table 2 for FM data). The cell density found on smooth substrates in static and low strain (4% at 0.1Hz) conditions was significantly (*p<0.05) higher (13,460±140 cells/cm^2 and 14,600±510 cells/cm^2 for SEM and FM setups respectively) as compared with the rest of the conditions. The cell density found on both types of substrates in the 16% at 1.0Hz conditions was significantly (#p<0.05) lower (5,600±270 cells/cm^2 and 5,800±100 cells/cm^2 for SEM and FM setups respectively) as compared with the rest of the conditions. No significant difference in cell density was found when comparing between cells on smooth and micro-textured substrates in the 4% at 0.5Hz and 1.0Hz, 8% and 16% at 0.1Hz, 0.5Hz and 1.0Hz conditions.

Figure 32a and Figure 32b shows the percentage of neurites aligned in three angular ranges: 0°-30°, 31°-60° and 61°-90° for cells on smooth and micro-textured substrates, respectively measured in all groups using an SEM. Cells on both types of substrates in the 4% at 1.0Hz and 16% at 0.1Hz conditions had a dominating number (>50%) of neurites aligned in the 0°-30° range as compared with the rest of the groups. Cells on both types of substrates in the 16% at 1.0Hz condition had a dominating number of neurites aligned in the range 61°-90° as compared with the rest of the groups. Cells on both types of substrates subjected to the 8% at 0.5Hz condition had a greater percentage of neurites aligned in the 31°-60° range as compared with the rest of the groups but not with a dominating number. Cells on both types of substrates in the 8% at 0.1Hz had a dominating number of neurites aligned in the 0°-30° range. Cells on both type of substrates in the 8% at 1.0Hz and 16% at 0.5Hz conditions had a greater proportion of neurites in the 61°-90° range, but not with a dominating number. However, in the rest of conditions; neurites were aligned almost randomly without a dominating preferential orientation among the three angular ranges.

These results addressed the objectives of the Research Question 2 by providing a comparative analysis on the effect of micro-textured substrate topography and different mechanical strain conditions on neurite development. The findings of the quantitative analysis suggest that when comparing the 4% at 0.1Hz condition with the static condition in each substrates group no major difference in neurite length, neurite density and cell density was seen. This indicates that the low strain condition of 4% at 0.1Hz did not have any stimulatory effect on the cells. This non-stimulatory phenomenon was also observed with cardiac fibroblasts and rat tibiae when they were subjected to a small magnitude strain level (3%) and strain rate (0.1Hz) [64].

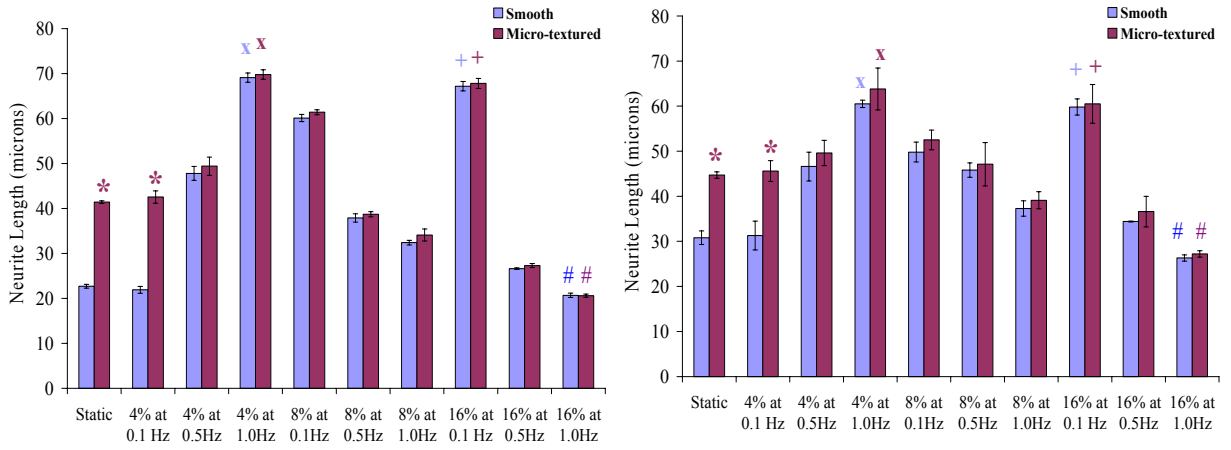

(a) (b)

Figure 29. Bar graphs show the mean value for the neurite lengths observed in the respective conditions. Mean neurite length quantified by SEM analysis (a) and FM analysis (b). Values reported are mean ± standard error; n = 3; # p<0.05 (16% at 1.0Hz compared with the rest of the conditions), +p<0.05 (16% at 0.1Hz compared with the rest of the conditions), xp < 0.05 (4% at 1.0Hz compared with the rest of the conditions), *p <0.05 (micro-texture in static condition compared with smooth in static condition).

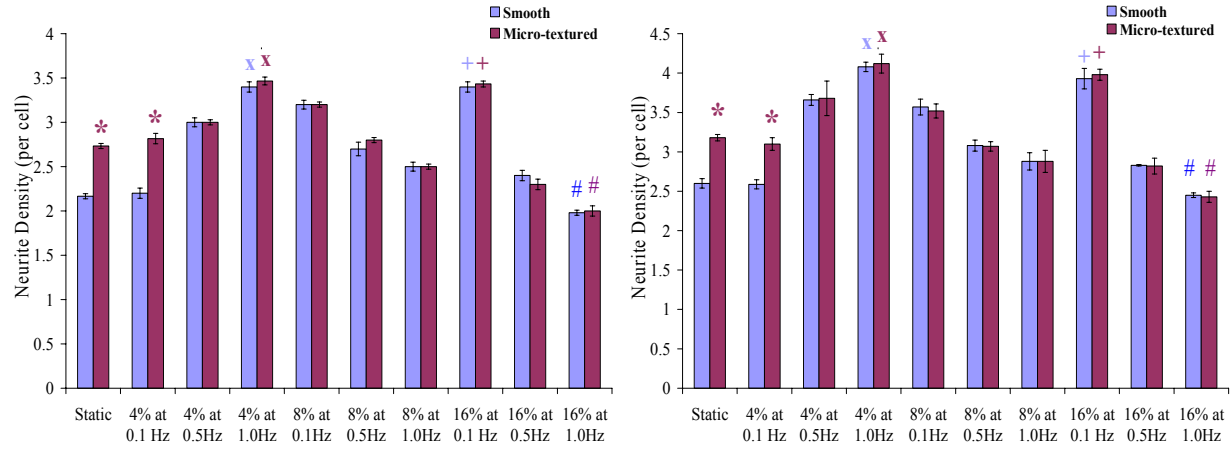

(a) (b)

Figure 30. Bar graphs show the mean value for the neurite density observed in the respective conditions. Mean neurite density quantified by SEM analysis (a) and FM analysis (b). Values reported are mean ± standard error; n = 3; # p<0.05 (16% at 1.0Hz compared with the rest of the conditions), +p<0.05 (16% at 0.1Hz compared with the rest of the conditions), xp<0.05 (4% at 1.0Hz compared with the rest of the conditions), *p<0.05 (micro-texture in static condition compared with smooth in static condition).

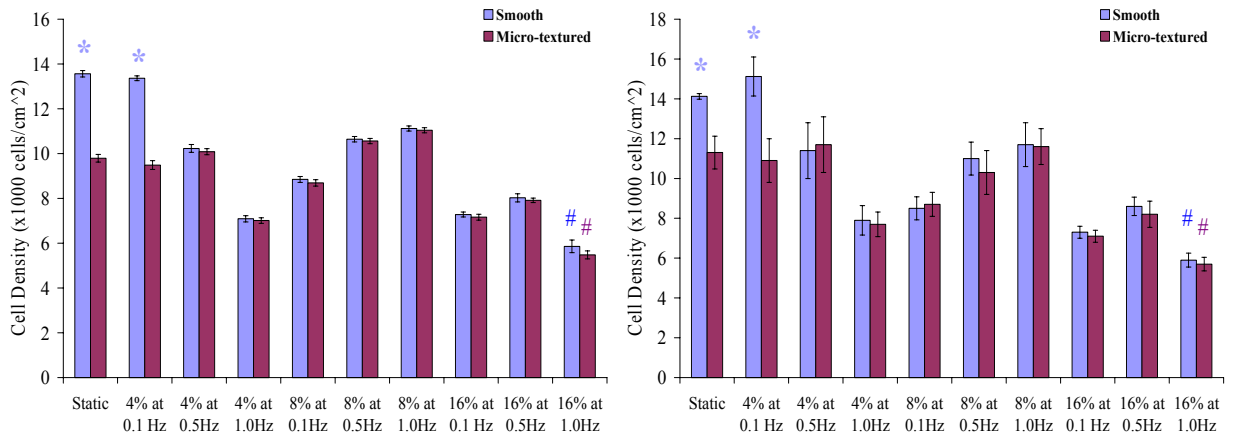

(a) (b)

Figure 31. Bar graphs show the mean value for the cell density observed in the respective conditions. Mean cell density enumerated using an optical microscope in cultures for the SEM analysis (a) and FM analysis (b). Values reported are mean ± standard error; n = 3; # $p < 0.05$ (16% at 1.0Hz compared with the rest of the conditions), *$p < 0.05$ (smooth in static condition compared with the rest of the conditions).

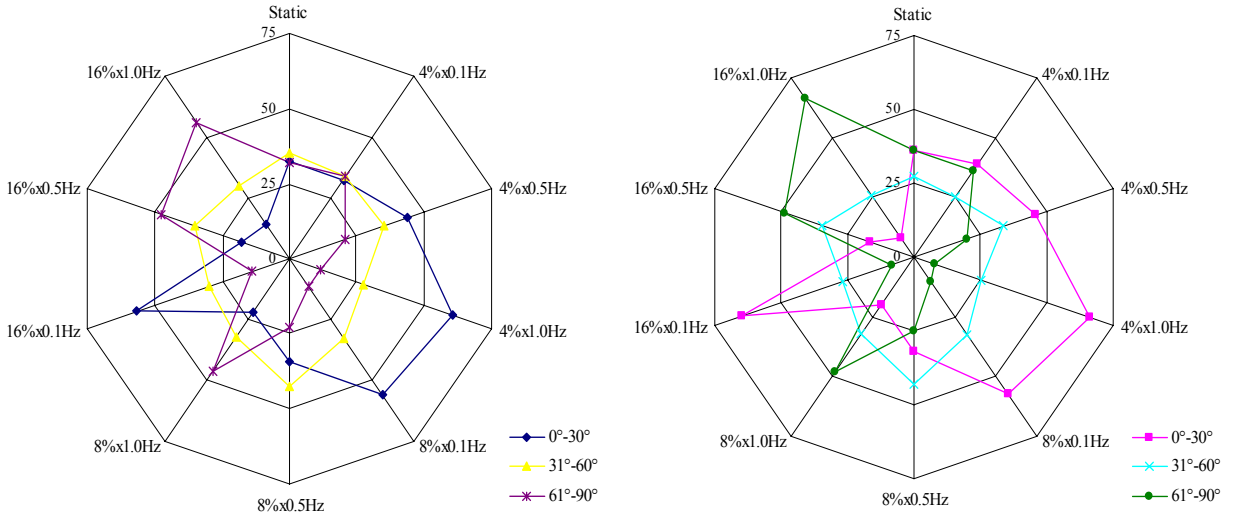

(a) (b)

Figure 32. Radar graphs show the mean values for the percentage of neurites aligned in the three angular ranges: 0°-30°, 31°-60°, 61°-90°. Cells on smooth (a) and micro-textured (b) substrates in different strain conditions. Values reported are the percentage of neurites along the vertical axis and the strain conditions along the circumferential axis. Greater than 50% of neurites in a specified angular defined as a dominating number.

At the strain level of 4%, a higher strain rate enhanced the neurite development, while at the strain levels of 8% or 16% a lower strain rate induced a similar stimulatory effect on neurite development. But the highest strain condition (16% at 1.0Hz) in this study had limited neurite development. These facts suggest that there is an interrelated relationship between strain rate and strain level. Specifically, at high strain levels, increasing strain rate decreases the development of neurite extensions, while at low strain rates, increasing strain rate increases the development of neurites.

Different neurite development in response to different strain conditions can be explained by intracellular cytoskeleton changes that may control or regulate the cell morphology. Studies have shown that periodic application of high strain level (>20%) and strain rate (9.5Hz) in skeletal muscle cells can rupture the actin network [92]. In our study, the strain condition of 16% at 1.0Hz might be responsible for causing a similar actin network rupture leading to neurite retraction, while the strain conditions of 4% at 1Hz, 8% at 0.1Hz and 16% at 0.1Hz might be responsible for promoting F-actin assembly and facilitating the microtubules to advance thereby leading to neurite outgrowth.

High strain condition (16% at 1.0Hz) caused most of the neurites to orient away (see Table 1, page 74) from the direction of the applied strain. It is possible that in this case the neurites were trying to avoid being overstrained by reorienting themselves in the direction of the minimum substrate strain. A similar phenomenon was observed by Wang et. al. [93] when they subjected human melanocyte cells on smooth substrates to cyclic (1Hz) stretching at 4%, 8% and 12% strain levels. They hypothesized that at a higher strain level (12%) the cells oriented in the direction of the minimal axial strain (about 60° to the direction of the applied strain) to avoid being overstretched.

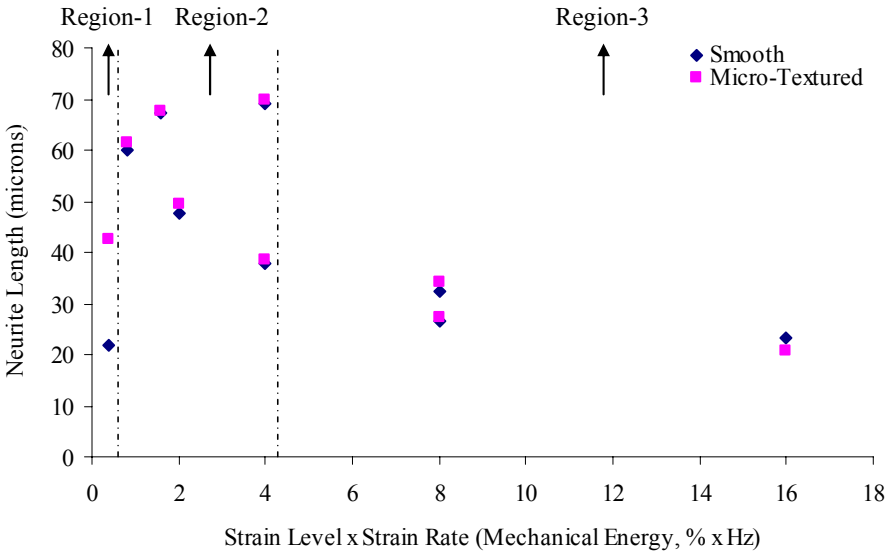

(a)

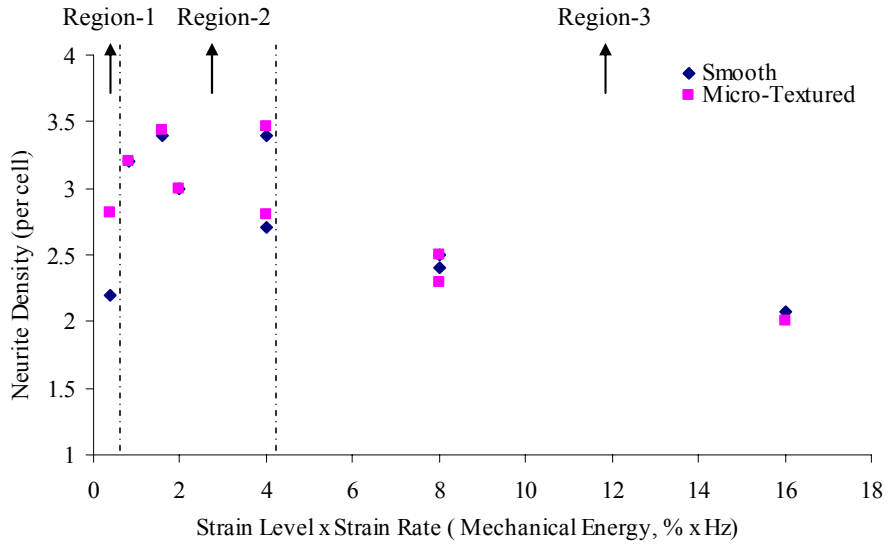

(b)

Figure 33. Variation of neurite development with mechanical energy imparted to the cells. Development of neurite length (a) and neurite density (b) in setups subjected to different mechanical energy levels.

To determine the effect of mechanical energy on the neurite development of cells, the calculated neurite lengths and neurite densities were correlated to the mechanical energy (product of the applied strain level and strain rate) from the triplicates cultures for all the setups. Figure 33 shows the effect of different mechanical energy level on neurite development. The correlation between the neurite length and mechanical energy in cells on smooth and micro-textured substrates (Figure 33a) is R = -0.52 and -0.74, respectively. Similarly, the correlation between the neurite density and mechanical energy in cells on smooth and micro-textured substrates (Figure 33b) is R = -0.60 and -0.81, respectively. The correlation, however, is found to be significant ($p<0.05$) for micro-textured cases, and is not significant for the smooth cases.

A negative correlation was found between the neurite development and the mechanical energy over the entire range. However, when the data was divided into three separate regions a totally different relationship between the neurite development and mechanical energy was observed. A regional analysis of neurite development and mechanical energy (see Figure 33) shows that the neurite length and neurite density were higher in Region-2 (between 0.5-4.5) and lower in Region-1 (between 0-0.5) and Region-3 (between 4.5-16). These findings suggest that an intermediate mechanical energy level was highly stimulatory for neurite development while high and low mechanical energy levels were less stimulatory.

This study did not investigate the effect of substrate topography and mechanical strain on the regulation of gene expression. Future work should address the role of physical conditions (substrate topography and mechanical strain) in the cell's environment in modulating the phenotype of neurons through the activation of specific gene expression.

CHAPTER 6

CONCLUSIONS

The dimensions of the substrate topography had a profound impact on the cellular activities of PC12 cells. Specifically, nano-featured substrates elicited increased cell proliferation, and micro-featured substrates promoted cell differentiation. These findings may suggest the possibility of using substrates with topographical features at the nanometer or micrometer scales to control cell growth, such as using nano-substrates to promote cell proliferation and using micro-substrates to promote cell differentiation in neuron cells. The dimensions of the micro-islands patterned on the micro-substrates can further control and regulate differentiation. Micro-substrate patterned with higher micro-islands and a diameter close to the size of the neurites promoted greater differentiation. Furthermore, PC12 cells on nano-substrates developed extensive number of filopodia, indicating that the cells were spatially aware of their nano-featured surrounding. But these extensive numbers of filopodia did not lead to any significant neurite outgrowth in cells on nano-substrates during a culture period in which substantial neurite outgrowth was observed in cells on micro-substrates.

Nano-featured substrates, namely, nanopillars and nanopores, had a different effect on the neurite development of PC12 cells. Nanopillars elicited increased cell proliferation, and nanopores promoted intermediate cell proliferation and differentiation. Smooth substrates, namely, gold coated coverslips and bare coverslips promoted the greatest cell differentiation. These findings suggest the use of substrates with nanopillars or nanopores for controlled proliferation or differentiation of neuron cell lines.

When combined with mechanical stretching, in the static and low strain (4% at 0.1Hz) condition, micro-textured substrates enhance the development of neurite extension and neurite density. However, in the 4% at 0.5Hz and 1.0Hz, 8% and 16% at 0.1Hz, 0.5Hz and 1.0Hz conditions, cells on both substrates showed similar neurite development. Furthermore, strain level and strain rate have an interrelated effect on neurite development in cells on smooth and micro-textured substrates. Specifically, on both types of substrates, a low strain level at a high strain rate condition of 4% at 1.0Hz strain elicited an enhanced development of neurite length and neurite density while a high strain level at a low strain rate condition of 16% at 0.1Hz elicited a similar degree of neurite development. Low strain condition of 4% at 0.1Hz did not have any stimulatory effect on neurite development, while high strain condition of 16% at 1.0Hz had an adverse effect on neurite development. Strain conditions of 4% at 1.0Hz and 16% at 0.1Hz promote neurite development. Intermediate mechanical energy level was stimulatory and promoted neurite development while high and low mechanical energy levels were less stimulatory and induced limited neurite development, suggesting that the level of mechanical energy can be used to control and regulate neurite development.

Both topography and mechanical strain had an influence on cellular activities such as differentiation and proliferation in PC12 cells. In the case of substrate topography, the size and shape of the substrate feature was a determining factor in eliciting a specific cellular response. In the case of mechanical strain, the magnitude of the strain level and strain frequency of the applied strain was a determining factor in modulating these cellular activities. Furthermore, in the case of combined effect of topography and strain conditions, the magnitude and frequency of the applied strain determined the impact of topography on these cellular activities.

CHAPTER 7

FUTURE DIRECTION

Only a select few substrate topographies and a small range of strain conditions were used to determine the effect of physical cues on cellular activities in PC12 cells. Further work needs to be done to better understand the influence of spacing, diameter and height of nano and micro-featured substrates on neurite development. Results from such a future study will complement the results of Research Question 1 in this study in addressing the role of substrate topography on neurite development. Similarly, the combined effect of substrate topography and mechanical strain was investigated using only one type of micro-textured substrates and a limited range of strain levels and strain rates. Future work can be aimed at investigating the role of different micro-patterned deformable substrates on the effect of different strain conditions on neurite development. Furthermore, the effect of nano-patterned deformable substrate subjected to mechanical strain also needs to be investigated. It is possible that substrate topographic feature with different dimensions and shape might have a different influence on neurite development under specific strain conditions.

The results of Research Question 1 and 2 in this dissertation suggest the use of physiological relevant strain conditions and substrate topographies to control the differentiation and proliferation in neuron cells. Most cells found *in vivo* are also subjected to combined effect of mechanical strain and substratum topography. Hence, the combined effect of substrate topography and mechanical strain can be used to better understand the influence of the physical cues on cellular activities in other cell lines. This has significance in design and development of

in vitro models for understanding the effect of mechanical strain on influencing the topographical features on cell differentiation and proliferation found *in vivo*.

Future work should elucidate the mechanism by which physical cues such as substrate topography and mechanical strain are translated into biological signal. The role of cell surface receptors in regulating differentiation and proliferation in response to physical cues in neuronal cell line such as PC12 cells can be addressed by labeling the cells with a neuronal cell surface marker (NCAM). This marker is a member of the immunoglobulin super-family and is believed to play an important role in cell-cell interactions during development, especially in the regulation of neurite outgrowth [94]. As soluble NCAM is known to promote neurite outgrowth in addition to NGF, a future study should investigate the NCAM phosphorylation activity and neuronal differentiation in response to substrate topography and mechanical strain.

This study showed that substrate topography and mechanical strain influence neurite development and cell multiplication in PC12 cells. However, the association of cell morphology with specific gene expression levels needs to be established to understand how these physical cues are translated into biological signals that determine downstream processes such as cell adhesion, differentiation and proliferation. In differentiating neurons, the expression of growth associated gene (GAP-43) correlates with neurite outgrowth. GAP-genes upon activation by a signaling pathway induce gene transcription during neurite development and regeneration [95]. This interaction between neurite development and gene expression can be investigated by setting up parallel cultures for morphological analysis by SEM and gene expression by northern blots and quantitative real time polymerase chain reaction (RT-PCR). The relationship between the gene expression and the neurite outgrowth can thus be investigated for cells on different types of substrate topographies and mechanical strain conditions.

REFERENCES

1. Barbucci, R., Lamponi, S., Magnani, A. and Pasqui, D. (2002) Micropatterned surfaces for the control of endothelial cell behavior. J. Biomolecular Engineering 19, 161-170.

2. Karuri, N. W., Liliensiek, S., Teixeira, A. I., Abrams, G., Campbell, S., Nealey, P. F. and Murphy, C. J. (2004) Biological length scale topography enhances cell substratum adhesion of human corneal epithelial cells. Journal of Cell Science 117, 3153-3164.

3. Katsumi, A., Orr, W., Tzima, E. and Schwartz M. A. (2004) Integrins in mechanotransduction. J. Biol. Chem. 279, 12001-12004.

4. Teixeira, A. I. G., Abrams, A., Murphy, C. J. and Nealey P. F. (2001) Effects of nanoscale substrate topography on the behavior of human corneal epithelial cells. SRC Program review, U. of Wisconsin, Madison, Wisconsin.

5. Craighead, H. G., James, C. D. and Turner, A. M. P. (2001) Chemical and topographic patterning for directed cell attachment. J. Curr. Opin. Solid State Mater. Sci. 5, 177–84.

6. Flemming, R. G., Murphy, C. J., Abrams, G. A., Goodman, S. L. and Nealey, P. F. (1999) Effects of synthetic micro- and nano-structured surfaces on cell behavior. J. Biomaterials 20, 573-588.

7. Cyster, L. A., Parker, K. G., Parker, T. L. and Grant, D. M. (2004) The effect of surface chemistry and nanotopography of titanium nitride (TiN) films on primary hippocampal neurons. J. Biomaterials 25, 97–107.

8. Andersson, A. S., Olsson, P., Lidberg, U. and Sutherland, D. (2003) The effects of continuous and discontinuous groove edges on cell shape and alignment. J. Experimental Cell Research 288, 177–188.

9. Zhu, B., Zhang, Q., Lu, Q., Xu, Y., Yin, J., Hu, J. and Wang, Z. (2004) Nanotopographical guidance of C6 glioma cell alignment and oriented growth. Biomaterials 25; 4215–4223.

10. Pfister, B. J., Weihs, T. P., Betenbaugh, M. and Bao, G. (2003) An In vitro uniaxial stretch model for axonal injury. Annals of Biomedical Engineering 31, 589–598.

11. Geddes, D. M., LaPlaca, M. C. and Cargill, R. S. (2003) Susceptibility of hippocampal neurons to mechanically induced injury. Experimental Neurology 184, 420–427.

12. Slemmer, J. E., Matser, E. J. T., Zeeuw, C. I. and Weber, J. T. (2002) Repeated mild injury causes cumulative damage to hippocampal cells. Brain 125, 2699-2709.

13. Burger, E. H. and Nulend, J. K. (1999) Mechanotransduction in bone—role of the lacunocanalicular network. FASEB journal 13, S101-S112.

14. Mills, I., Cohen, C. R., Kamal, K., Shin, G. L., Du, W. and Sumpio, B. E. (1997) Strain activation of bovine aortic smooth muscle cell proliferation and alignment: study of strain dependency and role of protein kinase A and C signaling pathways. J. Cell Phys. 170, 228-234.

15. Lewis, A. K. and Birdgenan, P. S. (1992) Nerve growth core contains two populations of actin filaments that differ in organization and polarity. J. Cell Bio.119, 1219-1243.

16. Chen, C. S. (2000) The balance of intra- and extra-cellular forces in mechanosensation. Investigator abstracts, The Whitaker Foundation, Rosslyn, VA.

17. Huang, S. and Ingber, D. E. (1999) The structural and mechanical complexity of cell-growth control. Nat. Cell Biol. 1, E131-E138.

18. Suter, D. M. and Forschert, P. (1998) An emerging link between cytoskeletal dynamics and cell adhesion molecules in growth cone guidance. Current Opinion in Neurobiology 8,106-116.

19. Zhou, F. Q., Waterman-Storer, C. M. and Cohan, C. S. (2002) Focal loss of actin bundles causes microtubule redistribution and growth cone turning. J. Cell Biology 157, 839–849.

20. Gallo, G., Yee, G. and Letourneau, P. C. (2002) Actin turnover is required to prevent axon retraction driven by endogenous actomyosin contractility. J. Cell Biology 158, 1219-1228.

21. Polinsky M., Balazovich K. and Tosney K. W. (2000) Identification of an invariant response: stable contact with schwann cells induces veil extension in sensory growth cones. The Journal of Neuroscience 20, 1044–1055.

22. Kuhn, T. B., Moberg, P., Brown, M. D., Bernstein, B. W., Minamde, L. S., Jensen, J. R., Kade, K., Seda, E. A. and Bamberg, J. R. (2000) Regulating actin dynamics in neuronal growth cones by ADF/Coflin and Rho family GTPases. J. of Neurobio. 44, 126-144.

23. Abrams, G. A., Schaus, S. S., Goodman, S. L., Nealey, P. F. and Murphy, C. J. (2000) Nanoscale topography of the corneal epithelial basement membrane and Descemet's membrane of the human. J. Cornea and External Diseases 19, 57-64.

24. Abrams, G. A., Bentley, E., Nealey, P. F. and Murphy, C. J. (2002) Electron microscopy of the canine corneal basement membranes. J. Cells Tissues Organs 170, 251-257.

25. Abrams, G. A., Goodman, S. L., Nealey, P. F., Franco, M. and Murphy, C. J. (2000) Nanoscale topography of the basement membrane underlying corneal epithelium of the Rhesus Macaque. J. Cell Tissue Res. 299, 39-46.

26. Dalby, M. J., Riehle, M. O., Yarwood, S. J., Wilkinson, C. D. W. and Curtis, A. S. G. (2003) Nucleus alignment and cell signaling in fibroblasts: response to a micro-grooved topography. J. Experimental Cell Research 284, 274–282.

27. Dalby, M. J., Gadegaard, N., Riehle, M. O., Wilkinson, C. D. W. and Curtis, A. S. G. (2004) Investigating filopodia sensing using arrays of defined nano-pits down to 35 nm diameter in size. The International Journal of Biochemistry & Cell Biology 36, 2005–2015.

28. Mesfin, N. M. D., Karim, M. A. A., Turner, A. M. P. and Schanz, S. (2004) Topographically modified surfaces affect orientation and growth of hippocampal neurons. J. Neur. Eng. 1, 78–90.

29. Lee, J. K, Baac, H., Song, S. H., Lee, S. D., Park, D. and Kim, S. J. (2004) The topographical guidance of neurons cultured on holographic photo-responsive polymer. Proceedings of the 26th Annual International Conference of the IEEE EMBS, San Francisco, CA, USA. September 1-5, 2004.

30. Webb, A., Clark, P., Skepper, J., Compston, A. and Wood, A. (1995) Guidance of oligodendrocytes and their progenitors by substratum topography. J. Cell Science 108, 2747–60.

31. Nagata, I., Kawana, A. and Nakatsuji N. (1993) Perpendicular contact guidance of CNS neuroblasts on artificial microstructures. J. Development 117, 401-408.

32. Wang, H. J. C., Grood, E. S., Florer, J. and Wenstrup, R. (2000) Alignment and proliferation of MC3T3-E1 osteoblasts in microgrooved silicone substrata subjected to cyclic stretching. J. Biomechanics 33, 729-735.

33. Rice, J. M., Hunt, J. A., Gallagher, J. A., Hanarp, P., Sutherland, D. S. and Gold, J. (2003) Quantitative assessment of the response of primary derived human osteoblasts and macrophages to a range of nanotopography surfaces in a single culture model in vitro. J. Biomaterials 24, 4799–4818.

34. Dalby, M. J., Riehle, M. O., Johnstone, H. J. H., Affrossman, S. and Curtis, A. S. G. (2003) Nonadhesive nanotopography: fibroblast response to poly(n-butyl methacrylate)-poly(styrene) demixed surface features. J. Biomed. Mater. Res. 67A, 1025–1032.

35. Dalby, M. J., Riehle, M. O., Johnstone, H. J. H., Affrossman, S. and Curtis, A. S. G. (2002) Polymer demixed nano-topography: control of fibroblast spreading and proliferation. J. Tissue Engineering 8, 1099–1108.

36. Dalby, M. J., Yarwood, S. J., Riehle, M. O., Johnstone, H. J. H., Affrossman, S. and Curtis, A. S. G. (2002) Increasing fibroblast response to materials using nanotopography: morphological and genetic measurements of cell response to 13-nm-high polymer demixed islands. Experimental Cell Research 276, 1–9.

37. Turner, S., Kam, L., Isaacson, M., Craighead, H. G., Shain, W. and Turner, J. (1997) Cell attachment on silicon nanostructures. J. Vac. Sci. Technol. B. 15, 2848-2854.

38. Wojciak, S. B, Madeja, Z., Korohoda, W., Curtis, A. and Wilkinson, C. (1995) Activation of macrophage-like cells by multiple grooved substrata. Topographical control of cell behavior. J. Cell Bio. Int. 19, 485–90.

39. Oakley, C. and Brunette, D. M. (1995) Response of single, pairs, and clusters of epithelial cells to substratum topography. J. Biochem. Cell Bio. 73, 473–89.

40. Cooper, A., Munden, H. R. and Brown, G. L. (1976) The growth of mouse neuroblastoma cells in controlled orientations on thin films silicon monoxide. J. Exp. Cell Res. 103, 435–439.

41. Hoch, H. C., Staples, R. C., Whitehead, B., Comeau, J. and Wolf, E. D. (1997) Signaling for growth orientation and cell di§erentiation by surface topography in Uromyces. Science 235, 1659–1662.

42. Hunt, J. A., Williams, R. L., Tavakoli, S. M. and Riches, S. T. (1995) Laser surface modification of polymers to improve biocompatibility. J. Mat. Sci. Mat. Med. 6, 813–817.

43. Fewster, S. D., Coombs, R. H., Kitson, J. and Zhou, S. (1994) Precise ultrafine surface texturing of implant materials to improve cellular adhesion and biocompatibility. J. Nanobio. 3, 201–214.

44. Fujimoto, K., Takahashi, T., Miyaki, M. and Kawaguchi, H. (1997) Cell activation by the micropatterned surface with settling particles. J. Biomat. Sci. Poly. 8, 879–91.

45. Wojciak, S. B, Denyer, M., Mishra, M. and Brown, R. A. (1997) Adhesion, orientation, and movement of cells cultured on ultrathin fibronectin fibers. In Vitro Cell Dev. Bio. Animal 33, 110–7.

46. Polinsky, M., Balazovich, K. and Tosney, K. W. (2000) Identification of an invariant response: stable contact with schwann cells induces veil extension in sensory growth cones. J. Neuroscience 20, 1044–1055.

47. Goldberg, D. and Burmeister, D. (1986) Stages in axon formation: observations of growth of aplysia axons in culture using video-enhanced contrast-differential interference contrast microscopy. J. Cell Biology 103, 1021-1031.

48. Tanaka, H., Hirose, M., Osada, T., Miwa, H., Watanabe, S. and Sato, N. (2000) Implications of mechanical stretch on wound repair of gastric smooth muscle cells In vitro. J. Digestive Diseases and Sciences 45, 2470–2477.

49. Yang, G., Crawford, R. C. and Wang, J. H. C. (2004) Proliferation and collagen production of human patellar tendon fibroblasts in response to cyclic uniaxial stretching in serum-free conditions. Journal of Biomechanics 37, 1543–1550.

50. Wang, J. H. C., Yang, G., Li, Z. and Shen, W. (2004) Fibroblast responses to cyclic mechanical stretching depend on cell orientation to the stretching direction. Journal of Biomechanics 237, 573–576.

51. Wang, J. H. C., Jia, F., Yang, G., Yang, S., Campbell, B. H., Stone, D. and Woo, S. L. Y. (2003) Cyclic mechanical stretching of human tendon fibroblasts increases the production of prostaglandin E2 and levels of cyclooxygenase expression: A novel in vitro model study. J. Connective Tissue Research 44, 128–133.

52. Gopalan, S. M., Flaim, C., Bhatia, S., Hoshijima, M., Knoell, R., Chien, K. R., Omens, J. H. and McCulloch, A. D. (2003) Anisotropic stretch-induced hypertrophy in neonatal ventricular myocytes micropatterned on deformable elastomers. J. Biotechnol. Bioeng. 81, 578-587.

53. Bonacci, J., Harris, T. and Stewart, A. G. (2003) Impact of extracellular matrix and strain on proliferation of bovine airway smooth muscle. J. Clin. and Exp. Pharm. and Phys. 30, 324-328.

54. Asanuma, K., Magid, R., Johnson, C., Nerem, R. M. and Galis, Z. S. (2003) Uniaxial strain upregulates matrix-degrading enzymes produced by human vascular smooth muscle cells. Am. J. Physiol. Heart Circ. Physiol. 284, H1778–H1784.

55. Powell, C. A., Smiley, B. L., Mills, J. and Vandenburgh, H. H. (2002) Mechanical stimulation improves tissue-engineered human skeletal muscle. Am. J. Physiol. Cell Physiol. 283, C1557–C1565.

56. Sipkema, P., Linden, P. J. W., Westerhof, N. and Yin, F. C. P. (2003) Effect of Cyclic axial stretch of rat arteries on endothelial cytoskeletal. Journal of Biomechanics 36, 653–659.

57. Gilchrist, M. D. (2004) Experimental device for simulating traumatic brain injury resulting from linear accelerations. J. Strain 40, 180-192.

58. Ingber, D. E. (1999) How cells might sense gravity. The FASEB Journal. 13, S3-S15.

59. Wang, H. C., Clermont, P. J., Wille, J. and Yin, P. F. (2001) Specificity of endothelial cell reorientation in response to cyclic mechanical stretching. J. Biomechanics 34, 1563–1572.

60. Bischofs, I. B. and Schwarz, U. S. (2003) Cell organization in soft media due to active mechanosensing. PNAS 100, 9274-9279.

61. Takemasa, T., Sugimoto, K. and Yamashita, K. (1997) Amplitude-dependent stress fiber reorientation in early response to cyclic strain. J. Experimental Cell Research 230, 407–410.

62. Sotoudeh, M., Li, Y. S., Usami, S., Shyy, J. and Chien S. (1998) Strain-induced apoptosis in porcine vascular smooth muscle cells. J. Ann Biomed Eng 26, S34.

63. Li, Z., Yang, G., Khan, M., Stone, D., Woo, S. L. and Wang, J. C. (2004) Inflammatory response of human tendon fibroblasts to cyclic mechanical stretching. The American Journal of Sports Medicine 32, 435-440.

64. Gudi, S. V. P., Lee, A. A., Clark, C. B. and Frangos, J. A. (1998) Equibiaxial strain and strain rate stimulate early activation of G-proteins in cardiac fibroblasts. Am. J. Physiol. Cell Physiol. 274, C1424-C1428.

65. Morrison, B., Cater, H. L., Wang, C. C. B., Thomas, F. C., Hung, C. T., Ateshian, G. A. and Sundstrom, L. E. (2003) A tissue level tolerance criterion for living brain developed with an in vitro model of traumatic mechanical loading. J. Stapp Car Crash Journal 47, 93-105.

66. Tanone, M., Yamaga, M., Ide, J. and Takagi, K. (1996) Acute stretching of peripheral nerve inhibits retrograde axonal transport. J. Hand Surgery 21, 358-363.

67. Wu, Q. and Chen, Q. (2002) Mechanoregulation of chondrocyte proliferation, maturation, and hypertrophy: Ion-channel dependent transduction of matrix deformation signals. J. Experimental Cell Research 256, 383–391.

68. Guck, J., Ananthakrishnan, R., Mahmood, H., Moon, T. J., Cunningham, C. and Kas, J. (2001) The Optical Stretcher: A novel laser tool to micromanipulate cells. J. Biophysical 81, 767–784.

69. Mitton, K. P., Tumminia, S. J., Arora, J., Zelenka, P., Epstein, D. L. and Russell, P. (1997) Transient loss of a B-crystallin: An early cellular response to mechanical stretch. J. Biochemical and Biophysical Research Communications 235, 69–73.

70. Zhuang, J., Yamada, K., Saffitz, J. E. and Kleber, A.G. (2000). Pulsatile stretch remodels cell-to-cell communication in cultured mycocytes. J. Circulation Res. 87, 816.

71. Wang, J. H. C., Clermont, P. G., Willie, J. and Yin, F. C. (2001). Specificity of endothelial cells reorientation in response to cyclic mechanical stretching. J. Biomechanics 12, 1563-1572.

72. Yest, M. J., Simpson, D., Wren, K., Riddles, S., Plochu, H. J., Borg, T. K. and Terracio, L. (2000). Design and construction of uniaxial cell stretcher. AJP Heart and Circ. Physio. I6, H3124-H3130.

73. Jones, D. B., Lensoth, G., Sawada, Y. and Var de Sloter, J. B. (1994). Application of homogenous defined strain to cell cultures. Biomechanics & cells Ed. Lyalll and El Haj. Exp. Bio Series. Cambridge Univ. Press, Cambridge, England.

74. Wang, J. H., Steve, D. and Wo, S. L. (2000). A new method to align and orient human patellar tendon fibroblasts during cyclic mechanical stretching. 46th Annual Meeting Orthopedic Res. Society, Orlando, Fl.

75. Shaub, A. (1999) Unravelling the extracellular matrix. Nature Cell Biology I.7, E173-175.

76. Waters, C. M., Glucksberg, M. R., Laulenschlayer, E. P., Lee, C. W., Matre, R. M., Warp, R. J., Savla, U., Healy, K. E., Moran, B., Castner, D. G. and Bearinger J. P. (2001) A system to impose prescribed homogenous strains on cultured cells. J. App. Physio. 91, 1600 - 1610.

77. Zhao, Y. P., Ye, D. X., Wang, G. C. and Lu, T. M. (2003) Designing nanostructures by glancing angle deposition., SPIE Proceedings 59, 5219.

78. Haq, F., Rao, Y. L., Keith, C., Zhao, Y. and Zhang, G. (2005) Nano and micro-structured substrates for neuronal cell development. J. Biomedical Nanotechnology 1, 313-319.

79. Venkatramani, A., Rao, Y. and Zhang, G. (2005) Nanopillar array structures for enhancing biosensing performance. International Journal of Nanomedicine. In Press.

80. Krause, A., Cowles, E. A. and Gronowicz, G. (2003) Integrin-mediated signaling in osteoblasts on titanium implant materials. J. Biomed. Mat. Res. 52, 738-747.

81. Walowitz, J. L. and Roth, J. A. (1999) Activation of ERK1 and ERK2 is required for manganese-induced neurite outgrowth in rat pheochromocytoma (PC12) cells. J. Neuroscience Research 57, 847–854.

82. Bershadsky, A., Chausovsky, A., Becker, E., Lyubimova, A. and Geiger, B. (1996) Involvement of microtubules in the control of adhesion dependent signal transduction. J. Current Biology 6, 1279-1289.

83. Mazia, D., Schatten, G. and Sale, W. (1975) Adhesion of cells to surfaces coated with polylysine. J. Cell Bio. 66, 198-200.

84. Rainaldi, G., Filippini, P., Ferrante, A., Indovina, P. L. and Santini, M. T. (2001) Fibronectin facilitates adhesion of K562 leukemic cells normally growing in suspension to cationic surfaces. J. Biomed. Mat. Res. 55, 104-113.

85. Ham, R. G. and McKeehan, W. L. (1979) Media and growth requirements. Methods in Enzymology 58, 44-93.

86. Greene, L. A., Farenelli, S. E., Cunningham, M. E. and Park, D. S. (1998) Culture and experimental use of PC12 rat pheochromocytoma cell line. In Banker, G. and Goslin, K. (editors), Culturing nerve cells. MIT Press, Cambridge, MA, p 161–188.

87. From the Laboratory of Dr. Allan Bradley “Use of hemacytometer for the determination of cell numbers”. Baylor College of Medicine, Houston, TX.

88. Ellman, C. L., Courtney, D., Andres, V. and Featherstone, R. J. (1961) A new and rapid colorimetric determination of acetylcholinesterase activity. J. Biochem. Pharmacology 7, 88-95.

89. Clark, P., Britland, S. and Connolly, P. (1993) Growth cone guidance and neuron morphology on micro-patterned laminin surfaces. J. Cell Science 105, 203-212.

90. Wood, W. and Martin, P. (2002) Structures in focus—filopodia. The International Journal of Biochemistry and Cell Biology 34, 726–730.

91. Foley, J. D., Grunwald, E. W., Nealey, P. F. and Murphy, C. J. (2005) Cooperative modulation of neuritogenesis by PC12 cells by topography and nerve growth factor. J. Biomaterials 26, 3639–3644.

92. Wagner, O., Zinke, J., Dancker, P., Grill, W. and Bereiter-Hahn, J. (1999) Viscoelastic properties of F-actin, microtubules, F-actin/A-actinin, and F-actin/Hexokinase determined in microliter volumes with a novel nondestructive method. J. Biophysical Journal 76, 2784–2796.

93. Wang, J. H. C., Ip, W., Boissy, R. and Grood, E. S. (1998) Cell orientation response to cyclically deformed substrates. J. Biomechanics 28, 1543-1552.

94. Beggs, H., Soriano, P. and Maness, P. (1994) NCAM-dependent neurite outgrowth is inhibited in neurons from Fyn-minus mice. J. Cell Biology 127, 825-833.

95. Reinhard, E., Nedivi, E., Wegner, J., Skene, J. H. P. and Westerfield, M. (1994) Neural selective activation and temporal regulation of a mammalian GAP-43 promoter in zebrafish. Development 120, 1767-1775.

APPENDICES

APPENDIX-A

SUBSTRATE TOPOGRAPHIES USED FOR STUDYING CELLULAR ACTIVITIES

Table 3. Various types of fabrication techniques used to develop topographies for studying cellular effects in different cell lines.

TYPE OF TOPOGRAPHY	FABRICATION TECHNIQUE	CELL LINE & CELLULAR EFFECT
Quartz wafer with 0.5, 5, 10, 25 μm width and 0.5, 5 μm depth grooves. Equal groove and ridge width [38].	Photolithography and reactive ion etching	Murine macrophage cells. Cells spread faster on shallow grooves but elongated faster on deeper grooves.
Titanium coated silicon with V-shaped 15 μm width and 3 μm depth grooves. Equal groove and ridge width [39].	Photolithography and anisotropic etching, glow discharge	Porcine epithelial cells. Cells oriented in direction of grooves; actin filaments and microtubules aligned along walls and edges
Silicon oxide on polystyrene with grooves of 4 μm width and 50 nm height arranged in a radial array [40].	Evaporative coating	Murine neuroblastoma cells. Cells adhered to lines and processes aligned along the lines; processes grew in bipolar manner.
Polystyrene cast of silicon mold with grooves of 0.5–100 μm width, 0.03–5.0 μm height and 0.5–62 μm between ridges [41].	Photolithography and reactive ion etching	Uramyces appendiculatus fungus. Maximum cell differentiation observed for ridges or plateaus 0.5 μm high; ridges higher than 1.0 μm or smaller than 0.25 μm were not effective signals; ridge spacing of 0.5–6.7 μm caused high degree of orientation of the fungus.
Polycarbonate, polyetherimide with square nodes of 7, 25, or 50 μm width and 0.5, 1.5, 2.5 μm height arranged in a square array [42].	Laser modification	Human neutrophils cells. None of the textured surfaces significantly stimulated neutrophil movement compared to chemical stimulators, although neutrophil movement was greater on some of the textured surfaces than on an untextured surface.
PMMA, PET, polystyrene with Circular pillars and pores 1, 5, 10, 50 μm diameter arranged in a uniform array [43].	Laser ablation used in conjunction with masks made by e-beam lithography, reactive ion etching	Human osteoblasts. Cells stretched between adjacent 1 and 5 μm pillars; cells attached to edges of pores, especially on 10 μm pores; texture caused increase in cell adhesion on all materials but PMMA; greatest increase in adhesion was on 50 μm PET pillars.
Poly(NIPAM) particles on polystyrene surface with 0.86–0.63 μm diameter arranged in a 2D hexagonal lattice, 0.96 μm avg. distance between sphere centers [44].	Particle setting	Neutrophil-like induced HL-60 cells. Cells loosely adhered but did not spread on sphere-coated surface and could roll easily.
Fibronectin tracks on glass with 0.2–5 μm width, Height and spacing not listed [45].	Glass coated with fibronectin tracks	Rat fibroblasts and macrophages. Increased spreading and alignment in direction of the tracks; actin aligned in fibroblasts; alignment of focal contacts in fibroblasts and macrophages; increased polymerization of F-actin; macrophages had actin-rich microspikes and became polarized and migratory.

APPENDIX-B

CELL STRETCHING DEVICES USED FOR STUDYING CELLULAR ACTIVITIES

Table 4. Various types of cell-stretching devices used for studying cell mechanics under micromechanical environment.

TYPE OF DEVICE	TYPE OF FORCE	CELLS STRETCHED
Linear pulsate stretch. Mechanical stretch to determine role in remodeling atrial and ventricular myocardium [70]	Uniaxial stretch. Transverse compression/ deformation of silicone membrane.	Neonatal-rat ventricular myocyte.
Cyclical Stretch. Cellular responses to mechanical stimuli depend on type of stimuli imposed [71].	a) Simple elongation (b) Pure uniaxial stretch (c) Equibiaxial stretch.	Human-aortic endothelial cells.
Linear Stretch. In vitro cell mechanics study to investigate the affect of mechanical stimulation on anchorage dependent cells [72].	Cyclic biaxial stretch.	Neonatal rat cardiac fibroblast.
Aclar DC motor device (product by Allied Signal inN.J., USA).	Actuator produces linear strains, which are controlled by microprocessor and calculated using optical measurement of defined displacement from the center.	Various cell-types e.g. endothelial, fibroblasts.
4-point bending machine allowed calculations of strain in the surface without need for measuring strain with a strain gauge [73].	Geometrical modeling to describe the strains in the tension and compression surfaces.	Osteoblast cells.
Affects of microgrooved surfaces on alignment & shape of tendon fibroblast cell's response to cyclic mechanical stretching [74].	Cyclic stretch imposed along microgrooves parallel and perpendicular to the axis of silicone membrane substrate for cultured cells.	Human patellar tendon fibroblasts.
Laser Trap Optical Stretcher to determine changes in cytoskeleton for characteristics found in pathology of cancer [75].	Conversion of momentum of beam gives an impulse to cell resulting in a stretching force on cell surface where light enters and leaves.	Fibroblast malignantly transforming to leukemia cell lines.
Pneumatic Actuator. Presents relationship of magnitude of mechanical cyclic strain and extent of wound closure & cell spreading [76].	Biaxial large strain homogenous stretch on a multi-well surface-treated silicone elastomer substrate.	Pulmonary epithelial cells.

APPENDIX-C

CELL COUNTING PROTOCOL

Cell Counting:

For tissue engineering applications in cell culturing it's necessary to determine cell concentration. This is necessary to determine healthy cell cultures. Cell count is a quantitative analysis to determine the efficacy of certain tests and procedures and hence assign significance to cell culture viability. A device used for cell counting is called a counting chamber. The most widely used type of chamber is called a hemacytometer, since it was initially designed for blood cell count. The protocol for using hemacytomer to determine cell density is given below.

Hemacytometer:

A hemacytometer (Fischer Scientific) was used for cell counting/cell density. Counting cells by the use of a hemacytometer is a convenient and practical method of determining cell numbers. Hemacytometer consists of two chambers, each of which is divided into nine 1.0 mm squares. A cover glass is supported 0.1 mm over these squares so that the total volume over each square is 1.0 mm x 0.1 mm or 0.1 mm_3, or 10^{-4} cm^3. Since 1 cm^3 is approximately equivalent to 1 ml, the cell concentration per ml will be the average count per square x 10^4 [87].

Cell distribution in the hemacytometer chamber depends on the particle number, not particle mass. Thus, cell clumps will distribute in the same way as single cells and can distort the result. Unless 90% or more of the cells are free from contact with other cells, the count should be repeated with a new sample. A sample will not be representative if the cells are allowed to settle before a sample is taken. Always mix the cell suspension thoroughly before sampling [87].

The cell suspension should be diluted so that each such square has between 20 - 50 cells (2-5 x 10^5 cells/ml). A total of 300 - 400 cells should be counted, since the counting error is approximated by the square root of the total count. A common convention is to count cells that touch the middle lines (of the triple lines) to the left and top of the square, but do not count cells similarly located to the right and bottom. Hemacytometer counts do not distinguish between living and dead cells. A number of stains are useful to make this distinction. Trypan blue among others (Erythrosin B, Nigrosin) can be used: the nuclei of damaged or dead cells take up the stain [87].